DIGITALCOMMONS
@WAYNESTATE

Wayne State University

Wayne State University Dissertations

1-1-2015

Preclinical Evaluation Of Infrared Light Therapy In A Rat Model Of Neonatal Hypoxic-Ischemic Encephalopathy

Christian Andrew Reynolds
Wayne State University,

Follow this and additional works at: http://digitalcommons.wayne.edu/oa_dissertations

Part of the Physiology Commons

Recommended Citation
Reynolds, Christian Andrew, "Preclinical Evaluation Of Infrared Light Therapy In A Rat Model Of Neonatal Hypoxic-Ischemic Encephalopathy" (2015). *Wayne State University Dissertations.* Paper 1294.

This Open Access Dissertation is brought to you for free and open access by DigitalCommons@WayneState. It has been accepted for inclusion in Wayne State University Dissertations by an authorized administrator of DigitalCommons@WayneState.

www.manaraa.com

PRECLINICAL EVALUATION OF INFRARED LIGHT THERAPY IN A RAT MODEL OF NEONATAL HYPOXIC-ISCHEMIC ENCEPHALOPATHY

by

CHRISTIAN ANDREW REYNOLDS

DISSERTATION

Submitted to the Graduate School

of Wayne State University,

Detroit, Michigan

in partial fulfillment of the requirements

for the degree of

DOCTOR OF PHILOSOPHY

2015

MAJOR: PHYSIOLOGY

Approved by:

_____

Advisor Date

_____

_____

_____

_____

www.manaraa.com

© COPYRIGHT BY

CHRISTIAN ANDREW REYNOLDS

2015

All Rights Reserved

www.manaraa.com

DEDICATION

I dedicate this dissertation to my fiancé, Dr. Zeljka Minic, and to all the friends, family and colleagues who supported me along the way.

www.manaraa.com

ACKNOWLEDGEMENTS

I would like to acknowledge my mentors, Drs. Karin Przyklenk and Thomas Sanderson, as well as my entire thesis advisory committee for their unwavering support. Without their expert guidance none of this work would have been possible.

All experiments presented in Chapter 4 of this dissertation were done in collaboration with Dr. Sarah Trimpin. The success of these experiments relied heavily on the support of Dr. Trimpin and the technology pioneered in the Trimpin Laboratory.

Finally, the ultimate success of this work was governed by a comprehensive understanding of the role of mitochondria in cell death caused by cerebral ischemia-reperfusion injury, and work from the Hüttemann and Sanderson laboratories has provided the prerequisite mechanistic insight essential for this project's completion.

www.manaraa.com

TABLE OF CONTENTS

www.manaraa.com

www.manaraa.com

www.manaraa.com

www.manaraa.com

www.manaraa.com

LIST OF TABLES

www.manaraa.com

LIST OF FIGURES

www.manaraa.com

www.manaraa.com

LIST OF ABBREVIATIONS

Δp_m	proton gradient across inner mitochondrial membrane
$\Delta \psi_m$	mitochondrial membrane potential
3-NBN	3-nitrobenzonitrile
ADP	adenosine diphosphate
AIF	apoptosis inducing factor
Apaf-1	apoptotic protease activating factor 1
ATP	adenosine triphosphate
BAK	Bcl-2 homologous antagonist/killer 1
BAX	Bcl-2 associated X protein
Bcl-2	a family of structurally related proteins involved in regulating the intrinsic pathway of apoptosis
Ca^{2+}	calcium
CcO	cytochrome *c* oxidase
CID	collision-induced dissociation
CL	cardiolipin
DCB	1,2-dicyanobenzene
DESI	desorption electrospray ionization
EDTA	ethylenediaminetetraacetic acid
EGTA	ethyleneglycoltetraacetic acid
ETC	electron transport chain
EtOH	ethanol
FAD^+	oxidized flavin adenine dinucleotide
$FADH_2$	reduced flavin adenine dinucleotide
GAPDH	glyceraldehyde 3-phosphate dehydrogenase
GBI	global brain ischemia

www.manaraa.com

H^+	proton
H_2O	water
H_2O_2	hydrogen peroxide
HEPES	4-(2-hydroxyethyl)-1-piperazineethanesulfonic acid
HIE	hypoxic-ischemic encephalopathy
HO_2	hydroperoxyl radical
HT22	an immortalized mouse hippocampal cell line
Iba-1	ionized calcium-binding adapter molecule 1
IMS	ion-mobility spectrometry
IRL	infrared light
KF	potassium fluoride
LED	light-emitting diode
LSI	laser spray ionization
m/*z*	mass-to-charge ratio
MAI	matrix-assisted ionization
MALDI	matrix-assisted laser desorption/ionization
MLCL	monolysocardiolipin
MS	mass spectrometry
MS/MS	tandem mass spectrometry
NAD^+	oxidized nicotinamide adenine dinucleotide
NADH	reduced nicotinamide adenine dinucleotide
NeuN	a neuronal nuclear antigen
NH_4OH	ammonium hydroxide
NO	nitric oxide
NO_2	nitrogen dioxide

www.manaraa.com

O_2^-	superoxide radical
O_2	oxygen
OGD	oxygen–glucose deprivation
OH^-	hydroxide radical
OxPhos	oxidative phosphorylation
PAGE	polyacrylamide gel electrophoresis
PBS	phosphate buffered saline
Pi	inorganic phosphate
PI3K	phosphoinositide 3-kinase
PKC	protein kinase C
PLA2	phospholipase A2
PMSF	phenylmethylsulfonyl fluoride
ROS	reactive oxygen species
SDS	sodium dodecyl sulfate
Ser	serine
Thr	threonine
TMRE	tetramethylrhodamine, ethyl ester
TMRM	tetramethylrhodamine, methyl ester
TOF	time of flight
TPP	tetraphenyl phosphonium
TTC	2,3,5-triphenyltetrazolium chloride
Tyr	tyrosine
UCP	uncoupling protein
VDAC	voltage-dependent anion channel

www.manaraa.com

CHAPTER 1

Hypoxia-induced Damage to the Adult and Immature Brain: Molecular Mechanism of Oxidative Damage

1 Neuropathology of Reperfusion Injury

Brain ischemia/reperfusion results in extensive injury and is a substantial medical burden because of the ensuing morbidity and mortality. In adults, ischemic insults to the brain typically result from stroke (caused by either thrombotic occlusion or rupture of a blood vessel) or cardiac arrest while, in infants, cerebral ischemia is initiated by complications during labor and delivery, resulting in neonatal hypoxic-ischemic encephalopathy. In both cohorts, restoring blood flow and thus reestablishing nutrient and oxygen delivery to the ischemic brain will undoubtedly salvage neurons. However, reperfusion itself causes additional, substantial brain damage termed “reperfusion injury”. The impact of cerebral ischemia/reperfusion injury on patient mortality is sizable irrespective of age or etiology.

1.1 Stroke

Stroke is the third leading cause of death and disability among Americans [1]. Strokes are most commonly ischemic in origin, caused by vascular obstruction in the cerebral circulation. If diagnosed in a timely manner, ischemic stroke can be reversed by administration of thrombolytic agents or, alternatively, the obstruction can be physically removed. Neurons that lie distal to the obstructed vessel, relying exclusively on blood supply from this vessel, die from the prolonged complete ischemia. These neurons comprise the infarcted region of the brain that is termed the “ischemic core”. Such neurons never regain function upon restoration of blood flow, and are dead prior to any window of therapeutic intervention. Of greater clinical interest are the populations of neurons that die in a delayed manner after reperfusion is initiated. These

www.manaraa.com

neurons, surrounding the ischemic core - referred to as the “penumbra” - are in part perfused by collateral blood flow (i.e., are not fully reliant on blood flow from the obstructed vessel), and are therefore more resistant to ischemic damage. Although neurons of the penumbra do not succumb to the initial ischemia-induced cell death, they go on to die during reperfusion in a delayed manner via mechanisms that resemble an apoptotic pathway. The delay in death of these cells offers a window for therapeutic intervention, thus it is critical that treatment of the penumbra be considered prior to recanalization of the obstructed vessel.

1.2 Cardiac Arrest/Resuscitation

Another leading cause of brain ischemia/reperfusion injury is cardiac arrest followed by resuscitation. In contrast to a focal brain insult caused by stroke, cardiac arrest results in complete ischemia throughout the entire brain. The brain is an extremely sensitive organ, hence even short durations of global ischemia (beyond 10 minutes) can result in debilitating neurologic deficits [2]. This sensitivity to ischemia may result from reliance on oxidative phosphorylation (OxPhos) for energy production, a concept we will address in detail in subsequent sections.

Successful resuscitation can rapidly restore blood flow and oxygen delivery to the body, including the brain. While approximately 70,000 patients are resuscitated from cardiac arrest each year, only ~10-35% of resuscitated patients survive to hospital discharge; this excessive death is likely a result of the severe brain damage caused by cerebral ischemia [2-4]. Whereas stroke results in a cerebral infarct, resuscitation from cardiac arrest results in neuronal death in select cell populations that are most sensitive to ischemic injury. The most sensitive populations of neurons, the CA1 hippocampal neurons [5, 6], die during the first days of reperfusion [7, 8]. The specific biochemical

www.manaraa.com

events that result in delayed neuronal death continue to be elucidated; however, overwhelming evidence has identified reactive oxygen species (ROS) generation as a key damaging event that leads to death of neurons [9-12].

1.3 Neonatal Hypoxic-Ischemic Encephalopathy

Ischemic insults to the infant brain cause hypoxic-ischemic encephalopathy (HIE), which leads to long-term neurocognitive deficits including cerebral palsy and epilepsy [13]. With an occurrence of approximately 2-4 per 1000 full-term in-hospital deliveries, HIE is a serious medical concern. The consequences of HIE are more severe among low birth weight and premature newborns [14, 15]. Various antepartum causes of HIE have been identified including maternal hypotension and fetal growth restriction, yet, the most prevalent cause is prolapse or compression of the umbilical cord and placenta abruption [16-18]. There is extensive heterogeneity in neuropathology following HIE, primarily due to variation in the etiology and severity of the hypoxic/ischemic events [19]. However, as in the adult, reperfusion undoubtedly contributes significantly to the overall pathologic progression of HIE and thus is of therapeutic interest.

2. A Mitochondrial Perspective on Reperfusion Injury

Mitochondria have long been known to play a critical role in the pathogenesis of cerebral ischemia/reperfusion injury, via ROS generation, mitochondrial failure or dysfunction, and mitochondrial (type II) apoptosis. In fact, during brain ischemia/reperfusion evidence exists for the three above deleterious events occurring within the mitochondria (see [20, 21]). The goal of Chapter 1 is to present a hypothesis developed largely in the Sanderson and Hüttemann laboratories and propose a common link between the three above events in mitochondrial pathologies seen during

www.manaraa.com

stroke, cardiac arrest, and HIE. In Section 3 the hypothesis is extended to unify these three events into a *novel paradigm that positions OxPhos as a central linchpin in the initiation and execution of cell death caused by ischemia/reperfusion.* However, before presenting this model of reperfusion injury, it is critical that we discuss: 1) how the OxPhos system functions; 2) the mechanism by which OxPhos generates and controls the mitochondrial membrane potential ($\Delta\Psi_m$); 3) control of OxPhos by phosphorylation; and finally 4) the role of the $\Delta\Psi_m$ in ROS generation.

2.1 The Electron Transport Chain and Oxidative Phosphorylation

The mitochondrial electrochemical gradient or protonmotive force (Δp_m) is generated and utilized by the OxPhos system, composed of the electron transport chain (ETC) and ATP synthase. A primary function of the ETC is to execute the transfer of electrons to the final electron acceptor, O_2. The molecular machinery that comprise the ETC include two major sites for electron entry, complex I (NADH dehydrogenase), and complex II (succinate dehydrogenase). Electrons donated to either of these protein complexes are transferred to complex III (bc_1 complex) via the non-protein electron carrier ubiquinone. Electrons are transferred from complex III to complex IV (cytochrome *c* oxidase, CcO) via the electron carrier cytochrome *c*.

CcO catalyses the final, and proposed rate limiting step in electron transfer; the donation of electrons to O_2, allowing conversion of O_2 and H^+ to H_2O. The energy stored in the electrons is stepwise extracted by complexes I, III, and IV, which couple electron transfer along the ETC to pumping of H^+ across the inner mitochondrial membrane. This pumping of protons across the inner mitochondrial membrane constitutes the largest contributing force of the mitochondrial membrane potential ($\Delta\Psi_m$), representing the overall charge difference across the inner mitochondrial

www.manaraa.com

membrane (see Section 2.2). In addition, these chemical protons that are taken up from the matrix site contribute to the generation of Δp_m. Finally, Δp_m is utilized by ATP synthase (complex V), which drives the conversion of ADP and Pi to ATP (Figure 1-1). This process provides the vast majority (90%) of ATP in the brain under normal conditions.

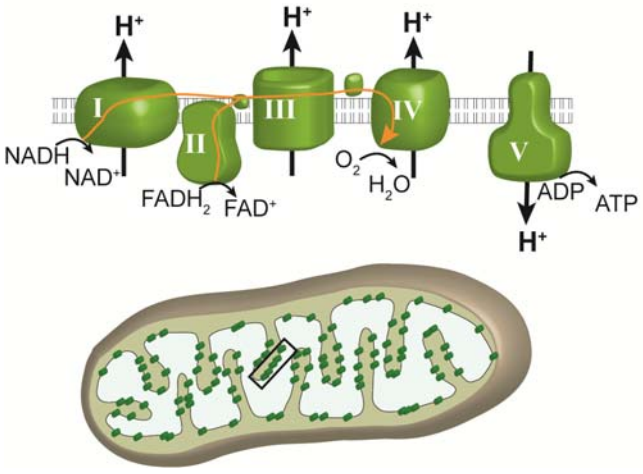

Figure 1-1: The Mitochondrial Electron Transport Chain and Oxidative Phosphorylation. The mitochondrial OxPhos components include: complex I (NADH dehydrogenase), complex II (succinate dehydrogenase complex III (bc1 complex), complex IV (cytochrome *c* oxidase, CcO) and complex V (ATP synthase). Electrons donated to either complex I or complex II are transferred to complex III via the non-protein electron carrier ubiquinone. From there, electrons are transferred to complex via cytochrome *c*. Electron flux through complexes I, III, and IV is couple to the pumping of H^+ across the inner mitochondrial membrane. The generation of a proton gradient across the inner mitochondrial membrane drives the conversion of ADP and Pi to ATP by complex IV.

Under non-stressed conditions, the transfer of electrons is a tightly regulated process. In fact, the vast majority of electrons that are donated to the ETC complete the entire reaction, culminating in reduction of O_2. However, a small percentage of electrons escape the ETC and can react with O_2 to form superoxide (O_2^-), a potent ROS. The specific sites of ROS generation along the ETC are complexes I and III. Although CcO (complex IV) produces several radical intermediates during the reduction of O_2, no electrons are allowed to escape; as a result CcO does not directly produce ROS. Under normal conditions, endogenous antioxidant systems are sufficient to scavenge the modest amounts of ROS generated and prevent cellular damage. However, under pathologic conditions antioxidants become overwhelmed or exhausted, allowing the unopposed and uncontrolled production of ROS and resultant ROS-initiated damage to

www.manaraa.com

cellular proteins, lipids, nucleic acids, and polysaccharides in an indiscriminate fashion [22-26]. To fully understand how ROS generation occurs and how this is controlled in a normal physiologic context, an appreciation of Δp_m and its primary component, the mitochondrial membrane potential $\Delta\Psi_m$, is required.

2.2 The Proton Motive Force and Mitochondrial Membrane Potential

Δp_m consists of two components, 1) an electrical constituent, simply referred to as the mitochondrial membrane potential $\Delta\Psi_m$, and 2) a chemical constituent, the pH difference across the inner mitochondrial membrane. Their relationship is defined as $\Delta p_m = \Delta\Psi_m - 59\ \Delta pH$. The electrical component, $\Delta\Psi_m$, represents the major portion of Δp_m in higher organisms.

In the traditional view, Δp_m (and $\Delta\Psi_m$) are determined by two basic components, substrate availability and respiratory control, which both act on the OxPhos complexes. The most basic means of mitochondrial OxPhos regulation is dependent on both availability of substrate (e.g., NADH, O_2, ADP, Pi) and its product, ATP. ATP and ADP are allosteric inhibitors and activators of CcO, respectively, and this control mechanism was proposed to adjust ETC activity to energy demand [27, 28]. Another major OxPhos regulatory mechanism is provided by Δp_m itself, and is called respiratory control, as was demonstrated in isolated mitochondria more than five decades ago [29]. Respiratory control is a mechanism by which Δp_m causes inhibition of the ETC proton pumps when the proton gradient exceeds a threshold value, preventing further proton pumping at high Δp_m levels. When ATP synthase converts ADP to ATP by utilizing the proton gradient, the reduction in Δp_m allows the proton pumps (i.e., complexes I, III, and IV) to resume electron transfer and to pump protons across the inner membrane. In resting mitochondria, when the vast majority of ADP has been converted into ATP, synthesis of

www.manaraa.com

ATP slows and Δp_m increases, inhibiting the proton pumps and thus mitochondrial respiration. This feedback mechanism pairs the ETC activity to $\Delta\Psi_m$ and serves to maintain $\Delta\Psi_m$ at physiologic levels of 80-140mV - a range in which ATP production is efficient and ROS generation is minimal.

Due to the difficulty of measuring absolute Δp_m in intact cells, most publications report $\Delta\Psi_m$ values, which constitute the majority of Δp_m. $\Delta\Psi_m$ can be monitored in living cells using voltage-dependent fluorescent probes such as the rhodamine dye TMRE (tetramethyl-rhodamine ethyl ester), and changes in fluorescence indicate relative changes in $\Delta\Psi_m$. Absolute $\Delta\Psi_m$ levels in millivolts can also be determined in isolated mitochondria by measuring the distribution of a membrane permeable cation such as tetraphenylphosphonium (TPP) with a TPP-sensitive electrode. In addition, absolute mV values for $\Delta\Psi_m$ can be determined in live cells by monitoring the redox states of the redox centers in bc_1 complex, thus allowing the precise calculation of $\Delta\Psi_m$ [30].

Since $\Delta\Psi_m$ could be measured readily, studies investigating $\Delta\Psi_m$ revealed an important difference of $\Delta\Psi_m$ levels observed in isolated mitochondria versus intact cells. In isolated mammalian mitochondria from liver and brain under state 4 conditions, $\Delta\Psi_m$ values were measured ≥150 mV, often exceeding 200 mV [31-38]. In contrast, the majority of studies performed in a more physiological context with a variety of intact mammalian cells or even intact organs showed lower $\Delta\Psi_m$ values in the range of 80 to 140 mV [39-43], with few studies reporting higher values between 140 – 161 mV [41, 43-47]. This discrepancy may be explained by differences in the regulation of OxPhos activity in higher organisms.

Respiratory control has traditionally been viewed as a key regulator of OxPhos. While this may be correct for OxPhos systems in bacteria, it appears that, in

www.manaraa.com

eukaryotes, additional regulatory mechanisms are in place. This idea is further supported by the fact that OxPhos enzymes are more complex in higher organisms. For example, CcO from bacteria contains 2 to 4 subunits whereas the mammalian enzyme is composed of 13 subunits per monomer and functions as a dimer, suggesting divergence with enhanced regulation [48, 49]. Although some differences between studies may be explained by different experimental conditions and the use of cells from different species and tissues, the emerging picture is that $\Delta\Psi_m$ values in isolated mitochondria are higher compared to those in intact cells. Explanations for this discrepancy, and the consequences of high $\Delta\Psi_m$ values, will be discussed in the next two sections.

2.3 OxPhos is Regulated by Reversible Phosphorylation

Higher $\Delta\Psi_m$ values observed in isolated mitochondria compared to intact cells suggest that the isolation procedure *per se* may induce modifications resulting in readings above the true physiologic range. Importantly, all mammalian OxPhos complexes are phosphorylated *in vivo* (reviewed in [50]), and we propose that these phosphorylations may be lost during traditional mitochondria isolation. A recent study analyzing mitochondrial morphology and function showed that the structure of isolated mitochondria is clearly different compared to the morphology found *in vivo* [51]. The authors further demonstrated a ~2-fold increase in CcO activity. Calcium is a buffer component used in some traditional protocols to purify mitochondria, and is a highly potent physiological second messenger and activator of mitochondrial function [52]. Calcium was shown to trigger dephosphorylation of most mitochondrial proteins [53], which may be mediated by calcium-dependent phosphatases as the Hüttemann laboratory and others have postulated [50, 54, 55]. A similar scenario likely takes place

www.manaraa.com

during ischemic stress, and this will be the focus of Section 3.

The Hüttemann and Sanderson groups have proposed that phosphorylation of OxPhos complexes is a critical regulatory mechanism in higher organisms to maintain healthy respiration rates and to prevent hyperpolarization of $\Delta\Psi_m$. Using novel methods of mitochondrial and OxPhos protein isolation that preserve protein phosphorylation sites [56], cytochrome *c* and CcO were found to be reversibly phosphorylated at multiple residues [57-59]. Moreover, phosphorylation of these proteins altered their electron transfer kinetics and affected allosteric regulation by ATP and ADP [57]. Phosphorylation of cytochrome *c* at either Tyr48 and Tyr97, caused reduced reaction rates with CcO, and is proposed to lead to normal physiologic electron transfer rates [60-62]. In all tissue types investigated, cytochrome *c* was normally present in both the phosphorylated and dephosphorylated state. Upon cellular stress (specifically, cerebral ischemia), the enzyme is rapidly dephosphorylated [63]. Interestingly, activation of cell signaling cascades that promote cell survival, such as insulin signaling [64], induce cytochrome *c* phosphorylation [63]. A residue on CcO was also identified that is reversibly phosphorylated (Tyr304), leading to inhibition of CcO [54]. Thus, dephosphorylation of CcO results in higher basal respiration.

The hypothesis was further expanded to propose that mitochondrial isolation procedures *or cellular stress, including ischemia,* alter the physiological phosphorylation state of the OxPhos complexes. This concept is supported by a study demonstrating hypoxia-induced changes in CcO phosphorylation in the heart [65]. In this model, phosphorylation of OxPhos proteins induce a healthy respiratory state where $\Delta\Psi_m$ values >140 mV inhibit further proton pumping, maintaining the 80-140 mV range where ROS production is minimal. In contrast, cellular stress *in vivo* and isolation of

www.manaraa.com

mitochondria *in vitro* causes changes and/or dephosphorylations of ETC complexes promoting maximal activity, and $\Delta\Psi_m$ only inhibits further proton pumping at very high $\Delta\Psi_m$ values; thus, in this state $\Delta\Psi_m$ is hyperpolarized. Support for the proposed model is provided by studies showing that phosphorylation of CcO and cytochrome *c*, as found *in vivo*, leads to partial inhibition and thus healthy cell respiration [54, 60, 66].

These studies demonstrate that stressful stimuli, such as ischemia, can result in changes in phosphorylation pattern of the OxPhos complexes, leading to ROS generation. Conversely, survival signaling promotes phosphorylation and 'controlled' electron transfer rates. Novel findings reported by Hüttemann et al. suggest a mechanism by which cell signaling cascades can regulate the overall basal activity rate of OxPhos [58]. Similar regulatory mechanisms may be discovered on other OxPhos complexes and functionally studied in the future. It is our hypothesis that mitochondria in intact cells under healthy conditions do not function at maximal capacity. This is reasonable because: 1) maximal rates of ATP synthesis by ATP synthase occur at $\Delta\Psi_m$=100-120 mV [67]; thus a further increase in $\Delta\Psi_m$ will not result in more ATP production, and 2) as discussed in Section 2.4, high $\Delta\Psi_m$ levels cause excessive ROS production.

2.4 Mitochondrial Membrane Potential Controls ROS Production

Under normal conditions, over 90% of oxygen is fully reduced to H_2O by CcO and only a small number of electrons 'leak' and lead to partial reduction of O_2 to superoxide. This ROS production takes place proximal to CcO, at complexes I and III, which release superoxide on the matrix and intermembrane space sides, respectively [68]. In complex I, two major sites of electron escape have been proposed, the flavoprotein component of electron entry into complex I [69] or the iron-sulfur cluster [70]. For complex III, ROS

www.manaraa.com

is produced by inhibition of electron transfer through the Q cycle [71]. Electron transfer from the cytochrome b_L heme to the b_H heme is inhibited at high $\Delta\Psi_m$, resulting in ubisemiquinone radical generation [72]. Ubisemiquinone generated near the intermembrane space then reduces O_2 to form superoxide.

Electron leak occurs at complex I, complex III, or both, depending on the type of stressful stimuli and cell type, however one common mechanism exists. It has been clearly demonstrated that ROS generation is dependent on $\Delta\Psi_m$. Specifically: 1) the maintenance of physiologically optimal $\Delta\Psi_m$ values, not exceeding 140 mV, prevents generation of ROS, while providing the full capability to produce ATP [67]; 2) although there are some conditions where ROS can be generated at low $\Delta\Psi_m$ levels through different mechanisms [73], it is generally accepted that pathophysiologic levels of ROS are produced at high $\Delta\Psi_m$ values; and 3) hyperpolarization of $\Delta\Psi_m$ (exceeding 140 mV) causes an *exponential* increase in ROS generation at both complexes I and III [71, 74-76]. It was also shown that the $\Delta\Psi_m$ component alone, and not ΔpH of the proton motive force, determines ROS production at complex III [77]. High $\Delta\Psi_m$ levels extend the half-life of reaction intermediates of electron transfer at sites capable of single electron reduction of O_2, thus allowing electron escape.

Once partially reduced to superoxide, this oxygen radical reacts with other molecules such as H_2O or H^+ to generate even more reactive species H_2O_2, HO_2, and OH. In addition, superoxide interacts with NO to form equally cytotoxic reactive nitrogen species. ROS generated in the mitochondria can freely cross mitochondrial membranes or exit via mitochondrial channels such as VDAC and, once released, can cause oxidative damage throughout the cell. Of note, ROS react quickly (half-life of nanoseconds to seconds) and irreversibly to damage cell constituents.

www.manaraa.com

An important question remains: why do mitochondria have an excess capacity to generate higher $\Delta\Psi_m$ levels with potentially disastrous consequences for the cell? One reason is that mitochondria must have the capacity to adapt to varying energy demands. However, a more plausible explanation is their involvement in mitochondrial (type II) apoptosis. Numerous studies have demonstrated that induction of apoptosis, which is accompanied by stress signaling and can involve: 1) excessive calcium release; 2) transient hyperpolarization of $\Delta\Psi_m$; and 3) a burst in the production of ROS, which has been proposed as a key signal for committing a cell to apoptosis (reviewed in [78]). Accordingly, in Sections 3 and 4, this mitochondrial-centric sequence of events leading to cellular demise is integrated into a model of ischemia/reperfusion injury, and the concept that modulation of $\Delta\Psi_m$ may provide a novel strategy to attenuate brain damage caused by ischemia/reperfusion is discussed.

3. Model of Ischemia/Reperfusion Injury

The preceding sections have provided insight regarding the role of mitochondria in cell death caused by brain ischemia/reperfusion, and are consistent with a hypothesis that focuses on changes of the phosphorylation state of mitochondrial OxPhos and subsequent $\Delta\Psi_m$ hyperpolarization (Figure 1-2). This model predicts that ischemic alterations of mitochondrial OxPhos primes the mitochondria for reperfusion-induced $\Delta\Psi_m$ hyperpolarization, an associated burst in mitochondrial ROS generation and loss of mitochondrial function, and subsequent delayed neuronal death. This progression is simplified into four main states that summarize the induction, progression, and execution of cell death during brain ischemia/reperfusion: 1) ischemic starvation; 2) reperfusion-induced hyperactivation; 3) mitochondrial dysfunction; and 4) delayed neuronal death (Figure 1-2).

www.manaraa.com

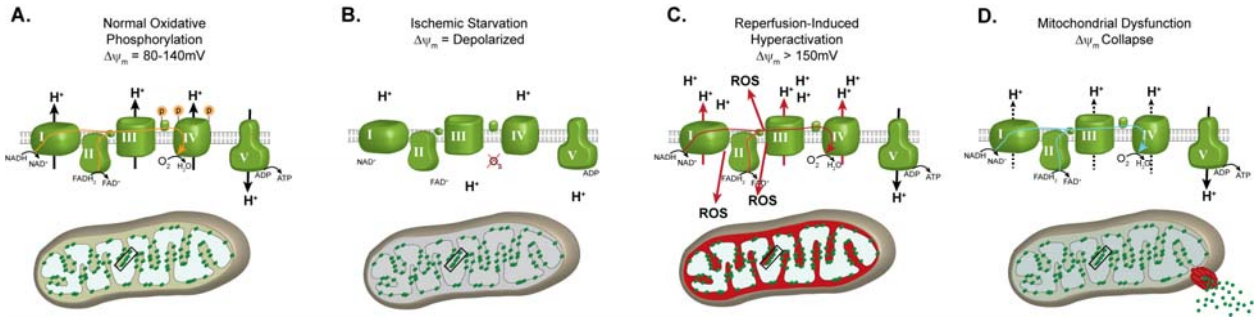

Figure 1-2: Progression of Ischemia/reperfusion Injury. (A) Under normal, non-stressed conditions, OxPhos components are phosphorylated (as illustrated for cytochrome *c* and CcO), promoting controlled electron transfer and maintaining the $\Delta\Psi_m$ in the 80-140mV range. This respiratory state is conducive to maximal ATP production and minimal ROS generation. **(B)** Ischemia induces a starvation state were the ETC cannot function due to lack of O_2. Dephosphorylation of OxPhos during ischemia renders these enzymes 'primed' for hyperactivity, however they cannot operate due to lack of the terminal substrate for respiration, O_2. **(C)** Reintroduction of O_2 with reperfusion initiates electron transfer, proton pumping and ATP synthesis. However, in this hyperactive (dephosphorylated) state, OxPhos hyperpolarizes the $\Delta\Psi_m$, causing an exponential increase in ROS generation at complexes I and/or III. **(D)** This burst in ROS can act as a signal for triggering apoptosis. In addition, damage caused by ROS induces a mitochondrial dysfunction state, with reduced electron transfer kinetics and reduced $\Delta\Psi_m$ levels, which results in energetic failure.

3.1 Ischemic-Starvation State: Ischemic OxPhos Dephosphorylation and the Role of Calcium

A unique feature of the brain is that it is almost exclusively dependent on oxidative phosphorylation to generate energy. Therefore it is necessary to have a constant supply of oxygen to sustain functionality. As discussed in previous sections, even under normal conditions, oxidative phosphorylation results in low-level production of ROS which immediately react with antioxidants and do not cause measurable cellular damage. Brain ischemia of even short durations (on the order of seconds-minutes) causes cessation of electron transport, as OxPhos cannot proceed under anoxic conditions. Electron stalling occurs when the rate of entry of electrons into complex I exceeds the rate of transit through the slowest step of the chain. During ischemia, limiting electron transit through complex IV causes upstream build-up of electrons at complexes I and III, thus leading to reduced ETC.

Without electron transfer and proton pumping across the inner mitochondrial

www.manaraa.com

membrane, the proton gradient quickly dissipates, thereby disabling Δp_m-driven ATP generation by ATP synthase. Ischemia has been found to cause depolarization of $\Delta\Psi_m$ following simulated ischemia *in vitro* [79] and *in vivo* during experimental stroke [80]. If ischemia persists, this eventually leads to ATP depletion and failure of all energy-dependent processes in the mitochondria and throughout the cell [81, 82]. Depletion of ATP during ischemia would not allow ATP synthase to maintain $\Delta\Psi_m$ by operating in the reverse mode via ATP hydrolysis, a mechanism that operates under certain conditions such as in some cancer cells [83], where it is driven by high ATP flux through glycolysis. Of particular importance to ischemia/reperfusion injury is the equilibration of Ca^{2+} across the plasma membrane and subsequent accumulation of Ca^{2+} in the cytosol. At high cytosolic [Ca^{2+}], mitochondria actively sequester Ca^{2+} to prevent pathologic increases in cytosolic [Ca^{2+}]. However, under the condition of ischemic depolarization, intramitochondrial [Ca^{2+}] increases to pathologic levels with evidence (by electron microscopy) of severe mitochondrial swelling and accompanying hallmarks of cell death [84].

Calcium is a potent activation signal for mitochondrial phosphatases. For example, the calcium-dependent Ser/Thr-phosphatase, calcineurin, can dephosphorylate proteins within the mitochondria [85]. Indeed, Ca^{2+} accumulation in the mitochondria induces dephosphorylation of multiple mitochondrial proteins [53, 57]. Moreover, it has been demonstrated that increased mitochondrial Ca^{2+} is a potent activation signal for mitochondrial respiration, leading to increased respiration and excessive ROS generation. This scenario is consistent with that suggested by McCormack and Denton who postulated that the main role of increased mitochondrial Ca^{2+} is to stimulate ATP production by activating enzymes involved in metabolism [86].

www.manaraa.com

The effect of Ca^{2+} on mitochondrial respiration does not appear to be due to a direct action of Ca^{2+} on ETC components, suggesting an intermediate step exists that could be activated by Ca^{2+}. The recent discoveries that dephosphorylation of CcO and cytochrome *c* lead to increased respiration rates provide a potential explanation for these early observations of the effect of Ca^{2+} on mitochondrial metabolism.

The proposed model represents a pathologic alteration as a response to an imbalance between energy availability and energy demand. Under conditions of mild hypoxia and inadequate ATP, energy demand would trigger Ca^{2+} signaling to increase mitochondrial respiration to increase ATP production in order to correct the deficiencies [87]. In contrast, under ischemic conditions, attempts to increase OxPhos activity in response to inadequate ATP are futile, as the final electron acceptor, O_2, is not present. One can speculate that this feed-forward mechanism caused by ischemia would eventually promote maximal activation of OxPhos. Indeed, others have questioned how a normal physiologic stimulus to increase energy production can lead to a pathologic increase in ROS generation [88]. When this process is viewed in the context of OxPhos dephosphorylation inducing subsequent hyperactivation of OxPhos, one can appreciate how ischemia could promote a mitochondrial state where substantial ROS can be generated upon reperfusion.

3.2 Reperfusion-Induced Hyperactivation State: OxPhos Hyperactivity, $\Delta\Psi_m$ Hyperpolarization, and ROS Generation

It is obvious that reperfusion of the ischemic brain is necessary for any attempt to salvage tissue. However, as previously discussed, reperfusion *per se* contributes significantly to tissue damage. From the perspective of ischemic mitochondria, reperfusion is necessary to restore the terminal substrate for OxPhos and nutrients to

www.manaraa.com

reinitiate cellular respiration. However, ischemia promotes a mitochondrial state that is conducive to hyperactive electron transfer upon reperfusion (Figure 1-3).

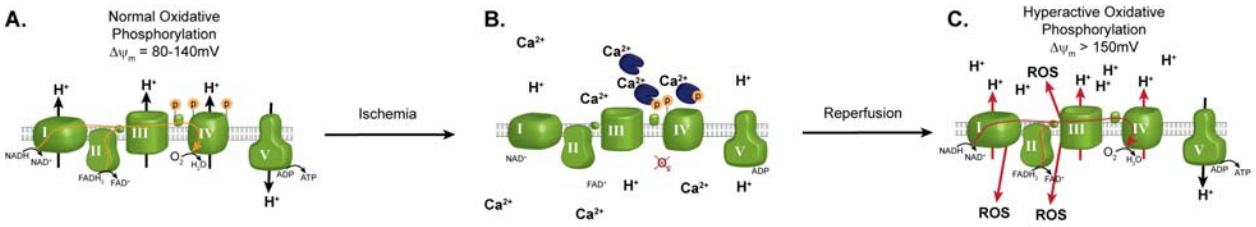

Figure 1-3: Mechanism of ROS generation during reperfusion. During extended brain ischemia, increased intramitochondrial Ca^{2+} activates phosphatases that dephosphorylate OxPhos components, as shown for cytochrome *c* and CcO in **B**. This promotes a state of OxPhos hyperactivity; however, because O_2 is absent electron transport cannot proceed. **(C)** Upon induction of reperfusion, OxPhos is allowed to operate at maximal activity, generating high $\Delta\Psi_m$ levels, which in turn promotes ROS generation.

According to the proposed model, ischemia evokes an increase in intermitochondrial Ca^{2+} [84, 89, 90], causing activation of mitochondrial phosphatases and dephosphorylation of OxPhos complexes [53], most notably cytochrome *c* and CcO (Figure 1-3). In addition to the effect on overall respiratory rate, dephosphorylation of CcO also leads to loss of allosteric inhibition by ATP [54, 55, 57, 60, 66]. Increased OxPhos activity alone could hyperpolarize $\Delta\Psi_m$ when reperfusion is initiated, and the loss of allosteric inhibition by ATP would further exacerbate this hyperpolarization. This effect could essentially 'reset' respiratory control to a higher level, leading to loss of feedback inhibition between OxPhos and $\Delta\Psi_m$ at the normal 120-140mV range. Under these conditions, hyperpolarization could be exacerbated and persist longer than otherwise possible without OxPhos dephosphorylation.

Enhanced and prolonged $\Delta\Psi_m$ hyperpolarization would have dramatic consequences. Liu et al. provided compelling evidence of the exponential nature of the relationship between ROS and $\Delta\Psi_m$ (reviewed in [71]). When $\Delta\Psi_m$ exceeds 140 mV the exponential nature becomes clear, resulting in a 70-90% increase in ROS generation with a modest 10 mV increase in $\Delta\Psi_m$ [71, 74]. Experimental measurements of $\Delta\Psi_m$ in

www.manaraa.com

this elevated range are plausible. In fact, as previously discussed, traditional mitochondrial isolation methods that do not take into account preservation of OxPhos phosphorylation often result in $\Delta\Psi_m$ above 200 mV [31-38]. These studies suggest that OxPhos dephosphorylation during ischemia would have profound consequences when reperfusion is initiated.

During the initial moments of reperfusion, OxPhos dephosphorylation would serve to promote rapid reestablishment of $\Delta\Psi_m$ and restoration of cellular ATP levels. Indeed, following reversal of brain ischemia, $\Delta\Psi_m$ is restored to contol levels within 1 minute, and cellular ATP levels are restored in less than 15 minutes [80]. However, if normal respiratory control mechanims are lost (including loss of alosteric inhibtion by ATP), $\Delta\Psi_m$ would surpass normal levels, resulting in pathologic $\Delta\Psi_m$ hyperpolarization. In this regard, Liu et al. demonstrated that rapid restoration of $\Delta\Psi_m$ is quickly followed by hyperpolarization of $\Delta\Psi_m$. A study in neuronal cell culture exposed to simulated ischemia/reperfusion injury demonstrated $\Delta\Psi_m$ hyperpolaization during the initial reperfusion stages [91]. Moreover, inhibition of $\Delta\Psi_m$ hyperpolarization by blocking complex I has been shown to prevent a stress-induced ROS burst and subsequent cell death [92]. Finally, this concept was extended by Starkov and Fiskum, who reported that mitochondria isolated from brain do, indeed, have an exponential relationship between $\Delta\Psi_m$ and ROS when assayed *in vitro* [74]. These studies suggest a pathologic condition where reperfusion results in $\Delta\Psi_m$ hyperpolarization which subsequently causes a significant ROS burst upon reperfusion.

Additional support for the OxPhos paradigm is provided by evidence demonstrating that the majority of ROS generation after brain ischemia occurs immediately upon reflow. For example, in the setting of global brain ischemia, ROS

www.manaraa.com

generation is most pronounced during the first 15 minutes of reperfusion [93]. Moreover, the predominant source of these ROS are the mitochondrial OxPhos complexes [11, 94, 95] and, in brain, escape of electrons from complex I appears to be responsible for most of the ROS produced [95-98].

As discussed in Section 2.4, the pivotal event that drives excessive electron escape and generation of ROS *in vivo* is $\Delta\Psi_m$ hyperpolarization. These data imply that interventions aimed at regulating $\Delta\Psi_m$ and preventing hyperpolarization may serve to attenuate ROS generation. Of particular interest is the dephosphorylation and hyperactivation of CcO, as CcO is the proposed rate-limiting step in OxPhos. Alternatively, direct targeting of $\Delta\Psi_m$ (for example, by using mitochondrial membrane uncoupling agents) may provide a feasible approach. However, before considering modulation of $\Delta\Psi_m$ as a therapeutic strategy (see Section 4), the cytotoxic consequences of ROS generation are reviewed.

3.3 Mitochondrial Dysfunction

Early studies into mitochondrial function following brain ischemia/reperfusion injury found that, by 30 minutes of reperfusion, mitochondrial respiration is dramatically decreased in cell populations that are destined to die [99, 100]. More recent reports have demonstrated that global brain ischemia/reperfusion leads to a reduction in complex I and CcO activity at later stages of reperfusion. This respiratory inhibition occurs within the first hour of reperfusion for CcO, and progresses more slowly for complex I (i.e., maximal inhibition by 24 hours of reperfusion [101]). This loss of respiratory function is accompanied by a reduction and eventual collapse of $\Delta\Psi_m$, leading to cell death. Interestingly, while traditional studies have demonstrated reduced OxPhos activity during later reperfusion, recent evidence by Chomova and colleagues

www.manaraa.com

has shown that, in the early minutes of reflow, OxPhos activities are increased over control levels [102]. These studies suggest that our current understanding of the responses of OxPhos to ischemia/reperfusion may be confounded by inappropriate mitochondrial extraction techniques employed in older reports.

Mitochondrial dysfunction during reperfusion has often been attributed to ROS-induced damage of mitochondrial components [70, 103]. The resulting OxPhos *hypo*-activation state (Figure 1-2) results in impaired proton pumping and reduced electron transfer kinetics. The mitochondrial switch from a hyperactive to dysfunctional hypoactive state has been attributed to oxidative damage of OxPhos complexes and/or oxidative damage to lipids important to OxPhos function. In support of this concept, direct oxidative damage of mitochondria has been shown to be involved in cellular damage following brain ischemia/reperfusion [104, 105].

A critical mitochondrial lipid target of ROS damage is cardiolipin. This is a unique phospholipid in that the majority of cardiolipin is found in the inner mitochondrial membrane where it is in tight association with OxPhos components. Cardiolipin plays a critical role in membrane insertion and function of cytochrome *c*, CcO, and other OxPhos complexes [106, 107], and there is growing evidence that cardiolipin plays a pivotal role in the regulation of mitochondrial bioenergetics [108, 109]. In fact, alterations in the structure and/or content of this phospholipid are responsible for mitochondrial dysfunction in a variety of pathological settings [110-113]. This concept is illustrated by the fact that disruption in the association of CcO with cardiolipin was accompanied by a ~50% reduction in activity of the enzyme [109]. Upon peroxidation, cardiolipin undergoes redistribution to the outer mitochondrial membrane [114] where it is required for release of apoptotic proteins from mitochondria into the cytosol [115].

www.manaraa.com

These effects could contribute to decreased CcO activity, impaired mitochondrial respiration, and mitochondrial failure.

Eventually, these pathologic alterations in mitochondrial function affect cellular functions and ultimately lead to cell death. Alterations in mitochondrial function are potent signals for induction of cell death cascades. Additionally, ROS have been implicated in directly activating cell death cascades. For example, under conditions of persistent impaired respiration, mitochondrial (type II) apoptosis is induced, with the release of apoptogenic factors (including cytochrome *c*) from the mitochondria purportedly serving as the final and irreversible trigger of neuronal death.

3.4 Delayed Neuronal Death: An Apoptotic-Like Phenotype

Cell death is often classified as apoptotic or necrotic, however, following cerebral ischemia/reperfusion, cell death often proceeds in a manner distinct from traditional apoptosis or necrosis. Morphologic and biochemical analysis indicate that both necrotic and apoptotic events occur simultaneously [84, 116], and evidence linking various pathways suggests that a degree of crosstalk exists that results in cell death occurring in a spectrum between apoptosis and necrosis [117]. The most common form of delayed, ischemia/reperfusion-induced neuronal cell death, and the type of insult that is the focus of the mechanism detailed in this Chapter, is characterized by an apoptotic-like phenotype. While all the specific characteristics of apoptosis may not be present, a key step – specifically, the release of apoptogenic factors from the mitochondria – appears critical in the initiation of cell death cascades [64, 118-120].

Many mechanisms have been proposed to explain the release of cytochrome *c* from mitochondria. Historically, it was hypothesized that mitochondria simply swell and burst, thereby releasing their contents into the cytosol. More recently, a large body of

www.manaraa.com

work has focused on the Bcl-2 family of proteins and their interactions as important regulators of mitochondrial permeability to cytochrome *c*. Of the Bcl-2 family, the primary candidates proposed to be involved in outer membrane permeabilization appear to be Bax and Bak; these proteins purportedly interact directly with mitochondria to promote the release of cytochrome *c* and other apoptogenic proteins (e.g. AIF, Smac/Diablo) [121, 122]. In addition, other investigators have focused on elucidating the formation of so-called 'permeability transition pores' that would facilitate cytochrome *c* release.

The caveat in all of these studies is that they are based on the premise that cytochrome *c* and other apoptogenic proteins are free within the mitochondria and, thus, could be released after pore formation or alterations in mitochondrial permeability. However, there is evidence that release of cytochrome *c* is a two-step process, involving 1) the release of proteins usually tethered to inner membrane by cardiolipin, combined with 2) pore formation [123]. Indeed, cytochrome *c* is among the proteins shown to be tethered to the inner mitochondrial membrane by cardiolipin [115, 124]. Exposure of mitochondria to ROS induces peroxidation followed by oxidation of cardiolipin, thereby releasing cytochrome *c* into the intermitochondrial space [123]. Subsequently, upon pore formation or alterations in permeability, the liberated cytochrome *c* is free to be released into the cytosol where it promotes formation of the apoptosome (a complex containing cytochrome *c*, caspase 9, and Apaf-1) that activates caspase 3. The apoptotic pathways activated following ischemia/reperfusion converge on caspase-3, the downstream cysteine protease, leading to the cleavage of hundreds of potential substrates within the brain and thus executing programmed cell death [125]. Indeed, activation of caspase-3, -8, and -9 have all been demonstrated to increase in

www.manaraa.com

the brain following ischemia/reperfusion [116, 126-128].

The aforementioned sequence of events identify multiple points of possible therapeutic intervention that, if appropriately targeted, could stop the progression of delayed neuronal cell death and thereby salvage tissue from ischemia/reperfusion injury. For example, intervening at the level of apoptosis (including prevention of mitochondrial outer membrane pore formation, cardiolipin peroxidation, or caspase activation), should have therapeutic benefits. However, attempts to prevent apoptotic cell death have revealed that multiple concurrent and redundant cell death pathways can be activated, making specific targeting of individual mediators or single pathways of apoptosis difficult or ineffective. Therefore, a focus on upstream targets (that is, molecular events that precede cytochrome *c* release) may yield a more logical and robust therapeutic approach to neuroprotection.

4. Intervention at OxPhos or $\Delta\Psi_m$ as a Potent Method of Neuroprotection

Targeting ROS to reduce or prevent brain ischemia/reperfusion injury is one potential strategy to target an early cell death signal. However, this method has been met with numerous clinical failures [129]. To understand this seemingly surprising lack of success, the traditional methodology for treatment of oxidative damage must be taken into consideration.

Current studies have shown that during reperfusion, ROS production exceeds the availability of endogenous antioxidants. Accordingly, previous attempts to design treatment modalities have focused on bolstering cellular antioxidant defenses to correct this imbalance. This strategy is primarily based on laboratory studies demonstrating robust neuroprotection in transgenic animals designed to overexpress endogenous mitochondrial antioxidants [104, 130-132]. These studies have provided substantial

www.manaraa.com

mechanistic insight into the pivotal role of ROS in cerebral ischemia/reperfusion injury. However, attempts to translate this concept and administer ROS scavengers as a clinical therapy have been futile [129]. This discrepancy could be explained by the multitude of potential pitfalls inherent in delivery of pharmacologic scavengers and antioxidants to the brain during reperfusion, including difficulties in delivery, rapid reaction kinetics due to the short half-life of ROS, multiple ROS generation sites, limited cellular drug uptake, and failure to cross the blood-brain barrier [133, 134]. Despite improvements in drug formulation and delivery, the efficacy of antioxidant strategies seen in animal studies has, nonetheless, not been realized in human trials [135-138].

As an alternative to this antioxidant approach, a cornerstone of the paradigm proposed by the Hüttemann and Sanderson labs is that interventions designed to *prevent* ROS generation (rather than scavenge ROS) will avoid many of the confounding issues associated with traditional scavenging techniques. In this regard, hyperpolarization of $\Delta\Psi_m$ is a critical regulatory step in multiple pathologies, including early reperfusion of multiple tissues [74, 80, 139]. Moreover, targeting of hyperpolarization has been shown to be a cytoprotective [91, 140, 141].

4.1 Uncoupling of Mitochondrial Membrane Potential

Cells express mitochondrial proteins, i.e., uncoupling proteins (UCPs) that allow H^+ to cross the inner mitochondrial membrane down the proton gradient. This bypasses ATP synthase and thus does not produce ATP by utilizing the proton gradient. The physiologic role of these proton channels is typically associated with heat generation. Recent studies have, however, found that UCPs have additional functions in the cell, including stabilizing the $\Delta\Psi_m$, thereby limiting electron escape and thus partial reduction of O_2 [75]. Interestingly, when UCPs were investigated in tissues where heat

www.manaraa.com

generation is not a primary function (such as brain), it was found that these proteins render the brain resistant to ischemia/reperfusion injury. For example, Haines et al. demonstrated that knockout of uncoupling protein 2 (UCP2) resulted in dramatically larger infarcts after stroke [142]. The converse was also true: overexpression of UCP2 was associated with a decrease in ischemia/reperfusion-induced brain damage, ROS generation, and induction of apoptosis after stroke [143]. Finally, pivotal data from Teshima et al. demonstrated that increased expression of UCP2 prevented ROS-induced cell death by stabilizing $\Delta\Psi_m$ [144]. These findings suggest that uncoupling proteins may play an important role in mitochondria by stabilizing $\Delta\Psi_m$ to prevent hyperpolarization and ROS production under stress. As a result, these proteins may represent a potent target for therapeutic intervention.

In addition to the use of UCPs to stabilize the $\Delta\Psi_m$, exogenous chemicals that allow protons to cross the inner mitochondrial membrane have also been tested to prevent ischemia/reperfusion injury. Proton ionophores (agents that allow proton leak across the inner membrane), have been shown to be effective in multiple disease states. For example, mild mitochondrial membrane uncoupling reduced $\Delta\Psi_m$ hyperpolarization, prevented ROS, and reduced cell death in models of myocardial ischemia [141], traumatic brain injury [140], and peroxide-induced neuronal damage [92].

It is important to note that small concentrations of mitochondrial membrane uncoupling agents are profoundly protective whereas, in contrast, higher concentrations *exacerbate* cellular damage [145]. These studies are consistent with the proposed mechanism of ischemia/reperfusion injury discussed in this Chapter: mild membrane uncoupling will prevent the hyperpolarization of $\Delta\Psi_m$ during stressful conditions, while

www.manaraa.com

complete uncoupling would allow excessive proton escape across the inner membrane and result in an energetic crisis. This biphasic effect makes the use of these compounds potentially dangerous, as overdose of an uncoupling agent could dramatically compromise the ability to produce energy through OxPhos. These compounds would also need to be present in the mitochondria during the time window of $\Delta\Psi_m$ hyperpolarization. As the majority of studies suggest that this phenomenon occurs during the early seconds-minutes of reperfusion [93], delivery to tissue prior to reperfusion may pose a therapeutic barrier. However, as discussed in the following section, there are potential methods capable of attenuating $\Delta\Psi_m$ hyperpolarization that do not require pharmacologic delivery.

4.2 Ischemic Preconditioning

Ischemic preconditioning is a phenomenon in which transient resistance to an ischemic insult is conferred to a tissue following brief episodes of sub-lethal ischemia. To investigate the effect of ischemic preconditioning on $\Delta\Psi_m$, Liu and Murphy utilized a customized laser scanning confocal microscope together with $\Delta\Psi_m$-specific fluorescent probes for real-time analysis of $\Delta\Psi_m$ in a mouse model of stroke [80]. The authors found that hyperpolarization of $\Delta\Psi_m$ was evident immediately following reflow, and that application ischemic preconditioning prevented $\Delta\Psi_m$ hyperpolarization and dramatically reduced the extent of neurologic injury.

Of specific interest is the mechanism by which preconditioning can prevent $\Delta\Psi_m$ hyperpolarization at the onset of reperfusion. Dave et al. demonstrated that brief episodes of antecedent preconditioning ischemia triggered the activation of PKCε and upregulated mitochondrial survival signaling [146]. Preconditioning applied prior to global brain ischemia provided multiple beneficial effects to the mitochondria, including

www.manaraa.com

phosphorylation of multiple OxPhos complexes, reduction of ROS generation, preservation of mitochondrial respiration during late reperfusion (the mitochondrial dysfunction phase) – events that culminated in decreased cytochrome *c* release, the putative trigger for apoptosis [146]. One could postulate that stimulation of cell signaling pathways that enhance phosphorylation of OxPhos complexes and limit cytochrome *c* release could promote controlled respiration and stabilize $\Delta\Psi_m$. Alternatively, a sub-lethal ischemic event could induce OxPhos dephosphorylation on a small scale, generate small amounts of ROS, and thereby stimulate survival signaling responsible for maintaining phosphorylation. If the activation of these kinases were increased during the subsequent 'lethal' ischemic event, this could provide protection from $\Delta\Psi_m$ hyperpolarization and ROS generation. In addition, preconditioning could induce the expression of UCPs, thereby maintaining lower basal $\Delta\Psi_m$ levels and limiting hyperpolarization. Indeed, Liu et al. demonstrated that preconditioning does increase UCP2 expression in brain [147]. However, whether this increase in expression in UCP2 contributes to preconditioning-induced neuroprotection – and, the precise mechanism by which preconditioning modulates $\Delta\Psi_m$ – remains unknown.

4.3 Induction of Cell Signaling to Induce OxPhos Phosphorylation

Our current knowledge of cytochrome *c* and CcO suggests that the primary role of the phosphorylation sites discovered to date is to sustain controlled respiratory rates and thereby prevent $\Delta\Psi_m$ hyperpolarization and ROS generation [54, 60, 62, 63, 66, 148]. Accordingly, it stands to reason that induction of cell signaling cascades that induce phosphorylation or prevent dephosphorylation would provide some protective effect. Evidence from our group has shown that phosphorylation of cytochrome *c* at Tyr97 can be induced by insulin [63]. Moreover, insulin treatment was found to be

www.manaraa.com

neuroprotective in a model of global brain ischemia/reperfusion by preventing the release of cytochrome *c* from mitochondria and inducing the upregulation of PI3K and other cell survival signaling cascades [64, 149]. Whether phosphorylation of cytochrome *c* at Tyr97 contributes to insulin-induced neuroprotection by stabilizing $\Delta\Psi_m$ is a focus of current investigation by our group.

5. Conclusions

This Chapter presents an overarching, mitochondrial-centric hypothesis describing the mechanisms that underlie mitochondrial ROS generation and cell death induced by reperfusion of ischemic brain tissue. There is evidence to support this injury mechanism in multiple scenarios of cerebral ischemia/reperfusion injury including stroke, cardiac arrest followed by resuscitation, and hypoxic-ischemic damage. The crux of the hypothesis is that $\Delta\Psi_m$ hyperpolarization and the ensuing ROS burst cause oxidative damage that precedes apoptosis in these pathologies. Specifically, our group has proposed that: 1) ischemia induces dephosphorylation of OxPhos, thereby 2) priming the mitochondria for hyperactive electron transport and $\Delta\Psi_m$ hyperpolarization upon reperfusion, 3) initiating a burst of ROS which overwhelms endogenous antioxidant systems that 4), damages cellular components and 5) culminates in the initiation of apoptotic-like cell death cascades. Most notably, this paradigm suggests that stabilization of $\Delta\Psi_m$ during early reperfusion provides a novel strategy to limit ROS generation and attenuate ischemia/reperfusion induced to brain.

www.manaraa.com

CHAPTER 2

Infrared Light Therapy: a Novel Approach for Attenuating Cerebral Reperfusion Injury

1. Rationale

Cerebral ischemia, sustained after cardiac arrest, is a major cause of death and disability [1-4]. Similarly, hypoxic events encountered during the perinatal period leading to pathologic decreases in fetal cerebral oxygen availability are detrimental resulting in neonatal hypoxic-ischemic encephalopathy (HIE) [13-15]. The current and only established and approved treatment to limit tissue damage and improve outcome after cerebral ischemia is prompt restoration of blood flow to the ischemic areas [150]. However (and as discussed in Chapter 1), while timely reflow is essential for the salvage of ischemic neurons, reperfusion can promote ROS production and lead to significant, irreversible tissue damage as a result of resuscitation/reoxygentation [151].

Many pharmacologic approaches have aimed at attenuating reperfusion injury by ROS scavenging. However, this approach has yielded inconsistent results in experimental models and failed to translate into the clinic, possibly due to the intrinsic impediments in delivering adequate concentrations of scavengers to the subcellular site(s) within the crucial early seconds-minutes of reflow. Thus, ongoing work in our laboratory, and by others, seeks to address this unmet need for an effective treatment of reperfusion injury by examining the preclinical efficacy of a novel non-invasive method. This approach relies on the ability of infrared light (IRL) to attenuate the production of (rather than scavenging) ROS. Unlike ultraviolet and visual light, IRL within the range of 700-1000nm readily passes through biological tissues [152, 153] and thus circumvents a major inherent limitation of traditional pharmacology-based treatments of reperfusion injury.

www.manaraa.com

1.1 Non-invasive Modulation of Mitochondrial Activity Using Infrared Light

The concept that IRL may be of therapeutic benefit and modulate mitochondrial function is not entirely new, and previous studies have used IRL as a non-invasive therapy [154-160]. Efficacy has been demonstrated for multiple pathologies including nerve regeneration, peripheral neuropathy, stroke, and wound healing [156, 161-169]; however, results have often been contradictory likely owing to an incomplete understanding of IRL's mechanism of action[170-173].

Work form the Hüttemann laboratory has demonstrated that IRL can directly modulate cytochrome *c* oxidase (CcO) activity *in vitro* (Figure 2-1). This tendency for photobiomodulation of CcO activity likely stems from the various heme and copper centers within the enzyme. These centers are influenced by light and directly modulate enzyme function [174, 175]. IRL with a wavelength of 750nm or 950nm was found to attenuate CcO activity, and this effect is exaggerated when used in combination. In contrast, IRL with a wavelength of 810nm modestly increased CcO activity, consistent with previous reports examining this IRL wavelength [156, 160].

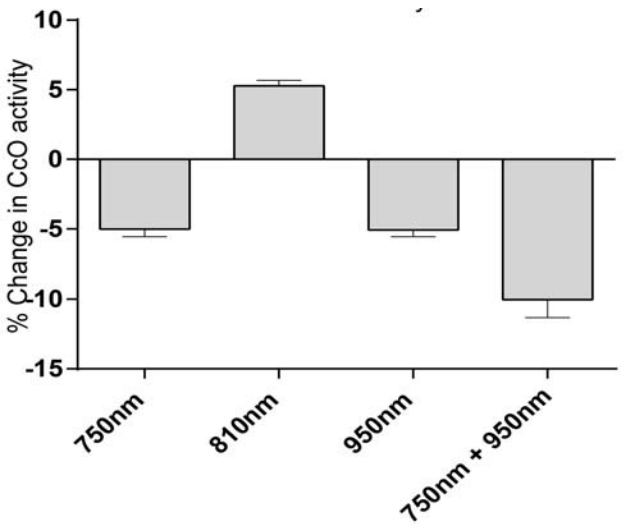

Figure 2-1: Modulation of CcO activity by IRL. Percent change in the activity of isolated bovine CcO in response to various IRL wavelengths alone or in combination is shown Data were obtained after 3 min of irradiation using low-power diodes and activities were normalized to non-irradiated samples. IRL with a wavelength of 750nm or 950nm attenuated CcO activity, and this effect is exaggerated when used in combination. In contrast, IRL with a wavelength of 810nm modestly increased CcO activity. From Hüttemann.

www.manaraa.com

1.2 IRL Attenuates Mitochondrial Membrane Hyperpolarization and ROS Production *In Vitro*

As introduced in Chapter 1 of this dissertation, the primary function of the mitochondrial ETC is to execute the transfer of electrons to O_2. CcO catalyses the last, and proposed rate limiting step in this process; the donation of electrons to O_2, allowing conversion of O_2 and H^+ to H_2O. Electron flux through complexes I, III, and IV, is coupled to pumping of H^+ across the inner mitochondrial membrane. This pumping of protons across the inner mitochondrial membrane constitutes the largest contributing force of the mitochondrial membrane potential ($\Delta\Psi_m$), which represents the overall charge difference across the inner mitochondrial membrane. During reperfusion, increases in $\Delta\Psi_m$ are believed to contribute to the generation of mitochondrial ROS. Thus, modulation of CcO activity via irradiation with IRL may provide a direct means of controlling $\Delta\Psi_m$ (and in turn ROS production) non-invasively.

Using live-cell imaging in conjunction with the $\Delta\Psi_m$-specific fluorescent probe, TMRM, the Sanderson laboratory observed that IRL irradiation with a wavelength of 950nm decreased $\Delta\Psi_m$ which quickly returned to control levels when irradiation was discontinued (Figure 2-2 A). These results indirectly demonstrate the ability the 950 nm wavelength of IRL to suppress ETC electron flux via its inhibitory effect on CcO. Using this *in vitro* method, the effect of IRL irradiation during simulated ischemia-reperfusion was examined using immortalized hippocampal neurons (HT22 cells). These studies confirmed the hyperpolarization of $\Delta\Psi_m$ during the first 30 minutes of reoxygenation, as predicted by the mechanism proposed above (Figure 2-2 B). Furthermore, as shown in Figure 2-2 B, IRL irradiation with a wavelength of 950nm during the initial 30 minutes of reoxygentaion attenuated mitochondrial membrane hyperpolarization.

www.manaraa.com

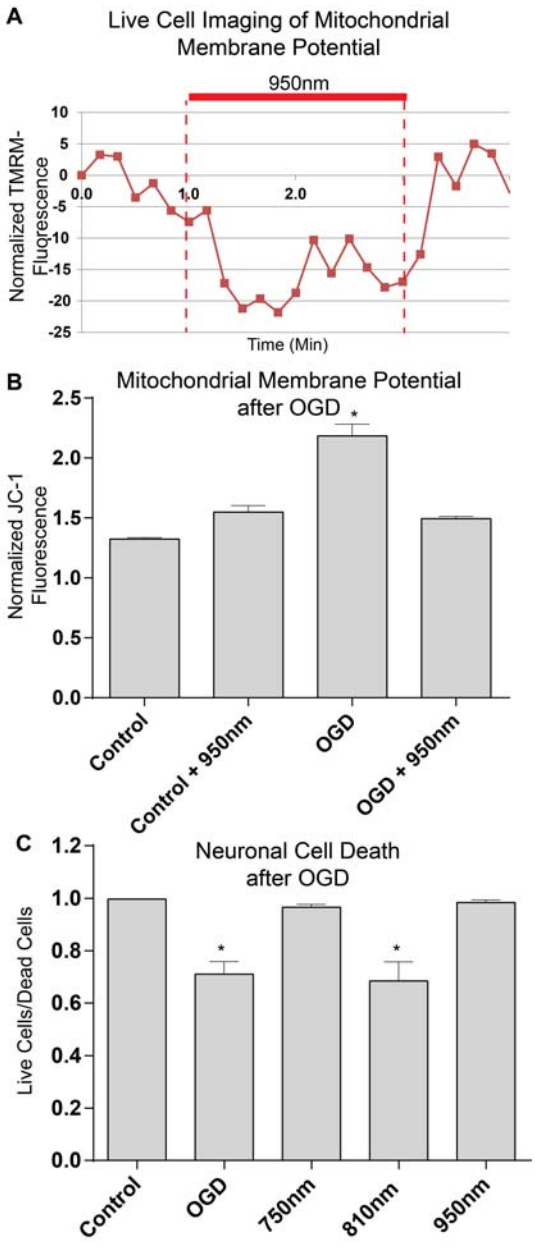

Figure 2-2: IRL modulates mitochondrial membrane potential and attenuates reperfusion injury in cultured neurons. A. Mitochondrial membrane potential ($\Delta\Psi_m$) during irradiation with 950 nm IRL (live cells using TMRM). **B.** $\Delta\Psi_m$ during the initial 30 min of reoxygenation after 1h O_2/glucose deprivation [OGD]. Expressed data are mean values of 96 live cell fluorescent well readings *p < 0.05. **C.** % viability in control cells, cells subjected OGD, and cells exposed to OGD treated with either excitatory IRL (810 nm) or inhibitory IRL (750 nm and 950 nm) wavelengths; *p < 0.05). From Sanderson.

The effect of IRL on neuronal cell survival after exposure to simulated ischemia-reperfusion was examined. Cells were irradiated with IRL via fiber-optic light guides for the initial hour of reoxygenation and cell death was quantified using a Live/Dead cell viability assay 24 hours later. A reduction in cell death was observed by irradiation with inhibitory IRL wavelength (750 nm and 950 nm) while the excitatory IRL wavelength (810 nm) was not protective (Figure 2-2 C). These insights into the effect of IRL during simulated ischemia-reperfusion *in* vitro have laid the foundation for subsequent *in vivo* efficacy testing. Accordingly, focus was directed to examining the preclinical efficacy of IRL using a rat model of adult global brain ischemia.

1.3 IRL Therapy Initiated at the Onset of Reperfusion Attenuates CA1 Hippocampal Damage Resulting from Global Brain Ischemia

Initial examination of the neuroprotective effect of IRL was evaluated in a rat

www.manaraa.com

model of adult global brain ischemia resulting from bilateral carotid-occlusion with hypotension [64, 176-180]. This model leads neuronal injury occurring specifically in populations of hippocampal CA1 neurons [5, 6]. These neurons are particularly sensitive to ischemic insults, and a near-complete loss is observed at 3-7 days after reperfusion [7, 8]. Consistent with previously published results using the rat model of adult global brain ischemia, untreated control animals had a significant loss of CA1 hippocampal neurons 14 days after the injury (Figure 2-3). Representative images of the CA1 hippocampus are shown in Figure 2-3 A, together with triple label immunofluorescence to detect neurons, microglia, and astrocytes. Quantification of

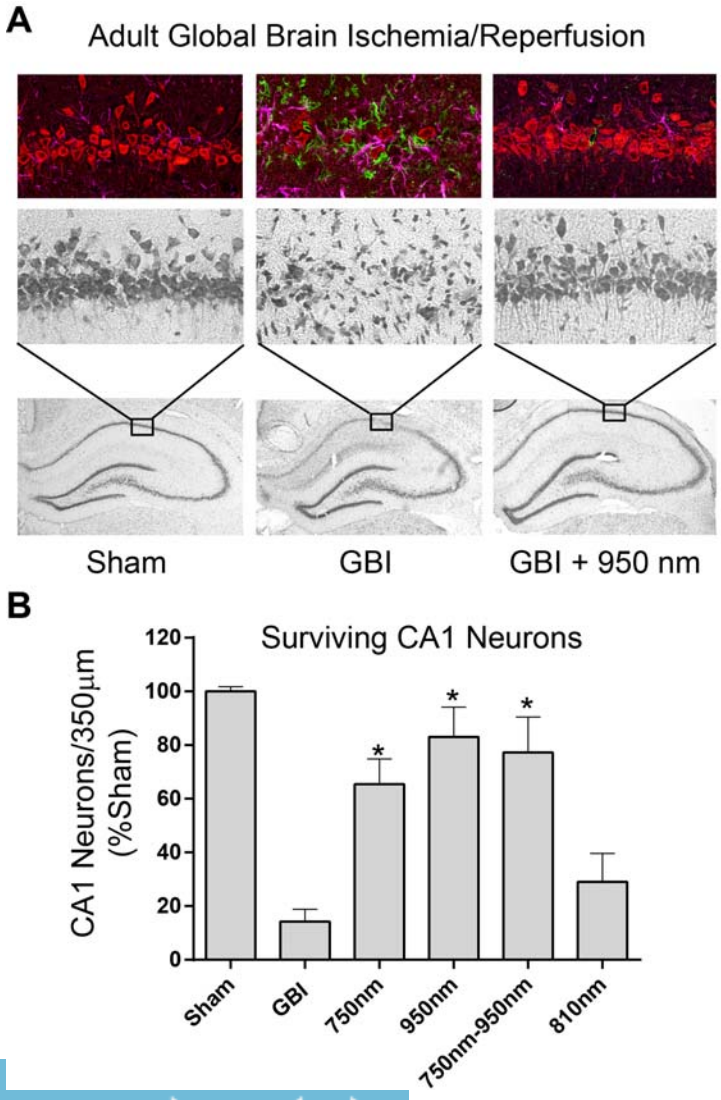

Figure 2-3: IRL treatment following global brain ischemia attenuates CA1 hippocampal damage. A. CA1 hippocampal damage. [bottom row] 10X image of Cresyl violet stained hippocampus [middle row] 40X magnification of CA1 hippocampus, [top row] Triple-label immuno-fluorescence for NeuN (red-neuron marker), Iba-1 (green-microglia marker) and GFAP (astrocyte marker). [Left column] Sham-operated animal (Sham), [center column] 8 min global brain ischemia followed by 14 days reperfusion (GBI), [right column] GBI plus IRL treatment (GBI + 950nm). **B.** Neuron counts in the CA1 hippocampus (mean ± SEM; *p<0.05 compared to GBI).

www.manaraa.com

CA1 neuronal counts is shown in Figure 2-3 B. When normalized to sham-operated animals, global brain ischemia resulted in an 88% reduction in viable pyramidal neurons and treatment with the CcO-inhibitory IRL wavelengths, 750 nm and 950 nm, significantly attenuated CA1 hippocampal damage when used alone or in combination (Figure 2-3 B). Treatment with the CcO-excitatory IRL wavelength, 810 nm, had no effect on neuronal viability in CA1 hippocampus.

1.4 IRL Therapy Initiated at the Onset of Reperfusion Attenuates Mitochondrial ROS Production within CA1 Hippocampal Neurons

In vitro studies outlined above suggest that inhibition of CcO at the onset of reperfusion is associated with a favorable reduction in mitochondrial ROS generation. To detect mitochondrial ROS generation *in* vivo, the fluorescent indicator MitoSOX® was used [181]. This colorless probe accumulates in mitochondria and becomes a red fluorescent dye upon oxidation. By pretreating rats with MitoSOX® via intra-carotid artery infusion, the effect of IRL treatment on mitochondrial ROS production was examined microscopically. As shown in Figure 2-4, inhibition of CcO at the onset of reperfusion was successful in attenuating mitochondrial ROS production following

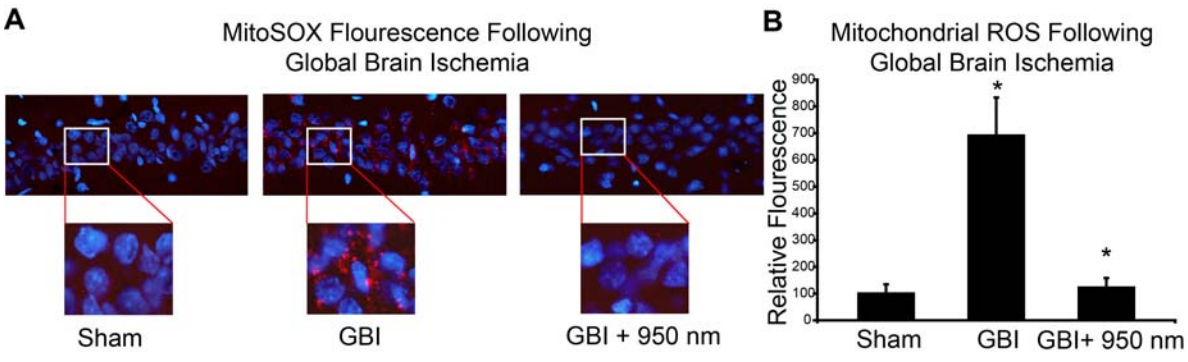

Figure 2-4: IRL treatment following global brain ischemia attenuates mitochondrial ROS production. A. MitoSOX® fluorescence. Nuclei labeled with DAPI and mitochondrial ROS was detected with MitoSOX® (red). [Left] sham-operated (Sham), [Center] global brain ischemia followed by 30 min of reperfusion (GBI), [Right] GBI plus IRL treatment (GBI + 950 nm). (**B)** Quantitation of red fluorescence (*p<0.05).

www.manaraa.com

cerebral ischemia. Representative fluorescent image overlays of the CA1 hippocampus are shown in Figure 2-4A. Consistent with the proposed model, global brain ischemia resulted in a significant increase in MitoSOX® fluorescence 30 minutes after the onset of reperfusion when compared to non-ischemic sham-operated controls (Figure 2-4 B). Furthermore, this increase in MitoSOX® fluorescence was abrogated in rats treated with IRL (Figure 2-4 B).

2. Summary

These data provide evidence of the preclinical efficacy of IRL therapy for the treatment of cerebral ischemia-reperfusion injury. As demonstrated above, treatment with IRL wavelengths shown to reversibly inhibit CcO activity and reduce ΔΨm *in vitro* significantly improved neuronal survival after global brain ischemia in the adult rat. Furthermore, IRL treatment initiated at the onset or reperfusion attenuated mitochondrial ROS production. Thus, this therapeutic approach may provide a novel means of neuroprotection by circumventing mitochondrial ROS-mediated cell death signaling cascades.

www.manaraa.com

CHAPTER 3

Modeling Neonatal Hypoxic-ischemic Encephalopathy in the Rat

1. Rationale

The robust neuroprotective effect of IRL observed in the rat model of adult global brain ischemia described in Chapter 2 demonstrates the utility of this treatment for cerebral reperfusion injury. The specific goal of my dissertation is to investigate the preclinical efficacy of this novel treatment paradigm in the neonatal brain – in particular,brain injuries arising as a result of perinatal asphyxia. As a critical first step in achieving this goal, Chapter 3 focuses on the evaluation and refinement of a widely used animal model of neonatal hypoxic-ischemic encephalopathy (HIE).

The 'Vannucci' rodent model of neonatal HIE is a commonly employed method based on the Levine preparation where unilateral common carotid artery ligation followed by systemic hypoxia produces significant injury in the hypoxic-ischemic cerebral hemisphere [182]. During the insult, systemic blood pressure and cerebral blood flow ipsilateral to the carotid artery ligation are reduced by approximately 25%. Although patency of the cerebral vasculature is maintained, hypoxia-ischemia results in a drastic reduction in cerebral perfusion owing to a loss in the cerebral vessel's autoregulatory capacity. Accordingly, ipsilateral to the carotid artery ligation cerebral perfusion pressure is reduced in proportion to the decline in systemic blood pressure.

Following cerebral hypoxia-ischemia in the neonatal rat, morphologic and biochemical analysis indicate that both necrotic and apoptotic events occur which ultimately contribute to cerebral infarction [84, 116]. The apoptotic pathways activated following hypoxia-ischemia likely converge on caspase-3, which can be activated by the intrinsic or extrinsic pathways [183]. As described in Chapter 1, under normal

www.manaraa.com

conditions mitochondrial ROS formation and degradation is balanced, thus, maintaining overall mitochondrial redox stability. During reperfusion following cerebral hypoxia-ischemia, mitochondrial ROS accumulate which likely promote apoptotic cell death by enhancing mitochondrial permeability leading to intrinsic activation of caspase-3 following the release of mitochondrial cytochrome *c* [184, 185].

The specific biochemical phenotype and extent of cerebral infarction in the rodent model of neonatal HIE varies considerably from laboratory to laboratory and across animal strains. Factors such as litter size and rodent diet, as well as the temperature during and duration of the hypoxic insult contribute significantly to the model's severity and variability. The broad distribution in the extent of brain injury produced by this model mandates that a large number of animal subjects be enrolled in a given study in order to demonstrate any treatment effect [186]. The experiments described here sought to evaluate the utility of the Vannucci rat model of neonatal HIE for use in our laboratory by (i) establishing the extent of variability in cerebral injury achieved, as well as (ii) determining the major biochemical conduit activated to promote cell death.

2. Materials and Methods

2.1 Reagents

All reagents were purchased from Sigma Aldrich (St. Louis, MO) unless indicated otherwise.

2.2 Animal Surgical Procedure.

Rat pups of either sex were subjected to HIE on postnatal day 7 using the Vannucci model [182]. Briefly, pregnant female Sprague-Dawley rats were maintained in a temperature controlled environment with a 12hr light/dark cycle and were allowed to give birth naturally. To minimize variability in feeding and body weight, litters were size-

www.manaraa.com

culled to 10 pups on postnatal day 3. On postnatal day 7, pups were anesthetized using isoflurane (3.0% induction, 1.5% maintenance) in NO_2/O_2 (1:1). The right common carotid artery was exposed via ventral midline neck incision and cut between double ligatures of 6.0 silk suture. Sham operated control animals underwent the entire surgical procedure except for ligation and cutting of the carotid artery. The incision was sutured and pups were returned to their dam to recover for 60min before being exposed to systemic hypoxia.

2.3 Hypoxia Chamber Design

Precise control of temperature during the hypoxic insult is critical in order to minimize the variability in cerebral injury. Accordingly, a custom designed hypoxia apparatus was constructed. The inner chamber consisted of a 2.8 L polypropylene container with an airtight removable lid equipped with a rubber gasket into which inlet and exhaust ports were drilled. The inlet was connected to the glass barb of a 1L Büchner flask via a 30 cm long section of polyethelene tubing with an internal diameter of 0.635 cm. The inner chamber and Büchner flask were submerged in a Plexiglas outer water bath (21L) with dimension of 33.3 cm (w) x 25.4 cm (h) x 45.7 cm (l) and a wall thickness of 6mm (VWR Internationa; Radnor, PA). During the insult, gas containing 8% O_2 (balanced in N_2) was bubbled through the Büchner flask containing 750 mL of dH_2O which served to warm and humidify the gas. Gas flow was maintained at a rate of 2.5 L/min. Inner chamber air temperature was monitored using a t-type digital thermocouple (Physitemp Instruments; Clifton, NJ). The outer water bath temperature was controlled by a submerged circulating water heater (Thermo Scientific; Waltham, MA) and the water temperature was set to 36.2^{o}C or 35.0^{o}C to achieve an inner chamber air temperature of 36.0±0.5^{o}C or 34.5±0.5^{o}C, respectively.

www.manaraa.com

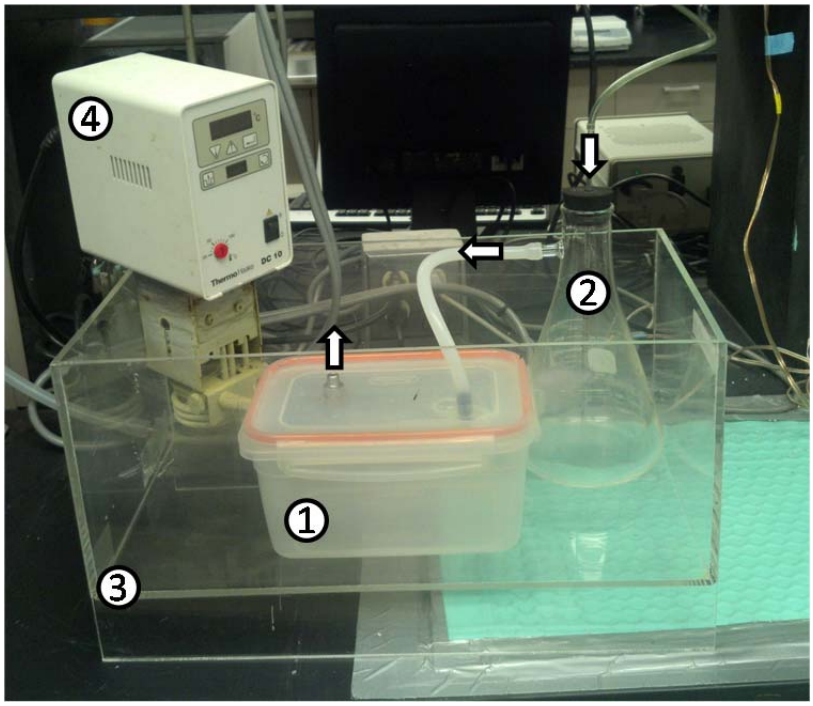

Figure 3-1: Custom designed hypoxia apparatus. The apparatus consists of an inner chamber (1), gas humidifier (2), water bath (3), and circulating water heater (4). Arrows indicate direction of gas flow.

2.4 Hypoxic Insult

After recovering from the carotid artery ligation surgery, pups were exposed to a constant flow of humidified 8.0% ± 0.1% oxygen balance in nitrogen (AirGas USA; Lansing, MI) in the custom-designed temperature-controlled chamber described above. The effect of hypoxia chamber temperature was evaluated by maintaining chamber air temperature at 34.5^{o}C or 36.0^{o}C and hypoxia was induced for 120 min or 180 min.

2.5 Infarct Volume Analysis

Forty-eight hours after the onset of reoxygenation, pups were euthanized via deep anesthesia with isoflurane. Brain tissue was perfused transcardially with ice-cold phosphate buffered saline, pH 7.4. Brains were removed and 1 mm coronal sections were cut using a vibratome (Campden Instruments; Lafayette, IN). Brain slices were immersed in 1% TTC in phosphate buffered saline, pH 7.4 and incubated at 37°C for 8 minutes [187]. Next, the slices were fixed in 4% paraformaldehyde overnight in the

www.manaraa.com

dark. Finally, TTC stained sections were scanned and (i) area of infarction (unstained area), (ii) area of the ipsilateral hemisphere, and (iii) area of the contralateral hemisphere were quantified using Quantity One ® software (Biorad). The percent infarcted area of each slice was determined by dividing the area of infarction (unstained area) by the area of the ipsilateral hemisphere of each slice and infarct volume was expressed as a percent of the ipsilateral hemisphere by summing the slices.

2.6 Subcellular Fractionation

To examine the effect of HIE on mitochondrial cytochrome *c* release and caspase 3 activation, subcellular fractions were obtained from injured and sham-operated control animals using differential centrifugation for subsequent analysis via western blot. At the indicated time points following the onset of reoxygenation, animals were transcardially perfused with ice-cold PBS and ipsilateral (hypoxia-ischemia) and contralateral (hypoxia-only) hemispheres were homogenized on ice in mitochondrial Isolation buffer (HEPES 25mM; pH7.7, Sucrose 250mM, KFl 10mM, Vanadate 1mM, EGTA 5mM, EGTA 2mM, PMSF 0.1mM). Following an initial centrifugation at 1000g for 10 min at 4^{o}C, the supernatant was centrifuged at 16,700g for 20min at 4^{o}C to isolate the crude mitochondrial fraction (pellet) and crude cytosolic fraction (supernatant). For sham-operated controls, animals were sacrificed 5 hours after the initial surgery (time-matched to 120 min reoxygenation).

2.7 Gel Electrophoresis and Immunoblotting

The protein concentration of mitochondrial and cytosolic fractions was determined using the method described by Bradford [188] and 50 µg of protein was loaded per lane and resolved via Tricine-SDS-PAGE as previously described [189]. Each gel was then transferred to a nitrocellulose membrane that was blocked with 5%

www.manaraa.com

nonfat dry milk in Tris-buffered saline containing 0.1% Tween 20. Membranes were incubated over night at 4°C with primary antibodies against cytochrome *c* (BD Biosciences, San Jose, CA), cleaved caspase 3, VDAC, and GAPDH (Cell Signaling Technology, Boston, MA). With the exception of anti-cleaved caspase 3, which was diluted 1:500, all primary antibodies were diluted 1:1000. Bands were visualized using horseradish peroxidase-conjugated secondary antibodies (Sigma-Aldrich, St Louis, MO) and the scanned and digitalized films were analyzed using Quantity One ® software (Biorad). Cytochrome *c* and cleaved caspase 3 immunoreactivity was normalized to GAPDH or VDAC to control for protein loading of cytosolic and mitochondrial fractions, respectively.

2.8 Statistical Analysis

All data were compared using Prism software (Graphpad; La Jolla, CA) and are presented as means ± SEM. Following a test for normality, a one-way ANOVA was performed and pairwise post-hoc comparisons were made using the Newman–Keuls method. Infarct data from the 120 min hypoxic insult were not normally distributed; accordingly, these data were analyzed using a Kruskal–Wallis one-way ANOVA by ranks followed by Dunn's post hoc analysis. P-values < 0.05 were considered statistically significant.

3. Results

3.1 Hypoxia-ischemia Results in Substantial Infarction

In accordance with previous studies employing this model, rat pups subjected to unilateral common carotid artery ligation followed by exposure to 8% oxygen sustained cerebral infarction ipsilateral to the carotid artery ligation (Figure 3-2). Importantly, neither hypoxia nor carotid ligation alone produced a discernible injury. Infarction

www.manaraa.com

primarily affects the cerebral cortex, however involvement of subcortical regions including the basal ganglia was also observed.

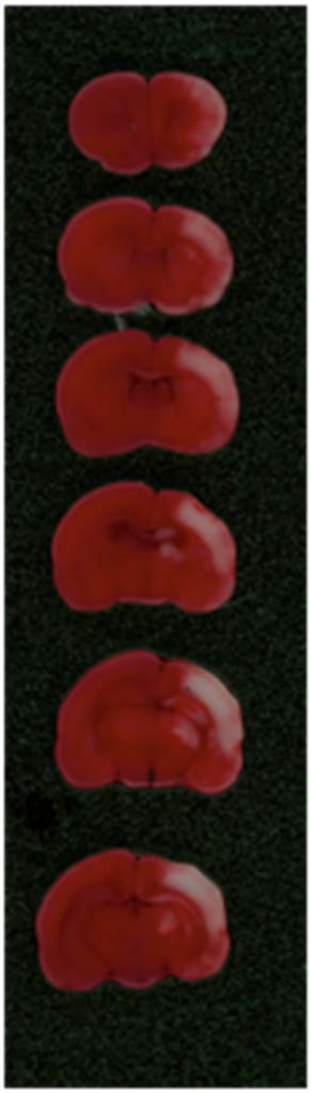

Figure 3-2: Hypoxia-ischemia results in substantial cerebral infarction. Postnatal day 7 rats were subjected to unilateral carotid artery ligation and subsequent hypoxia (8% O_2 balanced in N_2; 180 min). Forty-eight hours after the onset of reperfusion, brains were sliced and stained with TTC (Red= viable tissue; unstained regions = infarction)

3.2 Temperature and Duration of the Hypoxic Insult Influence Mortality and Infarct Severity in the Neonatal Rat Model of HIE

A total of 54 and 38 rat pups were enrolled to undergo 120 and 180 minutes of hypoxia at 36C, with an additional 43 and 56 animals subjected to hypoxia at 34.5C. Mortality following the shorter, 120 minute hypoxic insult was negligible ($\leq$3.7%), irrespective of temperature (Figure 3-3 A). However, in animals assigned to receive 180 minutes of hypoxia, mortality was greater in animals maintained at 36C versus

www.manaraa.com

34.5C (36.8% versus 3.6%; Figure 3-3-A).

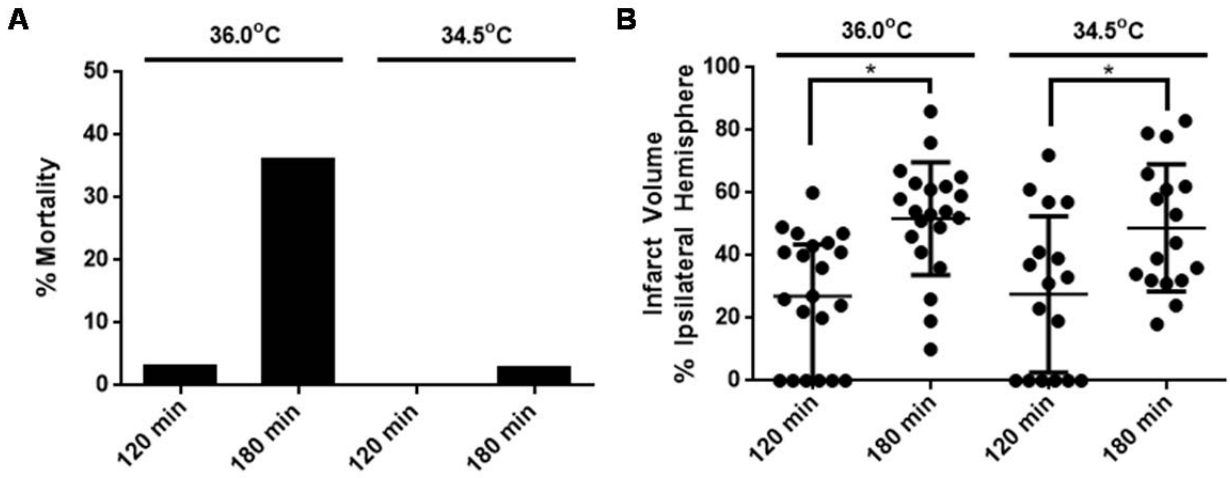

Figure 3-3. Temperature and duration of a hypoxic insult affect infarct volume and mortality. B. Infarct volume expressed as a percent of the ipsilateral hemisphere measured 48 hours after cerebral hypoxia-ischemia in the neonatal rat. Median infarct volume resulting from 180 minutes of hypoxia was significantly greater than that caused by 120 minutes at chamber temperatures of 36.0°C and 34.5°C (*P<0.05). Notably, chamber temperature had no significant effect on median infarct volume. **A.** Comparison of % mortality for 120 and 180 minute hypoxic insults at chamber temperatures of 36.0°C and 34.5°C.

Among survivors, ipsilateral median infarct volume resulting from 180 minutes of hypoxia was significantly greater than that caused by 120 minutes regardless whether the hypoxia chamber temperature was maintained at 36.0°C or 34.5°C (Figure 3-3 B). Importantly, and in contrast to results obtained with 120 minutes of hypoxia, all animals developed detectable (albeit variable) areas of infarction.

3.3 Cytosolic Accumulation of Cytochrome *c* is Associated with Increased Caspase 3 Activation during Early Reperfusion Following Cerebral Hypoxia-Ischemia in the Neonatal Rat

Cytosolic accumulation of cytochrome *c* leads to activation of caspase-3 via the intrinsic pathway resulting in apoptotic cell death. Accordingly, our next objective was to determine whether this pathway is activated in the neonatal rat brain following a 180 minute hypoxic insult at 34.5°C – the conditions identified in Section 4.2 to consistently

www.manaraa.com

yield infarction with minimal mortality. To address this issue, cytosolic fractions obtained from ipsilateral (hypoxic-ischemic) and contralateral (hypoxia-only) hemispheres were collected at the end of hypoxia-ischemia, as well as following 30 and 120 minutes of reoxygenation (n=4-5 replicates per time-point). Sham-operated animals time-matched to 120 min reoxygenation were used as controls (n=4). As shown in Figure 3-4, western blot analysis revealed a significant increase in cytochrome *c* accumulation within the cytosolic fraction following 120 minutes of reperfusion in the ipsilateral hemisphere (*P<0.05 versus sham). Importantly, increased cytosolic cytochrome *c* was not observed in the ipsilateral hemisphere at earlier time points of reperfusion, nor was increased cytosolic cytochrome *c* detected in the contralateral hemisphere.

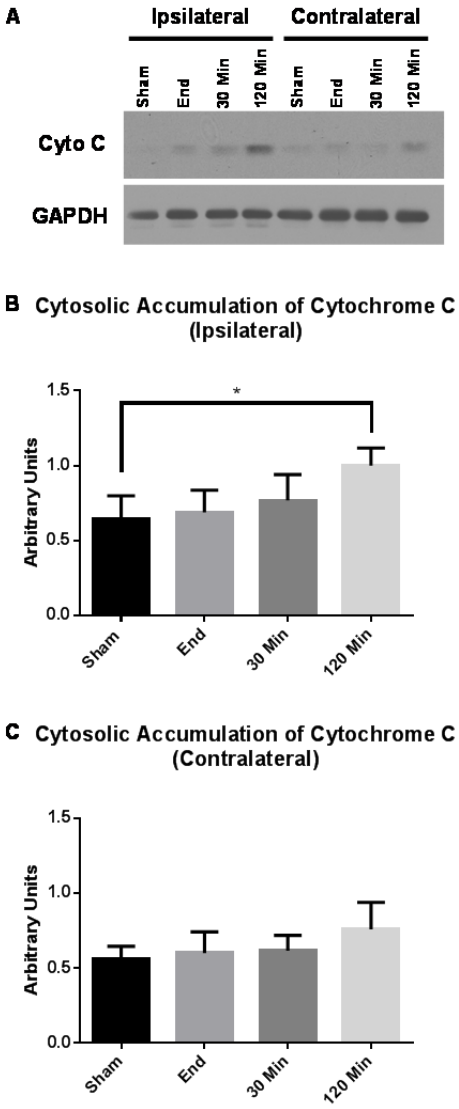

Figure 3-4: Cytosolic accumulation of cytochrome c following cerebral hypoxia-ischemia in the neonatal rat. A. Representative immunoblot for cytochrome *c* and GAPDH in the cytosol. Cytochrome c accumulation was normalized to GAPDH, and averaged data (mean ± SEM) are shown for sham-operated control, at the end of hypoxia-ischemia, as well as following 30 or 120 min of reperfusion from ipsilateral (**B**) and contralateral (**C**) hemispheres. (*P<0.05)

As shown in Figure 3-5 western blot analysis of the catalytic cleavage of caspase 3 indicates that this proapoptotic cysteine protease is activated acutely in the brain, following hypoxia-ischemia in the neonatal rat. Detection of cleaved caspase 3 within the cytosol of the ipsilateral hemisphere was possible as early as 30 minutes following the onset of reperfusion in two animals; and after 120 minutes of reperfusion all animals

www.manaraa.com

tested showed cleaved caspase 3 immunoreactivity confined to the ipsilateral hemisphere.

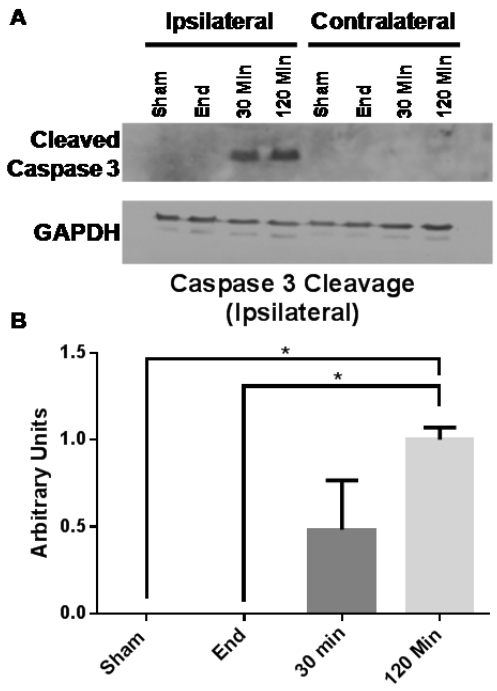

Figure 3-5: Activation of caspase 3 following cerebral hypoxia-ischemia in the neonatal rat. A. Representative immunoblot for cleaved caspase 3 (17kd) and GAPDH in the cytosol. **B.** Cleaved caspase 3 immunoreactivity was normalized to GAPDH, and averaged data (mean ± SEM) are shown for sham-operated control (Sham), at the end of hypoxia-ischemia (End), as well as following 30 or 120 min of reperfusion from the ipsilateral hemisphere. (*P<0.05)

4. Summary

Consistent with previously published literature, the extent of cerebral injury produced by this rodent model of HIE was variable. Hypoxia chamber temperature had an impact on mortality, but did not significantly change infarct volume with equal hypoxic duration. These findings demonstrate the critical importance of maintaining a suitable chamber temperature during the hypoxic insult when using this model. The duration of the hypoxic event also influenced both the *consistency* of developing cerebral infarction and *median infarct volume*, with larger infarcts observed with insults lasting 180 versus 120 minutes. While shorter hypoxic insults have been utilized in a small number of studies by other groups [84, 190], pilot studies using 60 and 90 minutes of hypoxia conducted using the chamber described above yielded no detectable infarct via TTC staining 48 hours after the insult.

www.manaraa.com

Although, the distribution of ipsilateral infarct volumes among animals subjected to either 120 or 180 minutes of hypoxia was broad, the longer hypoxic duration led to infarct detection in all animals. Accordingly, a hypoxic insult of 180 minutes in duration was chosen for use in examining mitochondrial permeability, cytosolic accumulation of cytochrome *c* and activation of caspase 3. To this end, hypoxia-ischemia, but not hypoxia alone, led to significant cytosolic accumulation of cytochrome *c* within 2 hours following the onset of reperfusion which was associated with caspase 3 activation. Consequently, using a hypoxic duration of 180 minutes and a chamber temperature of 34.5^{o}C, these findings suggest that the rat model of neonatal HIE causes mitochondrial permeability transition and ultimately leads to the induction of apoptosis which, presumably, contributes to the cerebral infarction observed.

www.manaraa.com

CHAPTER 4

Cardiolipin Oxidation and Hydrolysis in Neonatal HIE: Development and Application of a Novel Mass Spectrometry Method

1. Rationale

Cardiolipins (CL) [bis-(1,2-diaceyl-sn-glycero-3-phospho)-1'-3'-sn-glycerols] form a unique class of anionic phospholipid found nearly exclusively within the inner mitochondrial membrane in eukaryotic cells. CL influences a wider variety of fundamental functions including mitochondrial inner membrane curvature [191] and OxPhos supercomplex formation [192, 193]. Cleavage of CL by phospholipase A2 (PLA2) isoforms yields monolysocardiolipin (MLCL), which along with oxidized CL has been implicated in apoptotic signaling and cell death [107, 194].

In adult rat models of acute traumatic brain injury and cerebral ischemia-reperfusion, mitochondrial CL was observed to be selectively oxidized [195, 196]. Ongoing work by Kagan and collogues suggests that CL-oxidation occurs following the transfer of electrons directly from reduced cytochrome *c* and newly oxidized CL is hydrolyzed by calcium-independent PLA2 activity to form MLCL and oxidized free fatty acids [196, 197]. This chapter focuses on: i) the development of a novel mass spectrometry (MS) method for use in interrogating the integrity of mitochondrial CL; and ii) the application of this method to investigate the effect of cerebral hypoxia-ischemia on CL oxidation and hydrolysis using the neonatal rat model of HIE described in Chapter 3.

2. Traditional Mass Spectrometry for the Analysis of Phospholipids

Commonly, MS platforms used to study membrane phospholipids, including CL, are coupled to high-performance liquid chromatography and, more recently, to thin-layer chromatography [198]. While the enrichment effect of chromatographic separation is

www.manaraa.com

often necessary when lipids of extremely low abundance are the targets for analysis, these techniques require significant expertise and, importantly, introduce perturbations arising from the extraction and separation conditions used. Accordingly, ionization methods for use in MS that enable lipid extraction to be avoided altogether are emerging for use in lipid research [199-207].

Membrane phospholipids, including CL, are typically studied in the negative ion mode using electrospray ionization (ESI) and matrix-assisted laser desorption/ionization (MALDI)-MS. MALDI produces predominantly singly charged $[M-H]^-$ CL ions, whereas ESI readily generates abundant doubly charged $[M-2H]^{2-}$ CL ions. ESI and MALDI are considered to be *'soft'* ionization methods, and MALDI is particularly important for membrane lipid research applications because of its ability to ionize phospholipid species directly from intact biological membranes and tissues without prior lipid extraction [205]. Conversely, ESI is invaluable in lipidomics applications because of its ease of coupling with liquid chromatography [208] and its multiple charging which enhances the utility of ion mobility spectroscopy (IMS) and MS/MS applications.

Recently, alternative *'soft'* ionization processes have been discovered for use in MS that combine strengths of both ESI and MALDI. Specifically, desorption-ESI (DESI) and laserspray ionization (LSI) readily generate multiply charged lipid ions and have been successfully used analyze phospholipids directly from the surface of tissue slices without lipid extraction [199, 209]. While substantial progress has been made using these novel *'soft'* ionization methods in platforms for lipid research, their reliance on high-tech lasers or electrospray sources necessitates a reasonably high degree of skill for successful implementation. Conversely, matrix-assisted ionization (MAI) is a recently described *'soft'* ionization method capable of generating multiply charged ions

www.manaraa.com

[210-212]. The production of gas-phase ions is achieved through MAI matrix sublimation upon exposure of the matrix/analyte crystalline solid to the vacuum, inherent to mass spectrometers [212]. Owing to the sublimation-driven mechanism underlying ion formation by MAI, there is no need for external energy input in the form of laser ablation, electrospray voltages, or heat [212].

Within the last decade, ion mobility spectrometry (IMS)-MS has become an important analytical method in lipid research with IMS providing an additional dimension of gas-phase separation, analogous to liquid chromatography. For complex lipid mixtures like those found in the biological membranes, IMS-MS yields two-dimensional separation in a timescale of a few milliseconds [213, 214]. Unlike high performance liquid chromatography or thin layer chromatography, IMS provides real-time gas-phase separation as ions travel through an ion-mobility cell, allowing lipid classes and subclasses to be separated based on radial acyl chain length, degree of unsaturation and head group variance [206, 207, 214]. Both ESI and MALDI have been successfully coupled to IMS for lipid analysis; however, ionization methods that readily generate multiply charged ions are more ideally suited for use in multidimensional IMS-MS applications [213]. Additionally, given that IMS separation occurs in the gas-phase following ionization, its use is amenable to research applications focused on studying lipids from intact membranes where liquid-phase chromatography is unachievable.

The experiments described here, conducted in collaboration with Sarah Trimpin, PhD (Department of Chemistry), sought to evaluate the use of MAI-IMS-MS as a method for the characterization of CL species directly from intact mitochondrial membranes. The success of this work is largely due to the recent discovery of a novel MAI matrix, 1,2-dicyanobenzene (DCB). Using DCB, the Trimpin laboratory has

www.manaraa.com

achieved MAI-MS sensitivities as low as 5 fmol with purchased cardiolipin standards which is far superior to the sensitivities observed using the well-studied MAI matrix, 3-Nitrobenzonitrile (3-NBN).

3. Technical Development of the MAI-IMS-MS Method

3.1 Materials and Methods

3.1.1 Reagents

All reagents were purchased from Sigma Aldrich (St. Louis, MO) unless indicated otherwise.

3.1.2 Mitochondrial Isolation

Technical development of the MAI-IMS-MS method development and characterization of the MS spectra was performed using mitochondria isolated from naïve (nonischemic) heart, liver and brain of female retired breeder Sprague Dawley rats. Briefly, tissue was homogenized on ice in mitochondrial Isolation buffer (Hepes 25mM; pH7.7, Sucrose 250mM, EGTA 5mM, EGTA 5mM). Following an initial centrifugation at 1000g for 10 min at 4^{o}C, the supernatant was centrifuged at 16,700g for 20min at 4^{o}C to isolate the crude mitochondrial fraction (pellet). Mitochondria were diluted to a protein concentration of 1mg•mL^{-1} in 20:80 H_2O:EtOH containing 0.1% NH_4OH.

3.1.3 Matrix Assisted Ionization – Ion Mobility Spectrometry – Mass Spectrometry

The MAI matrix DCB (Alfa Aesar; Ward Hill, MA) was dissolved in acetonitrile (5mg in 50µL) and mixed with enriched mitochondrial samples (1:1,v/v). Immediately prior to analysis, the solution containing matrix and mitochondria was drawn into a pipet tip in 1µL aliquots and allowed to crystallize at the end of the tip. As previously described [210-212], samples were introduced directly into the vacuum of the mass

www.manaraa.com

spectrometer by placing the pipet tip against the skimmer cone inlet. Mass spectra were obtained using a Waters SYNAPT G2 quadrupole-TOF and ion mobility spectrometry was performed with N_2 as the ion mobility gas.

3.2 Results

3.2.1 Multidimensional MAI-IMS-MS Analysis of Mitochondrial Cardiolipin

The MAI matrix DCB performed well in the presence of mitochondrial isolation buffer with minimal chemical background, and no appreciable effect on ion abundance, charge state or ion adduction was observed in the negative mode. Figure 4-1c shows a two-dimensional plot of ion mobility drift time vs. mass-to-charge (*m/z*) ratio obtained from rat brain mitochondria via MAI-IMS-MS. Molecular ions fall along two clearly

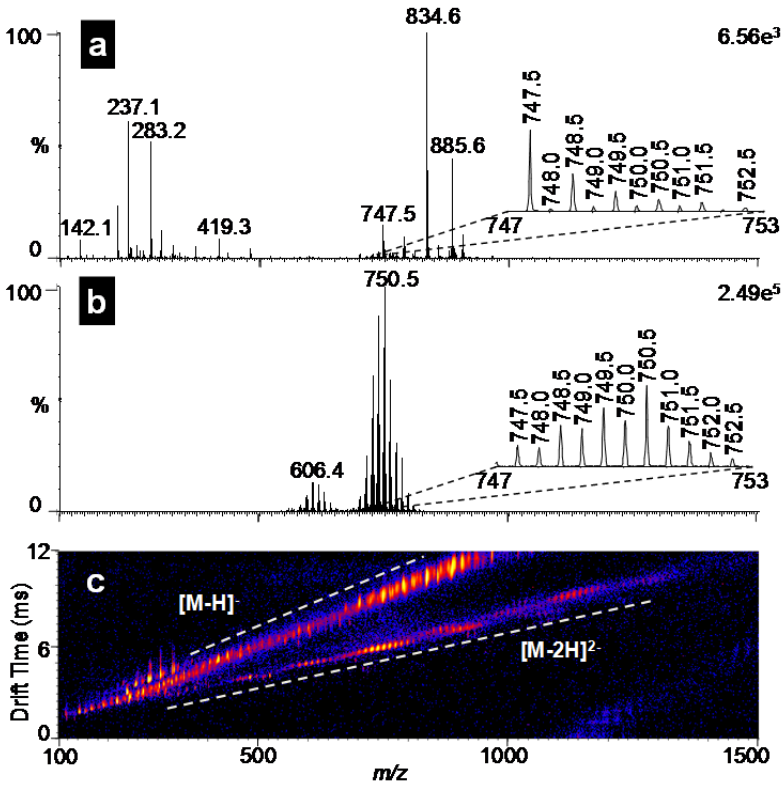

Figure 4-1: MAI-IMS-MS of rat brain mitochondria. Mass spectra of **a)** rat brain mitochondria and **b)** doubly charged $[M-2H]^{2-}$ MLCL and CL species extracted using IMS drift time. **c)** Two-dimensional plot of IMS drift time vs. *m/z*. Multidimensional IMS-MS analysis enables doubly charged $[M-2H]^{2-}$ and singly charged $[M-H]^-$ ions to be cleanly separated. The zoomed spectra highlight the extensive isotopic overlapping of doubly charged $[M-2H]^{2-}$ and singly charged $[M-H]^-$ ions which is eliminated through the use of IMS drift time deconvolution.

discerned trend lines determined by charge state where singly charged $[M-H]^-$ ions have longer drift times compared to doubly charged $[M-2H]^{2-}$ ions. As seen in Figure 4-1a, the mass spectra obtained from rat brain mitochondria is complex, and significant

www.manaraa.com

overlapping of singly charged $[M-H]^-$ phospholipid ions with the doubly charged $[M-2H]^{2-}$ CL ions occurs between *m/z* 650-850. Deconvolution using IMS drift time enables the mass spectrum of the doubly charged $[M-2H]^{2-}$ monolysocardiolipin (MLCL) and CL ions to be easily extracted (Figure 4-1b) from the two-dimensional plot.

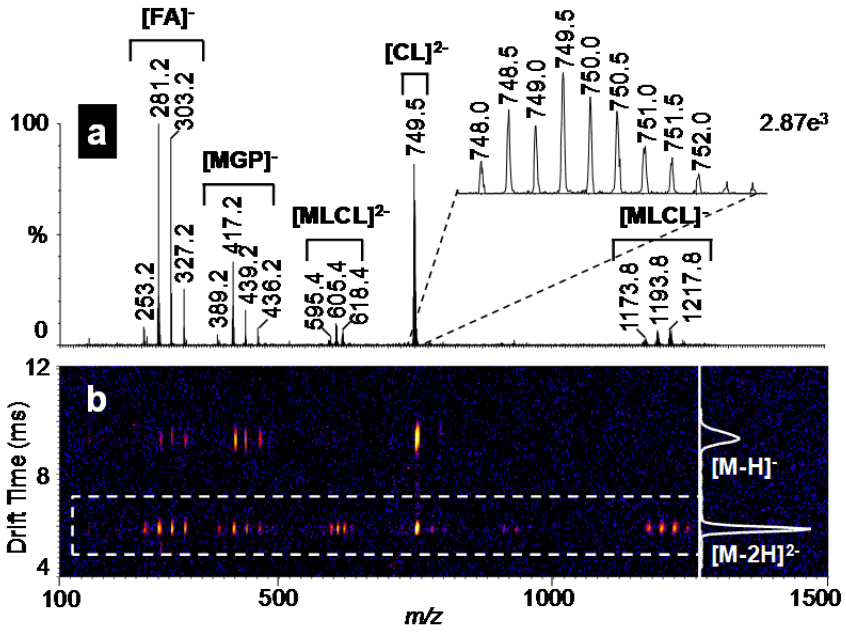

Figure 4-2: MAI-IMS-MS/MS characterization of cardiolipin species from brain mitochondria. a) MAI-IMS-MS/MS spectra of the doubly charged $[M-2H]^{2-}$ CL precursor ion at *m/z* 749.5 from rat brain mitochondria. Fatty acid fragment ions ($[FA]^-$) at *m/z* 253.2, 281.2, 303.2 and 327.2 correspond to palmitoleic (C16:1), oleic (C18:1), arachidonic (C20:4) and docosahexaenoic (C22:6) acids, respectively. Monoacylglycerol phosphate ($[MGP]^-$) fragment ions are observed at *m/z* 389.2, 417.2, 439.2, and 436.2. Doubly charged $[M-2H]^{2-}$ triacyl-monolyso-cardiolipin fragment ions ($[MLCL]^{2-}$) formed from the neural loss of a ketene, and singly charged $[M-2H]^-$ triacyl-monolyso-cardiolipin fragment ions ($[MLCL]^-$) are also observed. **b)** Two-dimensional plot of IMS drift time vs. m/z showing two precursor ions at *m/z* 749.5 with distinct IMS drift times were selected in the quadrupole and subjected to CID fragmentation. Using IMS drift time, fragment ions originating from the doubly charged $[M-2H]^{2-}$ CL precursor ion with a drift time of 5.86 milliseconds (white box) are cleanly separated from those originating from the singly charged $[M-H]^-$ precursor ion with a drift time of 9.26 milliseconds.

As anticipated, gas phase lipid ions generated during MAI matrix sublimation yield ESI-like fragmentation spectra during tandem MS using collision-induced dissociation (CID). The fragmentation spectra of tetra-linoleoyl-cardiolipin (Avanti Polar Lipids; Alabaster, AL) obtained using MAI-, ESI- and MALDI-MS/MS were compared (data not shown). Independent of the ionization method used, characteristic monoacylglycerol phosphate, diacylglycerol phosphate, and fatty acid fragment ions

www.manaraa.com

were observed. Additionally, the doubly charged $[M-2H]^{2-}$ CL precursor ions generated by MAI and ESI, yielded a doubly charged $[M-2H]^{2-}$ triacyl-monolyso-cardiolipin fragment ion resulting from the neutral loss of a ketene.

MAI-IMS-MS/MS characterization of CL species from mitochondrial samples is achieved using IMS drift time as an additional dimension by which precursor ions selected in the quadrupole can be isolated. Figure 4-2 shows the MAI-IMS-MS/MS fragmentation spectrum generated during CID fragmentation of the doubly charged $[M-2H]^{2-}$ CL precursor ion at *m/z* 749.5 of rat brain mitochondria. As observed in the 2-dimensional plot, two ions with distinct IMS drift times were selected in the quadrupole at *m/z* 749.5. Using IMS drift time, fragment ions origination from the doubly charged $[M-2H]^{2-}$ CL precursor ion with a drift time of 5.86 milliseconds are cleanly separated from those origination from the singly charged $[M-H]^{-}$ precursor ion with a drift time of 9.26 milliseconds.

Another noteworthy utility of IMS-MS is the rapid means of determining relative abundance ratios using the drift time peak area. Consequently, the relative ratio of any two lipid classes or subclasses, separated in the two-dimensional plot, can be easily determined. Figures 4-3, 4-4 and 4-5 show the mass spectra of the major CL species observed in rat heart, liver and brain mitochondria, respectively. The various acyl-groupings of CL are clustered based on the overall carbon content of their four acyl chains. The relative contribution of each acyl-grouping to the total CL pool was determined using drift time. To do this, the drift time peak area for each acyl-grouping was divided by the total CL peak area. These data are compared in Table 4-1.

In accordance with previously published results using traditional MS platforms [215, 216], the diversity of mitochondrial CL species detected using MAI-IMS-MS was

www.manaraa.com

tissue- dependent. The major CL species observed in the heart and liver were composed of four 18-carbon acyl-chains. In the heart mitochondria this accounted for 81.3% of the total CL pool and was exclusively tetra-linoleoyl-cardiolipin (723.5 *m/z; CL72:8)*. In the liver mitochondria both tetra-linoleoyl-cardiolipin (723.5 *m/z; CL72:8)* as well as tri-linoleoyl-mono-oleoyl-cardiolipin (724.5 *m/z*; CL72:7) were detected which together comprised 53.1% of the total CL pool. The CL profile of brain mitochondria contained more CL species than either the heart or liver mitochondria, and many of the brain CL species were comprised of long acyl chains including arachidonic (C20:4) and docosahexaenoic (C22:6) acids.

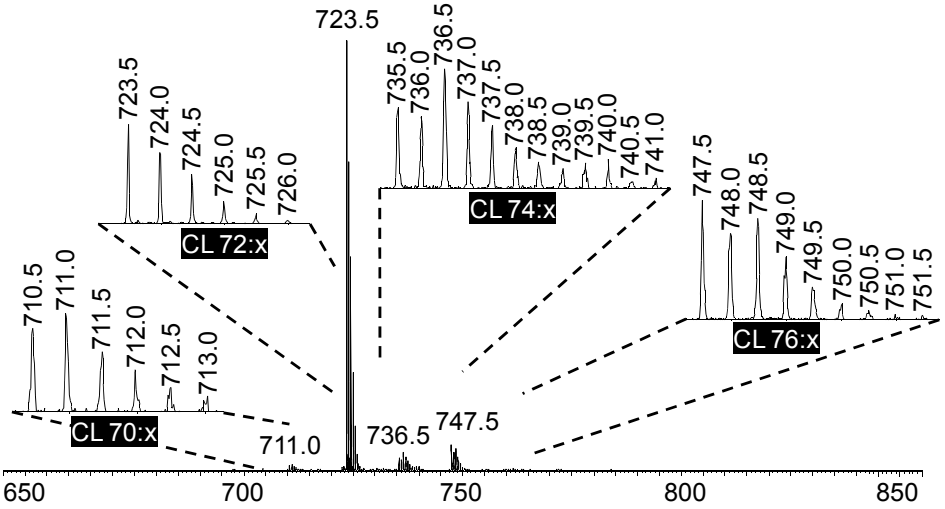

Figure 4-3: MAI-IMS-MS spectra of the cardiolipin content of rat heart mitochondria. The enlarged spectra highlight the isotopic distribution within each acyl-grouping.

www.manaraa.com

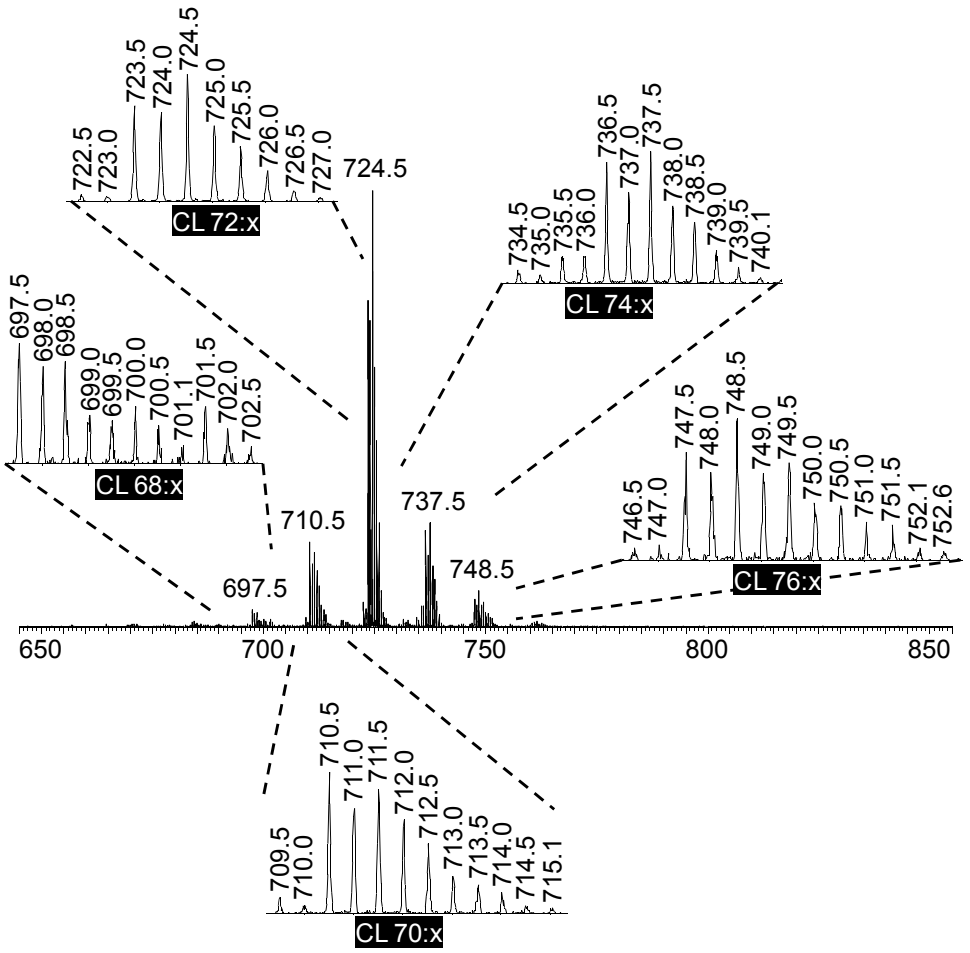

Figure 4-4: MAI-IMS-MS spectra of the cardiolipin content of rat liver mitochondria. The enlarged spectra highlight the isotopic distribution within each acyl-grouping.

www.manaraa.com

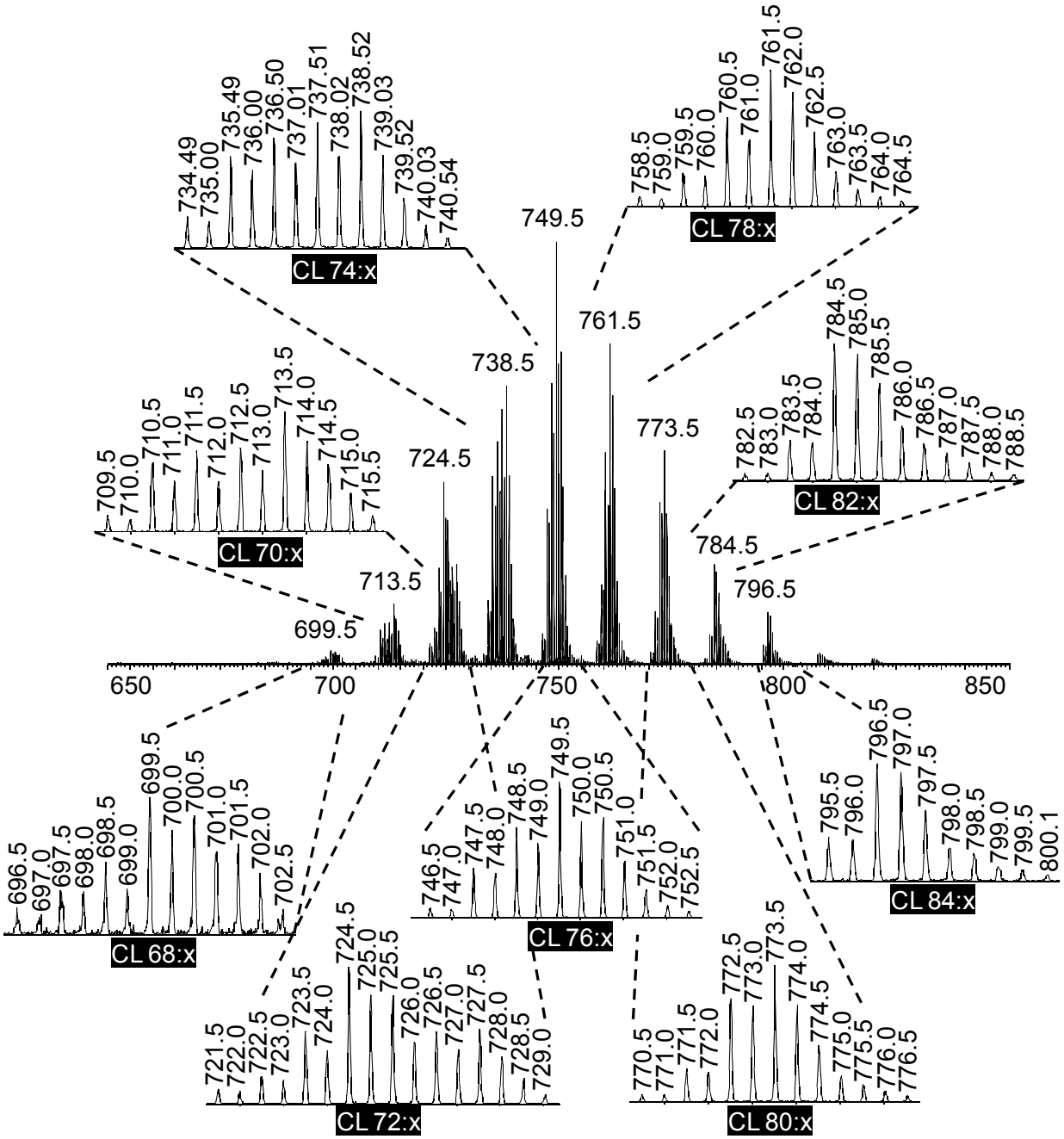

Figure 4-5: MAI-IMS-MS spectra of the cardiolipin content of rat brain mitochondria. The enlarged spectra highlight the isotopic distribution within each acyl-grouping.

www.manaraa.com

Table 4-1: Relative contribution of major cardiolipin Acyl-groupings observe in isolated mitochondria

	% of Total Cardiolipin Peak Area		
Acyl-Grouping	Heart Mitochondria (mean ± s.d.)	Liver Mitochondria (mean ± s.d.)	Brain Mitochondria (mean ± s.d.)
CL 68:x	not detected	3.7% ± 0.5%	1.2% ± 0.5%
CL 70:x	2.1% ± 0.2%	13.7% ± 2.1%	4.9% ± 0.9%
CL 72:x	81.3% ± 7.6%	53.1% ± 3.2%	5.1% ± 1.2%
CL 74:x	6.1% ± 1.8%	16.2% ± 3.2%	20.2% ± 3.2%
CL 76:x	4.9% ± 0.5%	6.8% ± 1.8%	21.8% ± 5.5%
CL 78:x	not detected	6.4% ± 0.4%	16.3% ± 0.6%
CL 80:x	not detected	not detected	11.3% ± 0.9%
CL 82:x	not detected	not detected	5.6% ± 0.8%
CL 84:x	not detected	not detected	2.8% ± 0.1%
CL 86:x	not detected	not detected	1.1% ± 0.2%
CL 88:x	not detected	not detected	0.5% ± 0.1%

4. Application of the Method in the Neonatal HIE Model

4.1 Materials and Methods

4.1.1 Induction of Cerebral Hypoxia-ischemia

Using MAI-IMS-MS, as described above, we next sought to determine whether cerebral hypoxia-ischemia influenced the overall mitochondrial CL profile. Neonatal rat pups of either sex were subjected to HIE on postnatal day 7 using the Vannucci model [182]. As described in chapter 3, pups were anesthetized using isoflurane (3.0% induction, 1.5% maintenance) in NO_2/O_2 (1:1) and the right common carotid artery was exposed via ventral midline neck incision and cut between double ligatures of 6.0 silk sutures. Sham operated control animals underwent the surgical procedure except for ligation and cutting of the carotid artery. The incision was sutured and pups were returned to their dam to recover for 60 min before being exposed to a constant flow of humidified 8% oxygen balance in nitrogen in the custom-designed temperature-

www.manaraa.com

controlled chamber described in chapter 3. Chamber air temperature was maintained at 34.5^{o}C and hypoxia was induced for 180 min.

Using the methods described in Section 2.1.2, mitochondria were isolated from ipsilateral (hypoxic-ischemic) and contralateral (hypoxia-only) cerebral hemispheres at the end of hypoxia-ischemia, as well as following 30 and 120 minutes of reoxygenation. Sham-operated animals time-matched to 120 min reoxygenation were used as controls. MAI-MS-MS was performed as detailed in Section 2.1.3 and interrogated as in Section 2.1.1.

4.1.2 Statistical Analysis

MLCL:CL ratios were determined by integration of extracted drift time curves to yield a peak area for CL and MLCL. The MLCL peak area was divided by the CL peak area to obtain an MLCL:CL ratio. These data were then analyzed using Prism software (Graphpad; La Jolla, CA) and are presented as means ± SEM. A one-way ANOVA was performed and pair wise post-hoc comparisons were made using the Newman–Keuls method.

4.2 Results

4.2.1 Cerebral Hypoxia-ischemia Increases the MLCL:CL Ratio

As shown in Figure 4-6, hypoxia-ischemia resulted in a significant increase in the MLCL:CL ratio during early reperfusion. Importantly, the increased MLCL:CL ratio was observed exclusively in the ipsilateral hemisphere (hypoxic-ischemic), while in the contralateral hemisphere (hypoxia-only) the ratio remained unchanged following the insult and throughout reoxygenation (Figure 4-7).

www.manaraa.com

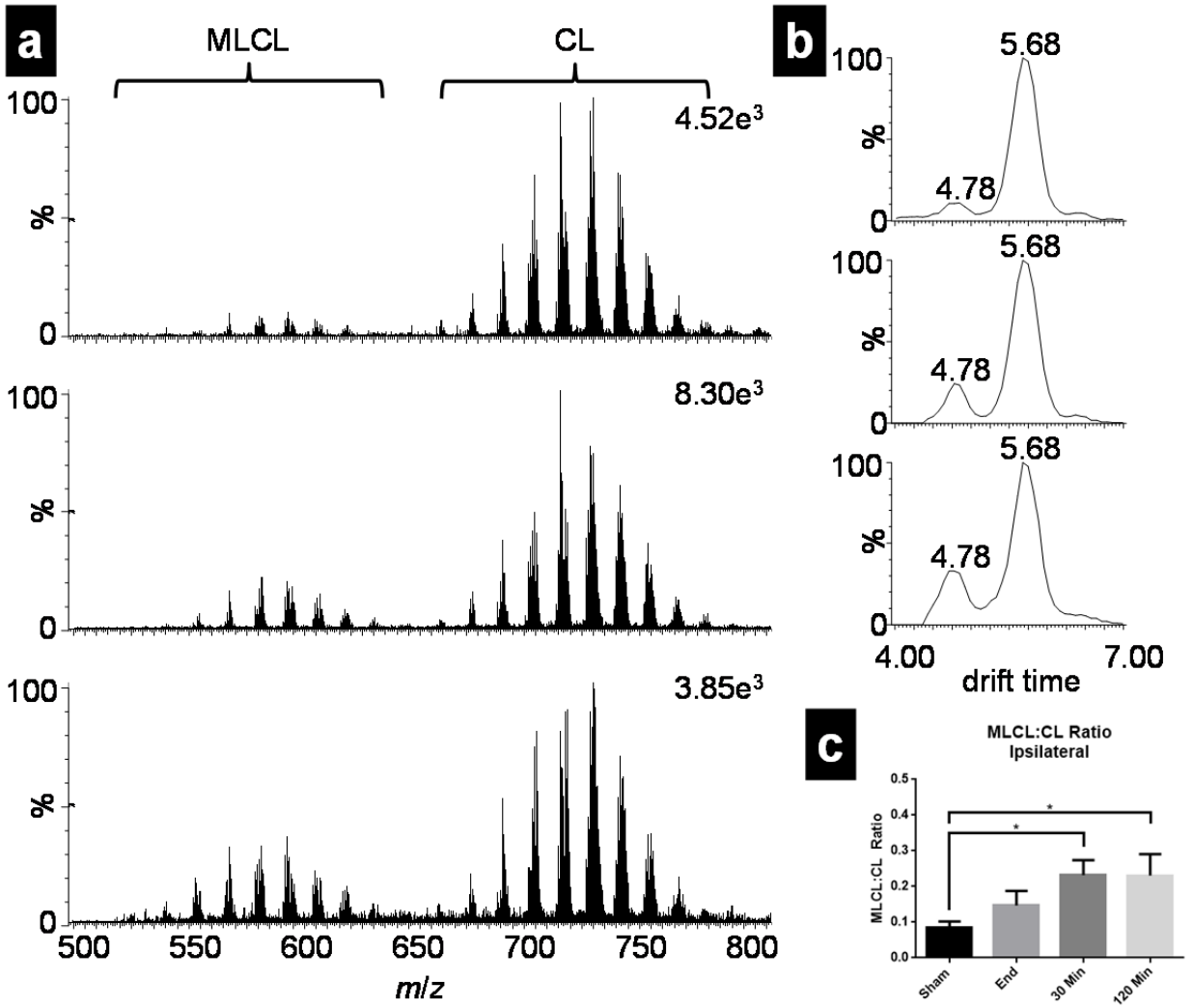

Figure 4-6: Cerebral hypoxia-ischemia leads to an increased ratio of MLCL:CL in mitochondria following reoxygentation. a) Representative mass spectra of the doubly charged $[M-2H]^{2-}$ MLCL and CL species observed in mitochondria of the ipsilateral cerebral hemisphere from a sham-operated control animal [top row], an animal exposed the hypoxia-ischemia [middle row], and an animal exposed to hypoxia-ischemia followed by 30 minutes of reperfusion [bottom row]. **b)** Extracted drift-time curves of MLCL (4.78ms) and CL (5.68ms) from sham-operated control [top row], hypoxia-ischemia [middle row], and hypoxia-ischemia + 30 minutes of reperfusion [bottom row]. **c)** An MLCL:CL ratio of each mitochondrial sample, was determined by dividing MLCL peak area by the CL peak area. Averaged data (mean ± SEM) are shown for sham-operated control (Sham), at the end of hypoxia-ischemia (End), as well as following 30 or 120 min of reperfusion. (*P<0.05)

www.manaraa.com

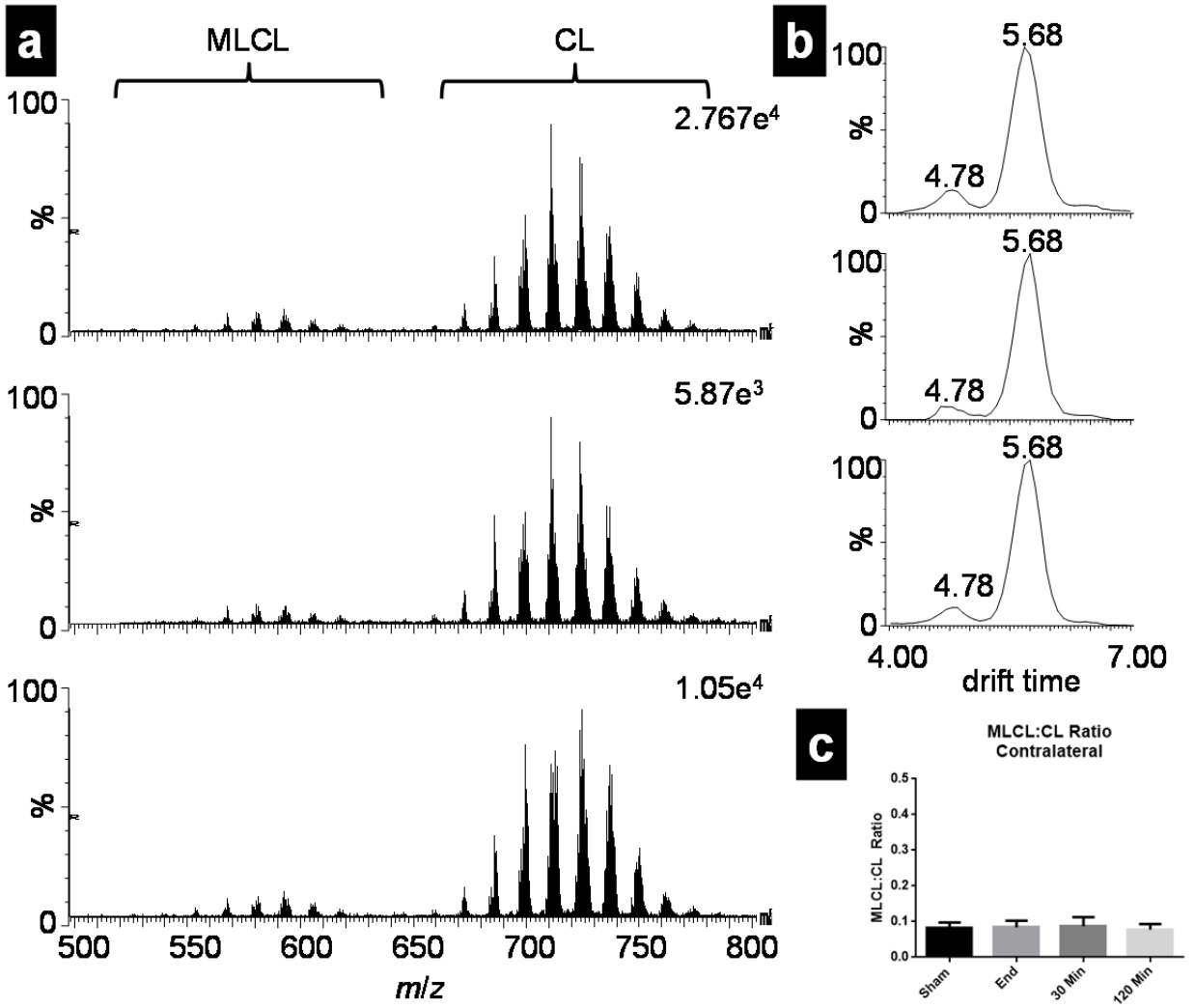

Figure 4-7: Cerebral hypoxia has no effect on mitochondrial MLCL:CL ratio. a) Representative mass spectra of the doubly charged $[M-2H]^{2-}$ MLCL and CL species observed in mitochondria of the contralateral cerebral hemisphere from a sham-operated control animal [top row], an animal exposed the hypoxia [middle row], and an animal exposed to hypoxia followed by 30 minutes of reoxygenation [bottom row]. **b)** Extracted drift-time curves of MLCL (4.78ms) and CL (5.68ms) from sham-operated control [top row], hypoxia [middle row], and hypoxia + 30 minutes of reoxygenation [bottom row]. **c)** An MLCL:CL ratio of each mitochondrial sample, was determined by dividing MLCL peak area by the CL peak area. Averaged data (mean ± SEM) are shown for sham-operated control (Sham), at the end of hypoxia (End), as well as following 30 or 120 min of reoxygenationn. (*P<0.05)

5. Summary

5.1 Technical Advantages of the Method

The central role of membrane lipids in impacting cellular and subcellular physiology is becoming more and more apparent; therefore, the ability to identify, quantify and characterize membrane lipids directly from their native and intact biological

www.manaraa.com

membranes is of vital importance. While ESI is easily coupled to liquid chromatography and is widely used in full-scale lipidomic studies, MALDI remains an attractive method for many membrane lipid research applications because of its ability to ionize phospholipid species without prior lipid extraction. MAI is a newly described ionization method that provides a novel means of combining many of the strengths of ESI and MALDI for use in studying membrane phospholipids. Unlike ESI and MALDI, where significant technological knowledge is necessary for successful experimentation, MAI is operationally simple and does not require the use of a laser or electrospray source. Thus, MAI is compatible with a wide array of commercially available mass spectrometers, requiring only the application of a MAI matrix such as 3-NBN or DCB.

5.2 Insights into Neonatal HIE

This work represents significant progress made in applying MAI-MS for the study of the membrane phospholipid, CL, from intact and native mitochondrial membranes. When used in conjunction with IMS-MS, this ionization method also provides a rapid and effective means of obtaining the biologically significant MLCL:CL ratio through analysis of extracted IMS drift time curves. Using this MAI-IMS-MS approach, cerebral hypoxia-ischemia in the neonatal rat was shown to result in a significant increase in the MLCL:CL ratio during early reperfusion.

While CL hydrolysis during cerebral ischemia-reperfusion may occur enzymatically following CL oxidation via PLA2 [217], it should be noted that in the current study, no appreciable CL oxidation was detected using MAI-IMS-MS. Subsequent MAI-IMS-MS/MS studies should be conducted to address this using an untargeted screen for oxidized fatty acyl fragment ions arising from doubly charged $[M-2H]^{2-}$ CL ions between *m/z* 650-850. Chemically, however, CL hydrolysis during

www.manaraa.com

ischemia-reperfusion may occur as a result of nucleophilic catalysis directly, and to this end, acid catalyzed CL hydrolysis has been reported [218, 219]. Independent of the underlying mechanism, an increase in the MLCL:CL ratio is highly suggestive of increased mitochondrial free radical production.

www.manaraa.com

CHAPTER 5

Preclinical Evaluation of Infrared Light Therapy Using a Rat Model of Neonatal Hypoxic-ischemic Encephalopathy

1. Rationale

As presented in Chapter 2, evidence of the preclinical efficacy of IRL therapy for the treatment of cerebral ischemia-reperfusion injury was initially obtained using a rat model of adult global brain ischemia. Treatment with two IRL wavelengths shown to reversibly inhibit CcO activity and reduce ΔΨm *in vitro* (750 nm and 950 nm) significantly improved survival of CA1 hippocampal neurons after global brain ischemia in the adult rat while, in contrast, treatment with the CcO-excitatory IRL wavelength, 810 nm, had no effect on neuronal viability in CA1 hippocampus. Additionally, when initiated at the onset of reperfusion, treatment with the CcO-inhibitory IRL wavelength, 950 nm, attenuated mitochondrial superoxide production. These findings provide direct support for the overarching hypothesis that reversible inhibition of CcO during early reperfusion reduces mitochondrial ROS production and in turn confers neuroprotectection. The experiments described here sought to evaluate the efficacy of this novel treatment paradigm using the neonatal rat model of HIE characterized in the preceding two chapters of this dissertation.

2. Materials and Methods

2.1 Reagents

All reagents were purchased from Sigma Aldrich (St. Louis, MO) unless indicated otherwise.

2.2 Induction of Cerebral Hypoxia-ischemia

Neonatal rat pups of either sex were subjected to HIE on postnatal day 7 using the Vannucci model [182]. As described in Chapter 3, pups were anesthetized using

www.manaraa.com

isoflurane (3.0% induction, 1.5% maintenance) in NO_2/O_2 (1:1) and the right common carotid artery was exposed via ventral midline neck incision and cut between double ligatures of 6.0 silk sutures. The incision was sutured and pups were returned to their dam to recover for 60 min before being exposed to hypoxia (i.e., a constant flow of humidified 8% oxygen balanced in nitrogen) in the custom-designed temperature-controlled chamber described in Chapter 3. Chamber air temperature was maintained at 34.5^{o}C and hypoxia was induced for 180 min.

2.3 Administration of IRL Treatment

At the onset of reoxygenation, rat pups were immobilized by securing them to the surface of 50 mm x 75 mm glass slides using laboratory tape, and animals were transferred to a dry-air incubator (Thermo) held at 35.0^{o}C. IRL was administered by direct illumination through the skull via a LED device placed 5 cm from the dorsal scalp (Figure 5-1). IRL treatment was conducted using low power, single-wavelength LED diodes (Roithner Lasertechnology) emitting light with a wavelength of 750, 810, or 950 nm. IRL irradiation was initiated at the onset of reoxygenation and was continued for 120 min.

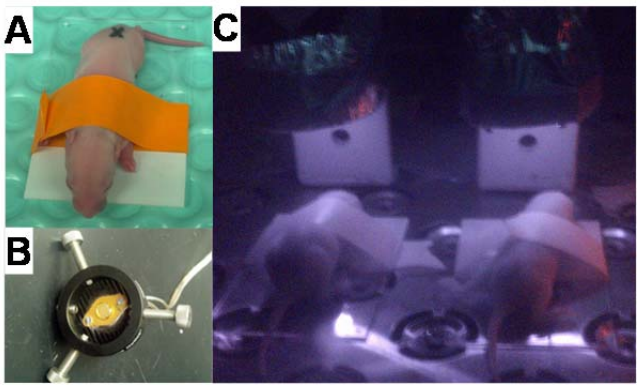

Figure 5-1: IRL administration. A. Postnatal day 7 rat pup immobilized for IRL treatment using a 50mm x 75mm glass slide and laboratory tape. **B.** IRL emmiting LED device equipped with single wavelength diodes (Roithner Lasertechnology). **C.** IRL administration of rat pups via direct illumination of the skull using the LED device.

www.manaraa.com

2.4 Infarct Volume Analysis

Infarct volume was determined 48 hours after the onset of reoxygenation via TTC staining of the coronally sectioned brain and infarct volume was expressed as a percent of the ipsilateral hemisphere as described in Section 2.5 of Chapter 3.

2.5 Subcellular Fractionation

Mitochondrial and cytosolic fractions were obtained 120 minutes following the onset of reoxygenation from animals treated with IRL (750 nm) as well as from non-treated controls. Subcellular fractionation was achieved using differential centrifugation as described in Section 2.6 of Chapter 3. Briefly, both the ipsilateral (hypoxia-ischemia) and contralateral (hypoxia-only) hemispheres were homogenized on ice in mitochondrial Isolation buffer (HEPES 25mM; pH7.7, sucrose 250mM, KFl 10mM, vanadate 1mM, EGTA 5mM, EGTA 2mM, PMSF 0.1mM). Following an initial centrifugation at 1,000g for 10 min at 4^{o}C, the supernatant was centrifuged at 16,700g for 20min at 4^{o}C to isolate the crude mitochondrial fraction (pellet) and crude cytosolic fraction (supernatant).

2.6 Gel Electrophoresis and Immunoblotting

The effect of IRL on HIE- induced accumulation of cytochrome *c* within the cytosol and activation caspase 3 was evaluated using the western blotting technique described in Section 2.7 of Chapter 3. Briefly, 50 µg of cytosolic protein was loaded per lane and resolved via Tricine-SDS-PAGE. Primary antibodies against cytochrome *c* (BD Biosciences, San Jose, CA), cleaved caspase 3, and GAPDH (Cell Signaling Technology, Boston, MA) were used. With the exception of anti-cleaved caspase 3, which was diluted 1:500, all primary antibodies were diluted 1:1000. Bands were visualized using horseradish peroxidase-conjugated secondary antibodies (Sigma-Aldrich, St Louis, MO) and the scanned and digitalized films were analyzed using

www.manaraa.com

Quantity One ® software (Biorad).

2.7 Matrix Assisted Ionization – Ion Mobility Spectrometry – Mass Spectrometry

The effect of IRL treatment on the mitochondrial MLCL:CL ratio was evaluated via MAI-IMS-MS as described in Section 3.1.3 of Chapter 4. Mitochondria were obtained 120 minutes following the onset of reoxygenation from IRL-treated animals and non-treated controls, and were diluted to a final protein concentration of 1mg•mL^{-1} in 20:80 H_2O:EtOH containing 0.1% NH_4OH. The MAI matrix DCB (Alfa Aesar; Ward Hill, MA) was dissolved in acetonitrile (5mg in 50µL) and mixed with enriched mitochondrial samples (1:1,v/v). Immediately prior to analysis, the solution containing matrix and mitochondria was drawn into a pipet tip in 1µL aliquots and allowed to crystallize at the end of the tip. As previously described in Chapter 4, samples were introduced directly into the vacuum of the mass spectrometer by placing the pipet tip against the skimmer cone inlet. Mass spectra were obtained using a Waters SYNAPT G2 quadrupole-TOF and ion mobility spectrometry was performed with N_2 as the ion mobility gas.

3. Results

3.1 IRL Therapy Initiated at the Onset of Reperfusion Reduces Cerebral Infarct Volume Following Hypoxia-ischemia in the Neonatal Rat

A total of 63 rat pups were enrolled to evaluate the effect of IRL treatment following hypoxia-ischemia. Pups were randomly assigned to receive 120 min of IRL-treatment with a wavelength of 750, 810, or 950 nm (n=15, 15 and 16, respectively). Non-treated littermates served as sham controls (n=17).

As shown in Figure 5-2, treatment with the CcO-inhibitory IRL wavelength, 750 nm, as well as the CcO-excitatory IRL wavelength, 810 nm, significantly attenuated

www.manaraa.com

cerebral infarction resulting from neonatal hypoxia-ischemia: mean infarct volumes were 31.3% and 29.0%, *versus* the value of 48.9% seen in untreated sham controls. Treatment with the 950 nm IRL wavelength resulted in a mean infarct volume of 34.3% which approached, but did reach, significance (p=0.127) when compared with controls.

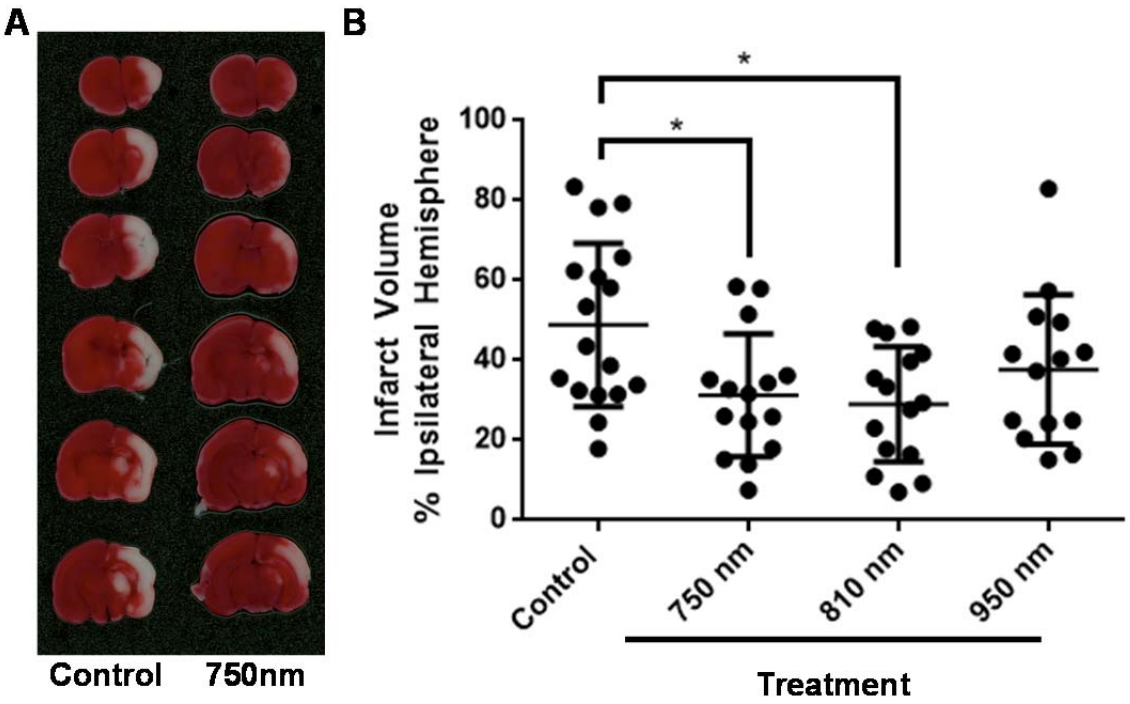

Figure 5-2: IRL treatment attenuates cerebral infarction resulting from hypoxia-ischemia in the neonatal rat. Postnatal day 7 rats were subjected to unilateral carotid artery ligation and subsequent hypoxia (8% O_2 balanced in N_2; 180 min). Animals were randomly assigned to receive 120 min of IRL-treatment with a wavelength of 750, 810, or 950 nm. Non-treated littermates served as controls. Forty-eight hours after the onset of reperfusion, brains were sliced and infarct volume was assessed. **A.** Representative TTC stained brain slices from a non-treated control and an IRL-treated animal (750 nm). Red= viable tissue; unstained regions = infarction. **B.** Mean infarct volume for all IRL treatments as well as non-treated controls (*p<0.05).

3.2 IRL Treatment Attenuates caspase 3 Activation during Early Reperfusion Following Cerebral Hypoxia-ischemia in the Neonatal Rat

As demonstrated in Chapter 3, the neonatal rat model of HIE results in mitochondrial permeability, cytosolic accumulation of cytochrome *c* and activation of caspase 3 in the ipsilateral (hypoxic-ischemic) hemisphere within 2 hours following the onset of reperfusion. Furthermore, using MAI-IMS-MS, cerebral hypoxia-ischemia in

www.manaraa.com

the neonatal rat was also shown to result in a significant increase in the mitochondrial MLCL:CL ratio during early reperfusion (Chapter 4). Thus, we next sought to examine whether the attenuation in cerebral infarction seen in the neonatal rat with IRL treatment was associated with favorable reductions in mitochondrial cardiolipin hydrolysis, mitochondrial permeability and caspase 3 cleavage.

Cytosolic fractions obtained from ipsilateral (hypoxic-ischemic) and contralateral (hypoxia-only) hemispheres were collected from non-treated and IRL-treated animals following 120 minutes of reoxygenation (n=4 per group). The wavelength of 750 nm was used for IRL treatment, and irradiation was initiated at the onset of reoxygenation and maintained until the time of sacrifice (120 min). Figure 5-3 shows the results of western blot analysis of cytosolic cytochrome *c* accumulation and caspase 3 cleavage in the ipsilateral (hypoxic-ischemic) hemisphere of IRL-treated and non-treated control animals. No difference in cytosolic cytochrome *c* accumulation was observed between IRL-treatment and control

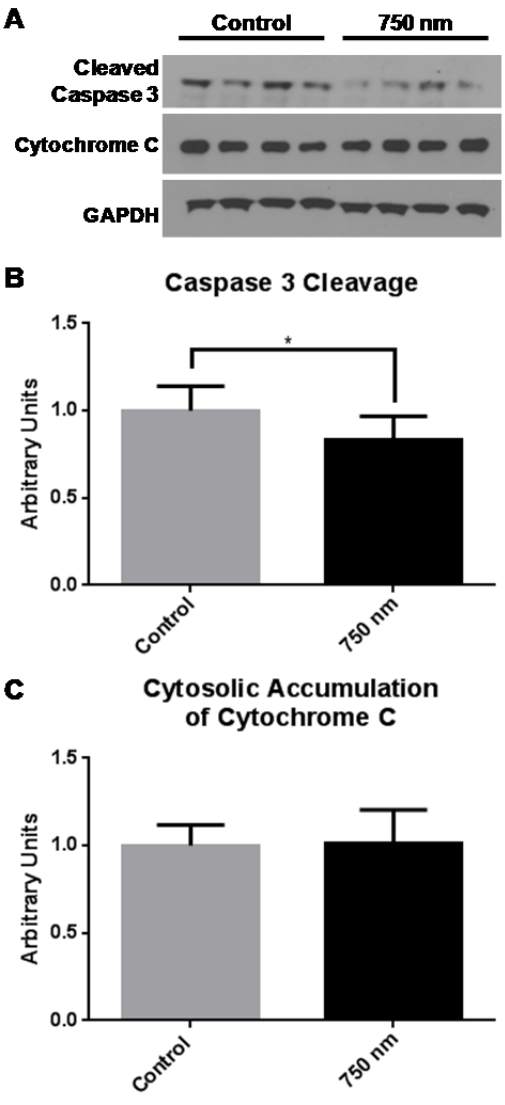

Figure 5-3: Effect of IRL treatment on cytosolic accumulation of cytochrome *c* and caspase 3 cleavage following cerebral hypoxia-ischemia in the neonatal rat. A. Representative immunoblot for cytochrome *c*, cleaved caspase 3, and GAPDH in the cytosolic fraction obtained from the ipsilateral hemisphere of IRL-treated and non-treated animals (control) subjected to hypoxia-ischemia. Cytochrome *c* accumulation and caspase 3 cleavage were normalized to GAPDH, and averaged data (mean ± SEM) are shown for control and IRL treated (750 nm) for cytochrome *c* (**B**) and cleaved caspase 3 (**C**). (*P<0.05)

www.manaraa.com

(Figure 5-3 A). However, cleavage of caspase 3 was nonetheless attenuated by treatment with IRL (Figure 5-3 B). As anticipated, no differences in cytosolic cytochrome *c* accumulation or caspase 3 cleavage were observed in the non-injured contralateral hemisphere between IRL-treated and non-treated control animals (data not shown).

Using the MAI-IMS-MS approach described in Chapter 4, the effect of IRL on the mitochondrial MLCL:CL ratio following hypoxia-ischemia was investigated. Mitochondria were obtained from the ipsilateral (hypoxic-ischemic) hemisphere of non-treated and IRL-treated (750 nm) animals following 120 minutes of reoxygenation (n=4 per group). Given that the mitochondrial MLCL:CL ratio was previously found to be unchanged in the contralateral (hypoxia-only) hemisphere using this rat model of neonatal HIE (Chapter 4), the current study focused exclusively on the ipsilateral (hypoxic-ischemic) hemisphere. Figure 5-4 A shows the mass spectra of the doubly charged $[M-2H]^{2-}$ MLCL and CL species observed in mitochondria of the ipsilateral cerebral hemisphere of a non-treated control animal as well as an animal treated with IRL (750 nm) for 120min. The MLCL:CL ratio was determined by integration of the extracted drift time curves for CL and MLCL, and the MLCL peak area was divided by the CL peak area. Using this method, no significant difference in the MLCL:CL ratio was observed between IRL-treatment and control (Figure 5-4 C).

www.manaraa.com

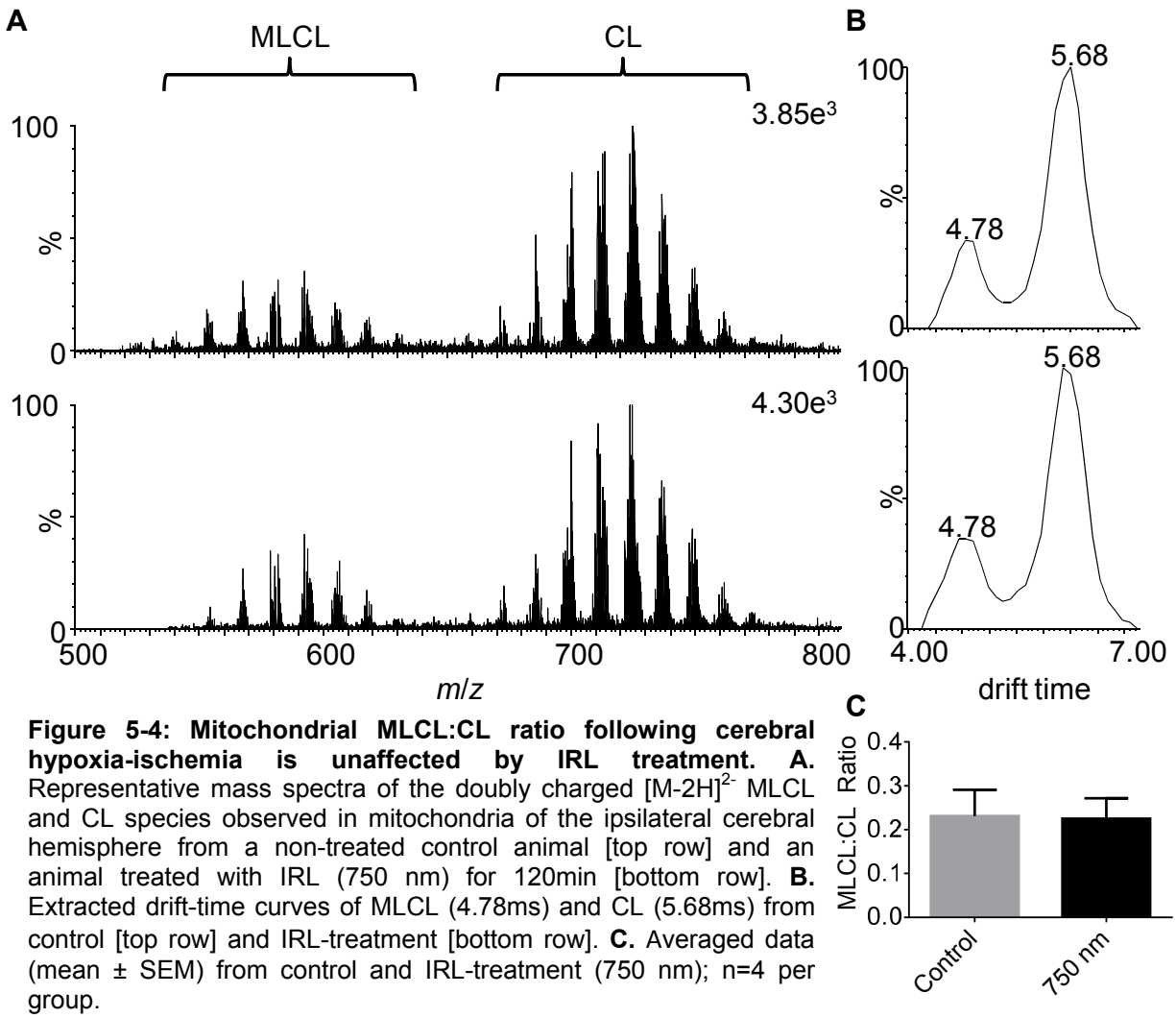

Figure 5-4: Mitochondrial MLCL:CL ratio following cerebral hypoxia-ischemia is unaffected by IRL treatment. A. Representative mass spectra of the doubly charged $[M-2H]^{2-}$ MLCL and CL species observed in mitochondria of the ipsilateral cerebral hemisphere from a non-treated control animal [top row] and an animal treated with IRL (750 nm) for 120min [bottom row]. **B.** Extracted drift-time curves of MLCL (4.78ms) and CL (5.68ms) from control [top row] and IRL-treatment [bottom row]. **C.** Averaged data (mean ± SEM) from control and IRL-treatment (750 nm); n=4 per group.

4. Summary

Consistent with results from previous IRL efficacy studies using a rat model of adult global brain ischemia, IRL treatment using the CcO-inhibitory IRL wavelength, 750 nm, attenuated cerebral injury resulting from hypoxia-ischemia in the neonatal rat. Furthermore, 750 nm IRL initiated at the onset of reperfusion, attenuated caspase 3 cleavage.

Experiments in the current chapter did, however, yield unexpected observations. First, in contrast to data obtained in the adult rat model of global brain ischemia (Chapter 2), treatment with the CcO-excitatory wavelength, 810 nm, reduced ipsilateral

www.manaraa.com

infarct volume in the neonate model. One potential explanation for this surprising result is that alternative and as-yet unexplored mechanisms of neuroprotection may be elicited by IRL therapy in the neonatal model of cerebral ischemia-reperfusion when compared to the previously studied adult model. These alternative mechanisms may work in conjunction with, or independent of, the hypothesized mechanism of mitochondrial modulation by CcO. To this end, a divergence of CcO isoform expression within mitochondria of the neonatal and adult brain may – in part – explain the discrepancy in observations between the two studies. CcO isoform switching has been described in lung mitochondria where CcO subunit IV isoforms 1 and 2 are preferentially expressed in the immature and mature lung, respectively [220]. Future studies should evaluate the effect of these specific IRL wavelengths (750, 810 and 950 nm) on CcO isolated from neonatal brain mitochondria to determine how exactly neonatal CcO activity responds to IRL irradiation *in vitro*.

It is also surprising that although neuroprotective, treatment with 750 nm IRL in the current study had no effect on the mitochondrial MLCL:CL ratio as measured by MAI-IMS-MS. Previous *in vitro* and *in vivo* studies using this CcO-inhibitory IRL wavelength support the hypothesis that 750 nm IRL treatment attenuates mitochondrial ROS production during early reperfusion following ischemia (Chapter 2). As suggested in Chapter 4, the mitochondrial MLCL:CL ratio may serve as an intrinsic indicator of mitochondrial ROS production as CL hydrolysis to form MLCL likely occurs directly as a result of – or enzymatically following – the production of mitochondrial ROS. Nonetheless, using MAI-IMS-MS no detectable difference was observed in the MLCL:CL ratio following cerebral ischemia-reperfusion between 750 nm IRL-treatment and non-treated control. Similarly, no detectable difference in cytosolic cytochrome *c*

www.manaraa.com

accumulation was observed between IRL-treatment and control. Subsequent studies should be conducted to verify this initial observation and additional delayed time points following the onset of reperfusion should be considered. It is possible that difference in these and/or other biochemical outcomes may become more apparent between IRL-treatment and control as the cerebral injury evolves.

www.manaraa.com

CHAPTER 6

Discussion

1. Summary of Results

Ongoing work from the Hüttemann and Sanderson laboratories has provided the fundamental mechanistic rationale for the use of IRL therapy as a treatment for cerebral reperfusion injury. The preclinical success of this approach stems from a comprehensive understanding of the role of mitochondria in cell death caused by cerebral ischemia-reperfusion injury. As summarized in Chapter 1, a model has been proposed in which ischemic alterations of mitochondrial OxPhos primes the mitochondria for subsequent reperfusion-induced $\Delta\Psi_m$ hyperpolarization leading to a burst in mitochondrial ROS generation and loss of mitochondrial function. These mitochondrial alterations ultimately culminate in delayed neuronal death following the release of proapoptotic factors from the mitochondria into the cytosol. This progression is simplified into four main states that summarize the induction, progression, and execution of cell death during brain ischemia-reperfusion: 1) ischemic starvation (i.e., ETC is rendered non-functional by the lack of O_2); 2) reperfusion-induced hyperactivation; 3) mitochondrial dysfunction; and 4) delayed neuronal death (Chapter 1, Figure1-2).

As discussed in Chapter 2, specific wavelengths of IRL can directly modulate CcO activity. IRL with a wavelength of 750nm or 950nm was found to inhibit CcO activity, while 810 nm IRL was found to modestly increased CcO activity (Chapter 2; Figure 2-1). Given that CcO catalyses the final, and proposed rate limiting step in mitochondrial electron transfer – the donation of electrons to O_2 – modulation of CcO activity via irradiation with IRL provides a novel mean of non-invasively regulating

www.manaraa.com

electron flux through the ETC and, by extension, the overall $\Delta\Psi_{m.}$ Treatment with IRL wavelengths shown to inhibit CcO activity *in vitro* was associated with a favorable reduction in mitochondrial ROS generation when initiated at the onset of reperfusion following global brain ischemia in the adult rat and resulted in significant neuroprotection (Chapter 2).

The overarching goal of this dissertation was to investigate the preclinical efficacy of this novel treatment paradigm in the neonatal brain – in particular, brain injuries arising as a result of perinatal asphyxia. Ischemic insults to the infant brain most often result from prolapse or compression of the umbilical cord during delivery and placental abruption [16-18]. Because these injuries are generally sustained while in a hospital setting at the time of delivery, this patient population is much more likely to receive therapeutic intervention early following the onset of reperfusion. Given that $\Delta\Psi_m$ hyperpolarization and mitochondrial ROS production likely occur rapidly following the onset of reoxygenation, treatment of asphyxiated infants with IRL may provide a non-invasive means of attenuating cerebral injury in this patient population.

The goal of the work described in Chapters 3 and 4 was to examine the utility of the Vannucci rat model of neonatal HIE for use in the preclinical evaluation of IRL therapy. Consistent with previously published literature, the extent of cerebral injury produced by this rodent model of neonatal HIE was variable. Not surprisingly, the duration of the hypoxic event influenced both the consistency of cerebral infarction and the median infarct volume. However, maintenance of a suitable chamber temperature during the hypoxic insult was also demonstrated to be critical. Experiments reported in Chapter 3 established that mitochondrial permeability, cytosolic accumulation of cytochrome *c* and activation of caspase 3 were manifest acutely following cerebral

www.manaraa.com

hypoxia-ischemia, but not hypoxia-alone. Additionally, using the MAI-IMS-MS approach described in Chapter 4, cerebral hypoxia-ischemia, but not hypoxia-alone, was shown to result in a significant increase in the MLCL:CL ratio during early reoxygenation. This latter observation is highly suggestive of mitochondrial ROS production, as CL hydrolysis to form MLCL occurs directly as a result of (or enzymatically following) the production of mitochondrial ROS. Taken together: although the inherent variability in injury severity of this animal model necessitates that a large number of animal subjects be enrolled in a given study in order to demonstrate any treatment effect, the acute biochemical phenotype produced by HIE appears to progress in accordance with predictions outlined in Chapter 1. Specifically, mitochondrial ROS production and mitochondrial permeability occur acutely following the onset of reoxygenation and precede the activation of apoptosis.

Consistent with results from previous IRL efficacy studies using the adult global brain ischemia, IRL treatment using the CcO-inhibitory IRL wavelength of 750 nm attenuated cerebral injury resulting from hypoxia-ischemia in the neonatal rat. Furthermore, IRL at 750 nm, initiated at the onset of reperfusion, attenuated caspase 3 cleavage. Unexpectedly, however, in contrast to data obtained in the adult rat model of global brain ischemia, treatment with the CcO-excitatory wavelength, 810 nm, also reduced ipsilateral infarct volume in the neonate model. As described in Chapter 5, one potential explanation for this surprising result is that alternative responses to IRL therapy may exist in the neonatal brain when compared to the mature brain.

2. Technical Limitations and Future Directions

One major limitation of this work stems from the inherent variability of cerebral injury produced by this rat model of neonatal HIE. Despite the significant effort invested

www.manaraa.com

in optimization, cerebral infarct size among untreated controls ranged from a minimum of 17.9% to a maximum of 83.5% of the ipsilateral hemisphere. This substantial variation confounds both the ability to identify therapies that will have a meaningful effect on infarct size, and, as discussed below, yield mechanistic insights into these therapies. Future preclinical studies investigating the optimal IRL wavelength and/or wavelength combinations as well as the overall safety of this therapeutic approach should be conducted in a large animal model.

Another significant limitation is that the mitochondrial MLCL:CL ratio has not been validated empirically as an intrinsic indicator of mitochondrial ROS production. While CL hydrolysis to form MLCL likely occurs directly as a result of (or enzymatically following) the production of mitochondrial ROS, it is conceivable that this process may occur enzymatically via a calcium-dependent PLA2 simply as a result of the mitochondrial calcium loading that likely occurs during ischemic starvation (see Chapter 1 Section 3). Ongoing work using isolated mitochondria seeks to address this possibility in an attempt to better interpret the physiological significance of an increased MLCL:CL ratio following cerebral ischemia-reperfusion.

As described in Chapter 5, using MAI-IMS-MS no detectable difference was observed in the MLCL:CL ratio following cerebral ischemia-reperfusion between 750 nm IRL-treatment and non-treated control. Similarly, no detectable difference in cytosolic cytochrome *c* accumulation was observed between IRL-treatment and control. Given the inherent variability in injury severity produced by this model, it is possible that these unanticipated observations are merely the result of insufficient sampling (n=4 per group), and that had a larger number of animals been enrolled (e.g. n =15-20 per group), a treatment effect would have been detected. This explanation (under-

www.manaraa.com

sampling) is strengthened further if a linear relationship is assumed to exist between early biochemical outcomes (mitochondrial MLCL:CL ratio and cytosolic cytochrome *c* accumulation) and cerebral infarct volume measured 48 hours after the onset of reperfusion. Subsequent studies should be conducted to address this limitation.

Finally, the current study focused exclusively on biochemical events occurring acutely following the onset of reperfusion while injury severity was assessed 48 hours later. Future studies would benefit from adding additional endpoints at delayed time points, as it is possible that pathophysiological and/or treatment-induced effects are occurring as the cerebral injury evolves.

3. Conclusions

This work has provided two major technical contributions to the field of cerebral ischemia-reperfusion injury. First, experiments in Chapter 3 have refined and provided biochemical characterization of the rat model of HIE. Second, Chapter 4 focused on the development of a method of characterizing membrane lipids directly from their native and intact biological membranes without prior lipid extraction using the MAI-MS technology pioneered in the Trimpin laboratory. While the current study used this new method exclusively to investigate alterations in the CL profile of brain mitochondria following cerebral hypoxia-ischemia, the approach can be employed in various membrane lipid research applications. Finally, consistent with results from previous IRL efficacy studies using a rat model of adult global brain ischemia, experiments in Chapter 5 establish that IRL treatment attenuated cerebral injury resulting from hypoxia-ischemia in the neonatal rat. Thus, and perhaps most importantly, this work contributes to the development of a potential novel therapeutic approach in the management of brain injuries arising as a result of perinatal asphyxia.

www.manaraa.com

APPENDIX A

Animal Protocol Approval Letters

Current:

WAYNE STATE UNIVERSITY

INSTITUTIONAL ANIMAL
CARE AND USE COMMITTEE
87 E. Canfield, Second Floor
Detroit, MI 48201-2011
Telephone: (313) 577-1629
Fax Number: (313) 577-1941

ANIMAL WELFARE ASSURANCE # A3310-01

PROTOCOL # A 09-01-13

Protocol Effective Period: October 16, 2013 – September 30, 2016

TO: Dr. Thomas Sanderson
Department of Emergency Medicine
1222 Elliman Clinical Research Building

FROM: Lisa Anne Polin, Ph.D.
Chairperson
Institutional Animal Care and Use Committee

SUBJECT: Approval of Protocol # A 09-01-13

"A novel non-invasive infrared light therapy to attenuate neonatal brain injury"

DATE: October 16, 2013

Your animal research protocol has been reviewed by the Wayne State University Institutional Animal Care and Use Committee, and given final approval for the period effective **October 16, 2013** through **September 30, 2016**. The listed source of funding for the protocol is **Kellogg Foundation--Perinatology Virtual Discovery Grant**. The species and number of animals approved for the duration of this protocol are listed below.

Species	Strain	Qty.	USDA Cat.
RATS	Sprague Dawley, Pregnant Dams (E15 timed pregnant)	88	D
RATS	Sprague Dawley, Pregnant Dams (E18 timed pregnant)	66	C

*To be purchased

RATS	Sprague Dawley, Male and Female, E21-22 Embryos	5	B
RATS	Sprague Dawley, Male and Female, E21-22 Embryos	875	D
RATS	Sprague Dawley, Male and Female, P7 pups	660	B

**To be bred in-house

Be advised that this protocol must be reviewed by the IACUC on an annual basis to remain active. Any change in procedures, change in lab personnel, change in species, or additional numbers of animals requires prior approval by the IACUC. Any animal work on this research protocol beyond the expiration date will require the submission of a new IACUC protocol form and full committee review.

The Guide for the Care and Use of Laboratory Animals is the primary reference used for standards of animal care at Wayne State University. The University has submitted an appropriate assurance statement to the Office for Laboratory Animal Welfare (OLAW) of the National Institutes of Health. The animal care program at Wayne State University is accredited by the Association for Assessment and Accreditation of Laboratory Animal Care International (AAALAC).

www.manaraa.com

WAYNE STATE UNIVERSITY

INSTITUTIONAL ANIMAL
CARE AND USE COMMITTEE
87 E. Canfield, Second Floor
Detroit, MI 48201-2011
Telephone: (313) 577-1629
Fax Number: (313) 577-1941

ANIMAL WELFARE ASSURANCE # A 3310-01

PROTOCOL # A 01-02-13

Protocol Effective Period: February 12, 2013 – January 31, 2016

TO: Dr. Thomas Sanderson
Department of Emergency Medicine
1222 Elliman Clinical Research Building

FROM: Lisa Anne Polin, Ph.D.
Chairperson
Institutional Animal Care and Use Committee

SUBJECT: Approval of Protocol # A 01-02-13

"Therapeutic targeting of perinatal ischemia"

DATE: February 12, 2013

Your animal research protocol has been reviewed by the Wayne State University Institutional Animal Care and Use Committee, and given final approval for the period effective **February 12, 2013** through **January 31, 2016**. The listed source of funding for the protocol is **Edward S. Thomas Endowment**. The species and number of animals approved for the duration of this protocol are listed below.

Species	Strain	Qty.	USDA Cat.
RATS	Sprague Dawley, Pregnant Dams (E15 timed pregnant)	23	D
RATS	Sprague Dawley, Pregnant Dams (E18 timed pregnant)	18	B
RATS	Sprague Dawley, Male and Female, E21-22 Embryos	22	B
RATS	Sprague Dawley, Male and Female, E21-22 Embryos	218	D
RATS	Sprague Dawley, Male and Female, P3 pups	180	B

Be advised that this protocol must be reviewed by the IACUC on an annual basis to remain active. Any change in procedures, change in lab personnel, change in species, or additional numbers of animals requires prior approval by the IACUC. Any animal work on this research protocol beyond the expiration date will require the submission of a new IACUC protocol form and full committee review.

The Guide for the Care and Use of Laboratory Animals is the primary reference used for standards of animal care at Wayne State University. The University has submitted an appropriate assurance statement to the Office for Laboratory Animal Welfare (OLAW) of the National Institutes of Health. The animal care program at Wayne State University is accredited by the Association for Assessment and Accreditation of Laboratory Animal Care International (AAALAC).

www.manaraa.com

Previous:

WAYNE STATE UNIVERSITY

INSTITUTIONAL ANIMAL
CARE AND USE COMMITTEE
87 E. Canfield, Second Floor
Detroit, MI 48201-2011
Telephone: (313) 577-1629
Fax Number: (313) 577-1941

ANIMAL WELFARE ASSURANCE # A 3310-01

PROTOCOL # A 04-06-11

Protocol Effective Period: May 17, 2011 – April 30, 2014

TO: Dr. Thomas Sanderson
Department of Emergency Medicine
51.1 Lande Medical Research Building

FROM: Lisa Anne Polin, Ph.D. Lisa Anne Polin
Chairperson
Institutional Animal Care and Use Committee

SUBJECT: Approval of Protocol # A 04-06-11

"Non-Pharmacologic Modulation of Mitochondrial Function: A Novel Strategy to Attenuate Reperfusion Injury Following Neonatal Hypoxia/Ischemia"

DATE: May 17, 2011

Your animal research protocol has been reviewed by the Wayne State University Institutional Animal Care and Use Committee, and given final approval for the period effective **May 17, 2011** through **April 30, 2014**. The listed source of funding for the protocol is **Edward S. Thomas Endowment**. The species and number of animals approved for the duration of this protocol are listed below.

Species	Strain	Qty.	USDA Cat.
RATS	Sprague Dawley, Pregnant Dams	37	B
RATS	Sprague Dawley, Male and Female, 7d-old neonates, 17+/-2g	303	D

Be advised that this protocol must be reviewed by the IACUC on an annual basis to remain active. Any change in procedures, change in lab personnel, change in species, or additional numbers of animals requires prior approval by the IACUC. Any animal work on this research protocol beyond the expiration date will require the submission of a new IACUC protocol form and full committee review.

The Guide for the Care and Use of Laboratory Animals is the primary reference used for standards of animal care at Wayne State University. The University has submitted an appropriate assurance statement to the Office for Laboratory Animal Welfare (OLAW) of the National Institutes of Health. The animal care program at Wayne State University is accredited by the Association for Assessment and Accreditation of Laboratory Animal Care International (AAALAC).

www.manaraa.com

WAYNE STATE UNIVERSITY

INSTITUTIONAL ANIMAL
CARE AND USE COMMITTEE
87 E. Canfield, Second Floor
Detroit, MI 48201-2011
Telephone: (313) 577-1629
Fax Number: (313) 577-1941

ANIMAL WELFARE ASSURANCE # A 3310-01

PROTOCOL # A 04-06-11
Protocol Effective Period: 5/17/2011 – 4/30/2014
AMENDMENT # 3

TO: Dr. Thomas Sanderson
Department of Emergency Medicine
51.1 Lande Medical Research Building

FROM: Lisa Anne Polin, Ph.D.
Chairperson
Institutional Animal Care and Use Committee

SUBJECT: Approval of Amendment **# 3** to Protocol # A 04-06-11

"Non-Pharmacologic Modulation of Mitochondrial Function: A Novel Strategy to Attenuate Reperfusion Injury Following Neonatal Hypoxia/Ischemia"

DATE: March 19, 2012

The following requested changes to the above protocol have been reviewed and approved for immediate effect:

Request dated March 8, 2012:

The following animals will be added to the protocol for additional treatment groups as described in the amendment request:

RATS, Sprague Dawley, Pregnant Dams; 12 "B"
RATS, Sprague Dawley, Male and Female, 7d-old neonates, 17+/-2g; 94 "D"

This protocol, as amended, will be subject to annual review on the anniversary date of the initial IACUC review. This protocol was last reviewed on May 17, 2011.

www.manaraa.com

APPENDIX B

Publisher Licensing Agreements

Copyright Clearance Center RightsLink®

Home | Create Account | Help | Live Chat

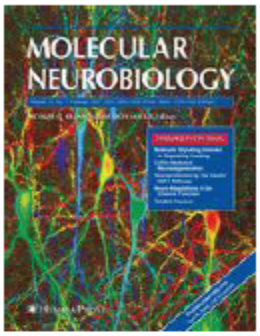

Title: Molecular Mechanisms of Ischemia–Reperfusion Injury in Brain: Pivotal Role of the Mitochondrial Membrane Potential in Reactive Oxygen Species Generation

Author: Thomas H. Sanderson

Publication: Molecular Neurobiology

Publisher: Springer

Date: Jan 1, 2012

Copyright © 2012, Springer Science+Business Media, LLC

LOGIN

If you're a copyright.com user, you can login to RightsLink using your copyright.com credentials. Already **a RightsLink user** or want to learn more?

Quick Price Estimate

This reuse request is free of charge although you are required to obtain a license through Rightslink and comply with the license terms and conditions. You will not be charged for this order. To complete this transaction, click the Continue button below.

I would like to...	use in a thesis/dissertation
Portion	Full text
Number of copies	1
Are you the author of this Springer article?	Yes
You are ...	a contributor of the new work
Select your currency	USD - $
Quick Price	0.00 USD

No content delivery. This service provides permission for reuse only. Once licensed, you may use the content according to the terms of your license.

Price quoted is an estimate based on this request for this title only. Final price will depend on the total amount of requested Springer material.

The material can only be used for the purpose of defending your thesis limited to university-use only. If the thesis is going to be published, permission needs to be re-obtained (selecting "book/textbook" as the type of use).

المنارة للاستشارات

www.manaraa.com

REFERENCES

1. Lloyd-Jones, D., et al., Heart disease and stroke statistics--2010 update: a report from the American Heart Association. Circulation, 2010. 121(7): p. e46-e215.
2. Krause, G.S., et al., Ischemia, resuscitation, and reperfusion: mechanisms of tissue injury and prospects for protection. Am Heart J, 1986. 111(4): p. 768-80.
3. Bloom, H.L., et al., Long-term survival after successful inhospital cardiac arrest resuscitation. Am Heart J, 2007. 153(5): p. 831-6.
4. Nichol, G., et al., Regional variation in out-of-hospital cardiac arrest incidence and outcome. JAMA, 2008. 300(12): p. 1423-31.
5. Kumar, K., et al., Ultrastructural and ionic studies in global ischemic dog brain. Acta Neuropathol, 1987. 73(4): p. 393-9.
6. Jenkins, L.W., et al., The role of postischemic recirculation in the development of ischemic neuronal injury following complete cerebral ischemia. Acta Neuropathol, 1981. 55(3): p. 205-20.
7. Ito, U., et al., Experimental cerebral ischemia in mongolian gerbils. I. Light microscopic observations. Acta Neuropathol, 1975. 32(3): p. 209-23.
8. Kirino, T. and K. Sano, Selective vulnerability in the gerbil hippocampus following transient ischemia. Acta Neuropathol, 1984. 62(3): p. 201-8.
9. Pulsinelli, W.A., et al., Ischemic brain injury and the therapeutic window. Ann N Y Acad Sci, 1997. 835: p. 187-93.
10. Hayashi, T., et al., Oxidative damage to the endoplasmic reticulum is implicated in ischemic neuronal cell death. J Cereb Blood Flow Metab, 2003. 23(10): p. 1117-28.
11. Piantadosi, C.A. and J. Zhang, Mitochondrial generation of reactive oxygen

www.manaraa.com

species after brain ischemia in the rat. Stroke, 1996. 27(2):327-31; discussion 332.

12. Sugawara, T. and P.H. Chan, Reactive oxygen radicals and pathogenesis of neuronal death after cerebral ischemia. Antioxid Redox Signal, 2003. 5(5): p. 597-607.

13. Al-Macki, N., et al., The spectrum of abnormal neurologic outcomes subsequent to term intrapartum asphyxia. Pediatr Neurol, 2009. 41(6): p. 399-405.

14. Vannucci, R.C., Hypoxic-ischemic encephalopathy. Am J Perinatol, 2000. 17(3):p. 113-20.

15. Volpe, J.J., Brain injury in the premature infant--current concepts of pathogenesis and prevention. Biol Neonate, 1992. 62(4): p. 231-42.

16. Badawi, N., et al., Intrapartum risk factors for newborn encephalopathy: the Western Australian case-control study. BMJ, 1998. 317(7172): p. 1554-8.

17. Sie, L.T., et al., MR patterns of hypoxic-ischemic brain damage after prenatal, perinatal or postnatal asphyxia. Neuropediatrics, 2000. 31(3): p. 128-36.

18. Cowan, F., et al., Origin and timing of brain lesions in term infants with neonatal encephalopathy. Lancet, 2003. 361(9359): p. 736-42.

19. Ferriero, D.M., Neonatal brain injury. N Engl J Med, 2004. 351(19): p. 1985-95.

20. Chan, P.H., Reactive oxygen radicals in signaling and damage in the ischemic brain. J Cereb Blood Flow Metab, 2001. 21(1): p. 2-14.

21. Fiskum, G., A.N. Murphy, and M.F. Beal, Mitochondria in neurodegeneration: acute ischemia and chronic neurodegenerative diseases. J Cereb Blood Flow Metab, 1999. 19(4): p. 351-69.

22. Stadtman, E.R. and R.L. Levine, Protein oxidation. Ann N Y Acad Sci, 2000. 899:

www.manaraa.com

p. 191-208.

23. Richter, C. and B. Frei, Ca2+ release from mitochondria induced by prooxidants. Free Radic Biol Med, 1988. 4(6): p. 365-75.

24. Kaur, H. and B. Halliwell, Aromatic hydroxylation of phenylalanine as an assay for hydroxyl radicals. Measurement of hydroxyl radical formation from ozone and in blood from premature babies using improved HPLC methodology. Anal Biochem, 1994. 220(1): p. 11-5.

25. LeDoux, S.P., et al., Repair of alkylation and oxidative damage in mitochondrial DNA. Mutat Res, 1999. 434(3): p. 149-59.

26. Rubbo, H., et al., Nitric oxide regulation of superoxide and peroxynitrite-dependent lipid peroxidation. Formation of novel nitrogen-containing oxidized lipid derivatives. J Biol Chem, 1994. 269(42): p. 26066-75.

27. Arnold, S. and B. Kadenbach, The intramitochondrial ATP/ADP-ratio controls cytochrome c oxidase activity allosterically. FEBS Lett, 1999. 443(2): p. 105-8.

28. Kadenbach, B., et al., New extension of the Mitchell Theory for oxidative phosphorylation in mitochondria of living organisms. Biochimica et biophysica acta, 2010. 1800(3): p. 205-12.

29. Chance, B. and G.R. Williams, Respiratory enzymes in oxidative phosphorylation. I. Kinetics of oxygen utilization. The Journal of biological chemistry, 1955. 217(1): p. 383-93.

30. Kim, N., M.O. Ripple, and R. Springett, Measurement of the Mitochondrial Membran Potential and pH Gradient from the Redox Poise of the Hemes of the bc1 Complex. Biochem J, 2012. Biophys J. 2012 Mar 7;102(5):1194-203.

31. Nicholls, D.G., The influence of respiration and ATP hydrolysis on the proton-

www.manaraa.com

electrochemical gradient across the inner membrane of rat-liver mitochondria as determined by ion distribution. Eur J Biochem, 1974. 50(1): p. 305-15.

32. Labajova, A., et al., Evaluation of mitochondrial membrane potential using a computerized device with a tetraphenylphosphonium-selective electrode. Anal Biochem, 2006. 353(1): p. 37-42.

33. Cossarizza, A., D. Ceccarelli, and A. Masini, Functional heterogeneity of an isolated mitochondrial population revealed by cytofluorometric analysis at the single organelle level. Exp Cell Res, 1996. 222(1): p. 84-94.

34. Barger, J.L., et al., Tissue-specific depression of mitochondrial proton leak and substrate oxidation in hibernating arctic ground squirrels. Am J Physiol Regul Integr Comp Physiol, 2003. 284(5): p. R1306-13.

35. Shears, S.B. and C.J. Kirk, Characterization of a rapid cellular-fractionation technique for hepatocytes. Application in the measurement of mitochondrial membrane potential in situ. Biochem J, 1984. 219(2): p. 375-82.

36. Brand, M.D., R.P. Hafner, and G.C. Brown, Control of respiration in non-phosphorylating mitochondria is shared between the proton leak and the respiratory chain. Biochem J, 1988. 255(2): p. 535-9.

37. da Silva, E.M., A.M. Soares, and A.J. Moreno, The use of the mitochondrial transmembrane electric potential as an effective biosensor in ecotoxicological research. Chemosphere, 1998. 36(10): p. 2375-90.

38. Moreira, P.I., et al., Amyloid beta-peptide promotes permeability transition pore in brain mitochondria. Biosci Rep, 2001. 21(6): p. 789-800.

39. Wan, B., et al., Effects of cardiac work on electrical potential gradient across mitochondrial membrane in perfused rat hearts. Am J Physiol, 1993. 265(2 Pt 2):

www.manaraa.com

p. H453-60.

40. Zhang, H., et al., Assessment of membrane potentials of mitochondrial populations in living cells. Anal Biochem, 2001. 298(2): p. 170-80.

41. Brand, M.D. and S.M. Felber, Membrane potential of mitochondria in intact lymphocytes during early mitogenic stimulation. Biochem J, 1984. 217(2):453-9.

42. Backus, M., et al., Microprobe analysis of Tc-MIBI in heart cells: calculation of mitochondrial membrane potential. Am J Physiol, 1993. 265(1 Pt 1): p. C178-87.

43. Porteous, W.K., et al., Bioenergetic consequences of accumulating the common 4977-bp mitochondrial DNA deletion. Eur J Biochem, 1998. 257(1): p. 192-201.

44. Nicholls, D.G., Simultaneous monitoring of ionophore- and inhibitor-mediated plasma and mitochondrial membrane potential changes in cultured neurons. J Biol Chem, 2006. 281(21): p. 14864-74.

45. Hoek, J.B., D.G. Nicholls, and J.R. Williamson, Determination of the mitochondrial protonmotive force in isolated hepatocytes. J Biol Chem, 1980. 255(4): p. 1458-64.

46. Nobes, C.D., et al., Non-ohmic proton conductance of the mitochondrial inner membrane in hepatocytes. J Biol Chem, 1990. 265(22): p. 12903-9.

47. Cortese, J.D., Rat liver GTP-binding proteins mediate changes in mitochondrial membrane potential and organelle fusion. Am J Physiol, 1999. 276(3 Pt 1):C611-20.

48. Iwata, S., et al., Structure at 2.8 A resolution of cytochrome c oxidase from Paracoccus denitrificans. Nature, 1995. 376(6542): p. 660-9.

49. Tsukihara, T., et al., The whole structure of the 13-subunit oxidized cytochrome c oxidase at 2.8 Å. Science, 1996. 272(5265): p. 1136-44.

www.manaraa.com

50. Hüttemann, M., et al., Regulation of mitochondrial oxidative phosphorylation through cell signaling. Biochimica et biophysica acta, 2007. 1773: p. 1701-20.

51. Picard, M., et al., Mitochondrial Structure and Function Are Disrupted by Standard Isolation Methods. PloS ONE, 2011. 6(3): p. e18317.

52. Robb-Gaspers, L.D., et al., Integrating cytosolic calcium signals into mitochondrial metabolic responses. Embo J, 1998. 17(17): p. 4987-5000.

53. Hopper, R.K., et al., Mitochondrial matrix phosphoproteome: effect of extra mitochondrial calcium. Biochemistry, 2006. 45(8): p. 2524-36.

54. Lee, I., et al., cAMP-dependent tyrosine phosphorylation of subunit I inhibits cytochrome c oxidase activity. J Biol Chem, 2005. 280(7): p. 6094-100.

55. Bender, E. and B. Kadenbach, The allosteric ATP-inhibition of cytochrome c oxidase activity is reversibly switched on by cAMP-dependent phosphorylation. FEBS Lett, 2000. 466(1): p. 130-4.

56. Lee, I., et al., Isolation of regulatory-competent, phosphorylated cytochrome c oxidase. Methods Enzymol, 2009. 345: p. in press.

57. Hüttemann, M., et al., Regulation of oxidative phosphorylation, the mitochondrial membrane potential, and their role in human disease. J Bioenerg Biomembr, 2008. 40(5): p. 445-56.

58. Huttemann, M., et al., Regulation of mitochondrial respiration and apoptosis through cell signaling: Cytochrome c oxidase and cytochrome c in ischemia/reperfusion injury and inflammation. Biochim Biophys Acta, 2012. 1817(4): p. 598-609.

59. Helling, S., et al., Multiple phosphorylations of cytochrome c oxidase and their functions. Proteomics, 2012. 12(7): p. 950-9.

www.manaraa.com

60. Lee, I., et al., New prospects for an old enzyme: mammalian cytochrome c is tyrosine-phosphorylated *in vivo*. Biochemistry, 2006. 45(30): p. 9121-8.

61. Yu, H., et al., Mammalian liver cytochrome c is tyrosine-48 phosphorylated *in vivo*, inhibiting mitochondrial respiration. Biochim Biophys Acta, 2008. 1777(7-8): p. 1066-71.

62. Pecina, P., et al., Phosphomimetic substitution of cytochrome C tyrosine 48 decreases respiration and binding to cardiolipin and abolishes ability to trigger downstream caspase activation. Biochemistry, 2010. 49(31): p. 6705-14.

63. Sanderson, T.H., et al., Cytochrome c is tyrosine 97 phosphorylated by neuroprotective insulin treatment. J Neurosci Res, 2012. Pending.

64. Sanderson, T.H., et al., Insulin blocks cytochrome c release in the reperfused brain through PI3-K signaling and by promoting Bax/Bcl-XL binding. J Neurochem, 2008. 106(3): p. 1248-58.

65. Prabu, S.K., et al., Protein kinase A-mediated phosphorylation modulates cytochrome c oxidase function and augments hypoxia and myocardial ischemia-related injury. The Journal of biological chemistry, 2006. 281(4): p. 2061-70.

66. Yu, H., et al., Mammalian liver cytochrome c is tyrosine-48 phosphorylated i*n vivo*, inhibiting mitochondrial respiration. Biochimica et biophysica acta, 2008. 1777(7-8): p. 1066-71.

67. Kaim, G. and P. Dimroth, ATP synthesis by F-type ATP synthase is obligatorily dependent on the transmembrane voltage. Embo J, 1999. 18(15): p. 4118-27.

68. St-Pierre, J., et al., Topology of superoxide production from different sites in the mitochondrial electron transport chain. The Journal of biological chemistry, 2002. 277(47): p. 44784-90.

www.manaraa.com

69. Han, D., et al., Effect of glutathione depletion on sites and topology of superoxide and hydrogen peroxide production in mitochondria. Mol Pharmacol, 2003. 64(5): p. 1136-44.

70. Kushnareva, Y., A.N. Murphy, and A. Andreyev, Complex I-mediated reactive oxygen species generation: modulation by cytochrome c and NAD(P)+ oxidation-reduction state. Biochem J, 2002. 368(Pt 2): p. 545-53.

71. Liu, S.S., Cooperation of a "reactive oxygen cycle" with the Q cycle and the proton cycle in the respiratory chain--superoxide generating and cycling mechanisms in mitochondria. J Bioenerg Biomembr, 1999. 31(4): p. 367-76.

72. Rottenberg, H., R. Covian, and B.L. Trumpower, Membrane potential greatly enhances superoxide generation by the cytochrome bc1 complex reconstituted into phospholipid vesicles. The Journal of biological chemistry, 2009. 284(29): p. 19203-10.

73. Suski, J.M., et al., Relation Between Mitochondrial Membrane Potential and ROS Formation. Methods in molecular biology, 2012. 810: p. 183-205.

74. Starkov, A.A. and G. Fiskum, Regulation of brain mitochondrial H2O2 production by membrane potential and NAD(P)H redox state. J Neurochem, 2003. 86(5): p. 1101-7.

75. Liu, S.S., Mitochondrial Q cycle-derived superoxide and chemiosmotic bioenergetics. Ann N Y Acad Sci, 2010. 1201: p. 84-95.

76. Korshunov, S.S., V.P. Skulachev, and A.A. Starkov, High protonic potential actuates a mechanism of production of reactive oxygen species in mitochondria. FEBS Lett, 1997. 416(1): p. 15-8.

77. Rottenberg, H., R. Covian, and B.L. Trumpower, Membrane potential greatly

www.manaraa.com

enhances superoxide generation by the cytochrome bc1 complex reconstituted into phospholipid vesicles. J Biol Chem, 2009. 284(29): p. 19203-10.

78. Kadenbach, B., et al., The possible role of cytochrome c oxidase in stress-induced apoptosis and degenerative diseases. Biochim Biophys Acta, 2004. 1655(1-3): p. 400-8.

79. Abramov, A.Y., A. Scorziello, and M.R. Duchen, Three distinct mechanisms generate oxygen free radicals in neurons and contribute to cell death during anoxia and reoxygenation. J Neurosci, 2007. 27(5): p. 1129-38.

80. Liu, R.R. and T.H. Murphy, Reversible cyclosporin A-sensitive mitochondrial depolarization occurs within minutes of stroke onset in mouse somatosensory cortex *in vivo*: a two-photon imaging study. J Biol Chem, 2009. 284(52): p. 36109-17.

81. Folbergrova, J., et al., Changes in the bioenergetic state of rat hippocampus during 2.5 min of ischemia, and prevention of cell damage by cyclosporin A in hyperglycemic subjects. Exp Brain Res, 1997. 114(1): p. 44-50.

82. Katsura, K., et al., Coupling among energy failure, loss of ion homeostasis, and phospholipase A2 and C activation during ischemia. J Neurochem, 1993. 61(5): p. 1677-84.

83. Domenis, R., et al., Mitochondrial bioenergetic profile and responses to metabolic inhibition in human hepatocarcinoma cell lines with distinct differentiation characteristics. J Bioenerg Biomembr, 2011. 43(5): p. 493-505.

84. Puka-Sundvall, M., et al., Subcellular distribution of calcium and ultrastructural changes after cerebral hypoxia-ischemia in immature rats. Brain Res Dev Brain Res, 2000. 125(1-2): p. 31-41.

www.manaraa.com

85. Ankarcrona, M., et al., Calcineurin and mitochondrial function in glutamate-induced neuronal cell death. FEBS Lett, 1996. 394(3): p. 321-4.

86. McCormack, J.G. and R.M. Denton, The role of intramitochondrial Ca2+ in the regulation of oxidative phosphorylation in mammalian tissues. Biochem Soc Trans, 1993. 21 (Pt 3)(3): p. 793-9.

87. Balaban, R.S., Cardiac energy metabolism homeostasis: role of cytosolic calcium. J Mol Cell Cardiol, 2002. 34(10): p. 1259-71.

88. Brookes, P.S., et al., Calcium, ATP, and ROS: a mitochondrial love-hate triangle. Am J Physiol Cell Physiol, 2004. 287(4): p. C817-33.

89. Zaidan, E. and N.R. Sims, The calcium content of mitochondria from brain subregions following short-term forebrain ischemia and recirculation in the rat. Journal of neurochemistry, 1994. 63(5): p. 1812-9.

90. Kristian, T., et al., Calcium-induced precipitate formation in brain mitochondria: composition, calcium capacity, and retention. J Neurochem, 2007. 102(4): p. 1346-56.

91. Iijima, T., et al., Neuroprotective effect of propofol on necrosis and apoptosis following oxygen-glucose deprivation--relationship between mitochondrial membrane potential and mode of death. Brain Res, 2006. 1099(1): p. 25-32.

92. Choi, K., et al., Oxidative stress-induced necrotic cell death via mitochondira-dependent burst of reactive oxygen species. Curr Neurovasc Res, 2009. 6(4): p. 213-22.

93. Kunimatsu, T., et al., Cerebral reactive oxygen species assessed by electron spin resonance spectroscopy in the initial stage of ischemia-reperfusion are not associated with hypothermic neuroprotection. J Clin Neurosci, 2011. 18(4): p.

www.manaraa.com

545-8.

94. Fabian, R.H., D.S. DeWitt, and T.A. Kent, *In vivo* detection of superoxide anion production by the brain using a cytochrome c electrode. J Cereb Blood Flow Metab, 1995. 15(2): p. 242-7.

95. Kudin, A.P., D. Malinska, and W.S. Kunz, Sites of generation of reactive oxygen species in homogenates of brain tissue determined with the use of respiratory substrates and inhibitors. Biochim Biophys Acta, 2008. 1777(7-8): p. 689-95.

96. Barja, G. and A. Herrero, Localization at complex I and mechanism of the higher free radical production of brain nonsynaptic mitochondria in the short-lived rat than in the longevous pigeon. J Bioenerg Biomembr, 1998. 30(3): p. 235-43.

97. Barja, G., Mitochondrial oxygen radical generation and leak: sites of production in states 4 and 3, organ specificity, and relation to aging and longevity. J Bioenerg Biomembr, 1999. 31(4): p. 347-66.

98. St-Pierre, J., et al., Topology of superoxide production from different sites in the mitochondrial electron transport chain. J Biol Chem, 2002. 277(47): p. 44784-90.

99. Sims, N.R. and W.A. Pulsinelli, Altered mitochondrial respiration in selectively vulnerable brain subregions following transient forebrain ischemia in the rat. J Neurochem, 1987. 49(5): p. 1367-74.

100. Sims, N.R., Selective impairment of respiration in mitochondria isolated from brain subregions following transient forebrain ischemia in the rat. J Neurochem, 1991. 56(6): p. 1836-44.

101. Racay, P., et al., Mitochondrial calcium transport and mitochondrial dysfunction after global brain ischemia in rat hippocampus. Neurochemical research, 2009. 34(8): p. 1469-78.

www.manaraa.com

102. Chomova, M., et al., Ischemia-Induced Inhibition of Mitochondrial Complex I in Rat Brain: Effect of Permeabilization Method and Electron Acceptor. Neurochemical research, 2012.

103. Zhang, Y., et al., The oxidative inactivation of mitochondrial electron transport chain components and ATPase. The Journal of biological chemistry, 1990. 265(27): p. 16330-6.

104. Murakami, K., et al., Mitochondrial susceptibility to oxidative stress exacerbates cerebral infarction that follows permanent focal cerebral ischemia in mutant mice with manganese superoxide dismutase deficiency. J Neurosci, 1998. 18(1): p. 205-13.

105. Friberg, H., T. Wieloch, and R.F. Castilho, Mitochondrial oxidative stress after global brain ischemia in rats. Neurosci Lett, 2002. 334(2): p. 111-4.

106. Shinzawa-Itoh, K., et al., Structures and physiological roles of 13 integral lipids of bovine heart cytochrome c oxidase. Embo J, 2007. 26(6): p. 1713-25.

107. Kagan, V.E., et al., Cytochrome c/cardiolipin relations in mitochondria: a kiss of death. Free Radic Biol Med, 2009. 46(11): p. 1439-53.

108. Kim, J., et al., Cardiolipin: characterization of distinct oxidized molecular species. J Lipid Res, 2011. 52(1): p. 125-35.

109. Robinson, N.C., Functional binding of cardiolipin to cytochrome c oxidase. J Bioenerg Biomembr, 1993. 25(2): p. 153-63.

110. Petrosillo, G., et al., *In vivo* hyperoxic preconditioning protects against rat-heart ischemia/reperfusion injury by inhibiting mitochondrial permeability transition pore opening and cytochrome c release. Free Radic Biol Med, 2011. 50(3): p. 477-83.

111. Paradies, G., et al., Oxidative stress, mitochondrial bioenergetics, and cardiolipin

www.manaraa.com

in aging. Free Radic Biol Med, 2010. 48(10): p. 1286-95.

112. Petrosillo, G., et al., Mitochondrial complex I dysfunction in rat heart with aging: critical role of reactive oxygen species and cardiolipin. Free Radic Biol Med, 2009. 46(1): p. 88-94.

113. Petrosillo, G., et al., Ca2+-induced reactive oxygen species production promotes cytochrome c release from rat liver mitochondria via mitochondrial permeability transition (MPT)-dependent and MPT-independent mechanisms: role of cardiolipin. J Biol Chem, 2004. 279(51): p. 53103-8.

114. Garcia Fernandez, M., et al., Early changes in intramitochondrial cardiolipin distribution during apoptosis. Cell Growth Differ, 2002. 13(9): p. 449-55.

115. Kagan, V.E., et al., Cytochrome c acts as a cardiolipin oxygenase required for release of proapoptotic factors. Nat Chem Biol, 2005. 1(4): p. 223-32.

116. Northington, F.J., et al., Early Neurodegeneration after Hypoxia-Ischemia in Neonatal Rat Is Necrosis while Delayed Neuronal Death Is Apoptosis. Neurobiol Dis, 2001. 8(2): p. 207-19.

117. Leist, M. and M. Jaattela, Four deaths and a funeral: from caspases to alternative mechanisms. Nat Rev Mol Cell Biol, 2001. 2(8): p. 589-98.

118. Hetz, C., et al., Bax channel inhibitors prevent mitochondrion-mediated apoptosis and protect neurons in a model of global brain ischemia. The Journal of biological chemistry, 2005. 280(52): p. 42960-70.

119. Cao, G., et al., Critical role of calpain I in mitochondrial release of apoptosis-inducing factor in ischemic neuronal injury. J Neurosci, 2007. 27(35): p. 9278-93.

120. Sugawara, T., et al., Mitochondrial release of cytochrome c corresponds to the selective vulnerability of hippocampal CA1 neurons in rats after transient global

www.manaraa.com

cerebral ischemia. J Neurosci, 1999. 19(22): p. RC39.

121. Cheng, E.H., et al., BCL-2, BCL-X(L) sequester BH3 domain-only molecules preventing BAX- and BAK-mediated mitochondrial apoptosis. Mol Cell, 2001. 8(3): p. 705-11.

122. Kuwana, T. and D.D. Newmeyer, Bcl-2-family proteins and the role of mitochondria in apoptosis. Curr Opin Cell Biol, 2003. 15(6): p. 691-9.

123. Ott, M., et al., Cytochrome c release from mitochondria proceeds by a two-step process. Proc Natl Acad Sci U S A, 2002. 99(3): p. 1259-63.

124. Berezhna, S., H. Wohlrab, and P.M. Champion, Resonance Raman investigations of cytochrome c conformational change upon interaction with the membranes of intact and Ca2+-exposed mitochondria. Biochemistry, 2003. 42(20): p. 6149-58.

125. Cohen, G.M., Caspases: the executioners of apoptosis. The Biochemical journal, 1997. 326 (Pt 1): p. 1-16.

126. Blomgren, K., et al., Synergistic activation of caspase-3 by m-calpain after neonatal hypoxia-ischemia: a mechanism of "pathological apoptosis"? J Biol Chem, 2001. 276(13): p. 10191-8.

127. Cheng, Y., et al., Caspase inhibitor affords neuroprotection with delayed administration in a rat model of neonatal hypoxic-ischemic brain injury. J Clin Invest, 1998. 101(9): p. 1992-9.

128. Zhu, C., et al., Post-ischemic hypothermia-induced tissue protection and diminished apoptosis after neonatal cerebral hypoxia-ischemia. Brain research, 2004. 996(1): p. 67-75.

129. Ginsberg, M.D., Neuroprotection for ischemic stroke: past, present and future.

www.manaraa.com

Neuropharmacology, 2008. 55(3): p. 363-389.

130. Chan, P.H., et al., Overexpression of SOD1 in transgenic rats protects vulnerable neurons against ischemic damage after global cerebral ischemia and reperfusion. J Neurosci, 1998. 18(20): p. 8292-9.

131. Fujimura, M., et al., The cytosolic antioxidant copper/zinc-superoxide dismutase prevents the early release of mitochondrial cytochrome c in ischemic brain after transient focal cerebral ischemia in mice. J Neurosci, 2000. 20(8): p. 2817-24.

132. Christophe, M. and S. Nicolas, Mitochondria: a target for neuroprotective interventions in cerebral ischemia-reperfusion. Curr Pharm Des, 2006. 12(6): p. 739-57.

133. Niizuma, K., H. Endo, and P.H. Chan, Oxidative stress and mitochondrial dysfunction as determinants of ischemic neuronal death and survival. J Neurochem, 2009. 109 Suppl 1: p. 133-8.

134. Chan, P.H., et al., Role of superoxide dismutase in ischemic brain injury: reduction of edema and infarction in transgenic mice following focal cerebral ischemia. Prog Brain Res, 1993. 96: p. 97-104.

135. Chan, P.H., S. Longar, and R.A. Fishman, Protective effects of liposome-entrapped superoxide dismutase on posttraumatic brain edema. Ann Neurol, 1987. 21(6): p. 540-7.

136. He, Y.Y., et al., Polyethylene glycol-conjugated superoxide dismutase in focal cerebral ischemia-reperfusion. Am J Physiol, 1993. 265(1 Pt 2): p. H252-6.

137. Shuaib, A., et al., NXY-059 for the treatment of acute ischemic stroke. N Engl J Med, 2007. 357(6): p. 562-71.

138. Weigl, M., et al., A systematic review of currently available pharmacological

www.manaraa.com

neuroprotective agents as a sole intervention before anticipated or induced cardiac arrest. Resuscitation, 2005. 65(1): p. 21-39.

139. Iijima, T., et al., Mitochondrial hyperpolarization after transient oxygen-glucose deprivation and subsequent apoptosis in cultured rat hippocampal neurons. Brain research, 2003. 993(1-2): p. 140-5.

140. Pandya, J.D., J.R. Pauly, and P.G. Sullivan, The optimal dosage and window of opportunity to maintain mitochondrial homeostasis following traumatic brain injury using the uncoupler FCCP. Exp Neurol, 2009. 218(2): p. 381-9.

141. Brennan, J.P., et al., Mitochondrial uncoupling, with low concentration FCCP, induces ROS-dependent cardioprotection independent of KATP channel activation. Cardiovasc Res, 2006. 72(2): p. 313-21.

142. Haines, B.A., et al., Deletion of mitochondrial uncoupling protein-2 increases ischemic brain damage after transient focal ischemia by altering gene expression patterns and enhancing inflammatory cytokines. Journal of cerebral blood flow and metabolism : official journal of the International Society of Cerebral Blood Flow and Metabolism, 2010. 30(11): p. 1825-33.

143. Mattiasson, G., et al., Uncoupling protein-2 prevents neuronal death and diminishes brain dysfunction after stroke and brain trauma. Nat Med, 2003. 9(8): p. 1062-8.

144. Teshima, Y., et al., Uncoupling protein-2 overexpression inhibits mitochondrial death pathway in cardiomyocytes. Circ Res, 2003. 93(3): p. 192-200.

145. Han, Y.H., et al., Carbonyl cyanide p-(trifluoromethoxy) phenylhydrazone (FCCP) as an O2(*-) generator induces apoptosis via the depletion of intracellular GSH contents in Calu-6 cells. Lung Cancer, 2009. 63(2): p. 201-9.

www.manaraa.com

146. Dave, K.R., et al., Ischemic preconditioning targets the respiration of synaptic mitochondria via protein kinase C epsilon. J Neurosci, 2008. 28(16): p. 4172-82.

147. Liu, Y., et al., Both ischemic preconditioning and ghrelin administration protect hippocampus from ischemia/reperfusion and upregulate uncoupling protein-2. BMC Physiol, 2009. 9: p. 17.

148. Samavati, L., et al., Tumor necrosis factor α inhibits oxidative phosphorylation through tyrosine phosphorylation at subunit I of cytochrome c oxidase. J Biol Chem, 2008. 283(30): p. 21134-44.

149. Sanderson, T.H., et al., Insulin activates the PI3K-Akt survival pathway in vulnerable neurons following global brain ischemia. Neurol Res, 2009. 31(9): p. 947-58.

150. Bolli, R., et al., Myocardial protection at a crossroads: the need for translation into clinical therapy. Circ Res, 2004. 95(2): p. 125-34.

151. Piper, H.M., K. Meuter, and C. Schafer, Cellular mechanisms of ischemia-reperfusion injury. Ann Thorac Surg, 2003. 75(2): p. S644-8.

152. Anderson, R.R. and J.A. Parrish, The optics of human skin. J Invest Dermatol, 1981. 77(1): p. 13-9.

153. Beek, J.F., et al., *In vitro* double-integrating-sphere optical properties of tissues between 630 and 1064 nm. Phys Med Biol, 1997. 42(11): p. 2255-61.

154. Yu, W., et al., Photomodulation of oxidative metabolism and electron chain enzymes in rat liver mitochondria. Photochem Photobiol, 1997. 66(6): p. 866-71.

155. Yeager, R.L., et al., Effects of 670-nm phototherapy on development. Photomed Laser Surg, 2005. 23(3): p. 268-72.

156. Wong-Riley, M.T., et al., Photobiomodulation directly benefits primary neurons

www.manaraa.com

functionally inactivated by toxins: role of cytochrome c oxidase. J Biol Chem, 2005. 280(6): p. 4761-71.

157. Streeter, J., L. De Taboada, and U. Oron, Mechanisms of action of light therapy for stroke and acute myocardial infarction. Mitochondrion, 2004. 4(5-6):569-76.

158. Eells, J.T., et al., Mitochondrial signal transduction in accelerated wound and retinal healing by near-infrared light therapy. Mitochondrion, 2004. 4(5-6):559-67.

159. Eells, J.T., et al., Therapeutic photobiomodulation for methanol-induced retinal toxicity. Proc Natl Acad Sci U S A, 2003. 100(6): p. 3439-44.

160. Wong-Riley, M.T., et al., Light-emitting diode treatment reverses the effect of TTX on cytochrome oxidase in neurons. Neuroreport, 2001. 12(14): p. 3033-7.

161. Whelan, H.T., et al., Effect of NASA light-emitting diode irradiation on molecular changes for wound healing in diabetic mice. J Clin Laser Med Surg, 2003. 21(2): p. 67-74.

162. Leonard, D.R., M.H. Farooqi, and S. Myers, Restoration of sensation, reduced pain, and improved balance in subjects with diabetic peripheral neuropathy: a double-blind, randomized, placebo-controlled study with monochromatic near-infrared treatment. Diabetes Care, 2004. 27(1): p. 168-72.

163. Bae, C.S., et al., Effect of Ga-as laser on the regeneration of injured sciatic nerves in the rat. *In Vivo*, 2004. 18(4): p. 489-95.

164. DeLellis, S.L., D.H. Carnegie, and T.J. Burke, Improved sensitivity in patients with peripheral neuropathy: effects of monochromatic infrared photo energy. J Am Podiatr Med Assoc, 2005. 95(2): p. 143-7.

165. Lim, J., et al., Effects of low-level light therapy on hepatic antioxidant defense in acute and chronic diabetic rats. J Biochem Mol Toxicol, 2009. 23(1): p. 1-8.

www.manaraa.com

166. Lapchak, P.A., et al., Transcranial near-infrared light therapy improves motor function following embolic strokes in rabbits: an extended therapeutic window study using continuous and pulse frequency delivery modes. Neuroscience, 2007. 148(4): p. 907-14.

167. Oron, A., et al., Low-level laser therapy applied transcranially to rats after induction of stroke significantly reduces long-term neurological deficits. Stroke, 2006. 37(10): p. 2620-4.

168. Detaboada, L., et al., Transcranial application of low-energy laser irradiation improves neurological deficits in rats following acute stroke. Lasers Surg Med, 2006. 38(1): p. 70-3.

169. Lapchak, P.A., J. Wei, and J.A. Zivin, Transcranial infrared laser therapy improves clinical rating scores after embolic strokes in rabbits. Stroke, 2004. 35(8): p. 1985-8.

170. Yaakobi, T., et al., Long-term effect of low energy laser irradiation on infarction and reperfusion injury in the rat heart. J Appl Physiol, 2001. 90(6): p. 2411-9.

171. Lampl, Y., et al., Infrared laser therapy for ischemic stroke: a new treatment strategy: results of the NeuroThera Effectiveness and Safety Trial-1 (NEST-1). Stroke, 2007. 38(6): p. 1843-9.

172. Zivin, J.A., et al., Effectiveness and safety of transcranial laser therapy for acute ischemic stroke. Stroke, 2009. 40(4): p. 1359-64.

173. Yip, S. and J. Zivin, Laser therapy in acute stroke treatment. Int J Stroke, 2008. 3(2): p. 88-91.

174. Karu, T.I. and N.I. Afanas'eva, [Cytochrome c oxidase as the primary photoacceptor upon laser exposure of cultured cells to visible and near IR-range

www.manaraa.com

light]. Dokl Akad Nauk, 1995. 342(5): p. 693-5.

175. Karu, T.I., L.V. Pyatibrat, and G.S. Kalendo, Photobiological modulation of cell attachment via cytochrome c oxidase. Photochem Photobiol Sci, 2004. 3(2): p. 211-6.

176. Sanderson, T.H. and J.M. Wider, 2-vessel occlusion/hypotension: a rat model of global brain ischemia. J Vis Exp, 2013(76).

177. Lagina, A.T., 3rd, et al., Combination therapy with insulin-like growth factor-1 and hypothermia synergistically improves outcome after transient global brain ischemia in the rat. Acad Emerg Med, 2013. 20(4): p. 344-51.

178. Hazelton, J.L., et al., Hyperoxic Reperfusion after Global Cerebral Ischemia Promotes Inflammation and Long-Term Hippocampal Neuronal Death. Journal of Neurotrauma, 2010. 27(4): p. 753-762.

179. Sanderson, T.H., et al., PKR-like endoplasmic reticulum kinase (PERK) activation following brain ischemia is independent of unfolded nascent proteins. Neuroscience, 2010. 169(3): p. 1307-14.

180. Sanderson, T.H., et al., Insulin activates the PI3K-Akt survival pathway in vulnerable neurons following global brain ischemia. Neurological Research, 2009. 31(9): p. 947-958.

181. Mallajosyula, J.K., et al., MAO-B elevation in mouse brain astrocytes results in Parkinson's pathology. PLoS ONE, 2008. 3(2): p. e1616.

182. Rice, J.E., 3rd, R.C. Vannucci, and J.B. Brierley, The influence of immaturity on hypoxic-ischemic brain damage in the rat. Ann Neurol, 1981. 9(2): p. 131-41.

183. Estaquier, J., et al., The mitochondrial pathways of apoptosis. Adv Exp Med Biol, 2012. 942: p. 157-83.

www.manaraa.com

184. Chernyak, B.V., Redox regulation of the mitochondrial permeability transition pore. Biosci Rep, 1997. 17(3): p. 293-302.

185. Liu, X., et al., Induction of apoptotic program in cell-free extracts: requirement for dATP and cytochrome c. Cell, 1996. 86(1): p. 147-57.

186. Sheldon, R.A., C. Sedik, and D.M. Ferriero, Strain-related brain injury in neonatal mice subjected to hypoxia-ischemia. Brain Res, 1998. 810(1-2): p. 114-22.

187. Bederson, J.B., et al., Evaluation of 2, 3, 5-triphenyltetrazolium chloride as a stain for detection and quantification of experimental cerebral infarction in rats. Stroke, 1986. 17(6): p. 1304-1308.

188. Bradford, M.M., A rapid and sensitive method for the quantitation of microgram quantities of protein utilizing the principle of protein-dye binding. Anal Biochem, 1976. 72: p. 248-54.

189. Schagger, H., Tricine-SDS-PAGE. Nat Protoc, 2006. 1(1): p. 16-22.

190. Taniguchi, H. and K. Andreasson, The hypoxic-ischemic encephalopathy model of perinatal ischemia. J Vis Exp, 2008(21).

191. Schlame, M. and M. Ren, The role of cardiolipin in the structural organization of mitochondrial membranes. Biochimica et Biophysica Acta (BBA)-Biomembranes, 2009. 1788(10): p. 2080-2083.

192. Zhang, M., E. Mileykovskaya, and W. Dowhan, Gluing the respiratory chain together Cardiolipin is required for supercomplex formation in the inner mitochondrial membrane. Journal of Biological Chemistry, 2002. 277(46): p. 43553-43556.

193. Pfeiffer, K., et al., Cardiolipin stabilizes respiratory chain supercomplexes. Journal of Biological Chemistry, 2003. 278(52): p. 52873-52880.

www.manaraa.com

194. Kagan, V.E., et al., Cytochrome c acts as a cardiolipin oxygenase required for release of proapoptotic factors. Nature chemical biology, 2005. 1(4): p. 223-232.

195. Bayir, H., et al., Selective early cardiolipin peroxidation after traumatic brain injury: an oxidative lipidomics analysis. Annals of neurology, 2007. 62(2): p. 154-169.

196. Ji, J., et al., Deciphering of mitochondrial cardiolipin oxidative signaling in cerebral ischemia-reperfusion. Journal of Cerebral Blood Flow & Metabolism, 2014.

197. Chu, C.T., et al., Cardiolipin externalization to the outer mitochondrial membrane acts as an elimination signal for mitophagy in neuronal cells. Nature cell biology, 2013. 15(10): p. 1197-1205.

198. Han, X., K. Yang, and R.W. Gross, Multi-dimensional mass spectrometry-based shotgun lipidomics and novel strategies for lipidomic analyses. Mass spectrometry reviews, 2012. 31(1): p. 134-178.

199. Lutomski, C.A., et al., Transmission Geometry Laserspray Ionization Vacuum Using an Atmospheric Pressure Inlet. Analytical chemistry, 2014. 86(13): p. 6208-6213.

200. Inutan, E. and S. Trimpin, Laserspray ionization (LSI) ion mobility spectrometry (IMS) mass spectrometry. Journal of the American Society for Mass Spectrometry, 2010. 21(7): p. 1260-1264.

201. Suni, N.M., et al., Analysis of lipids with desorption atmospheric pressure photoionization-mass spectrometry (DAPPI-MS) and desorption electrospray ionization-mass spectrometry (DESI-MS). Journal of Mass Spectrometry, 2012. 47(5): p. 611-619.

www.manaraa.com

202. Manicke, N.E., et al., Desorption electrospray ionization (DESI) mass spectrometry and tandem mass spectrometry (MS/MS) of phospholipids and sphingolipids: ionization, adduct formation, and fragmentation. Journal of the American Society for Mass Spectrometry, 2008. 19(4): p. 531-543.

203. Sun, G., et al., Matrix-assisted laser desorption/ionization time-of-flight mass spectrometric analysis of cellular glycerophospholipids enabled by multiplexed solvent dependent analyte− matrix interactions. Analytical chemistry, 2008. 80(19): p. 7576-7585.

204. Cheng, H., et al., Selective desorption/ionization of sulfatides by MALDI-MS facilitated using 9-aminoacridine as matrix. Journal of lipid research, 2010. 51(6): p. 1599-1609.

205. Angelini, R., et al., Lipidomics of intact mitochondria by MALDI-TOF/MS. Journal of lipid research, 2012. 53(7): p. 1417-1425.

206. Jackson, S.N., et al., Direct tissue analysis of phospholipids in rat brain using MALDI-TOFMS and MALDI-ion mobility-TOFMS. Journal of the American Society for Mass Spectrometry, 2005. 16(2): p. 133-138.

207. Woods, A.S. and S.N. Jackson, Brain tissue lipidomics: Direct probing using matrix-assisted laser desorption/ionization mass spectrometry. The AAPS journal, 2006. 8(2): p. E391-E395.

208. Sommer, U., et al., LC-MS-based method for the qualitative and quantitative analysis of complex lipid mixtures. Journal of lipid research, 2006. 47(4):804-814.

209. Wiseman, J.M., et al., Mass spectrometric profiling of intact biological tissue by using desorption electrospray ionization. Angewandte Chemie, 2005. 117(43): p. 7256-7259.

www.manaraa.com

210. Inutan, E.D. and S. Trimpin, Matrix assisted ionization vacuum (MAIV), a new ionization method for biological materials analysis using mass spectrometry. Molecular & Cellular Proteomics, 2013. 12(3): p. 792-796.

211. Trimpin, S. and E.D. Inutan, Matrix assisted ionization in vacuum, a sensitive and widely applicable ionization method for mass spectrometry. Journal of the American Society for Mass Spectrometry, 2013. 24(5): p. 722-732.

212. Trimpin, S. and E.D. Inutan, New ionization method for analysis on atmospheric pressure ionization mass spectrometers requiring only vacuum and matrix assistance. Analytical chemistry, 2013. 85(4): p. 2005-2009.

213. Trimpin, S. and D.E. Clemmer, Ion mobility spectrometry/mass spectrometry snapshots for assessing the molecular compositions of complex polymeric systems. Analytical chemistry, 2008. 80(23): p. 9073-9083.

214. Trimpin, S., et al., Profiling of phospholipids and related lipid structures using multidimensional ion mobility spectrometry-mass spectrometry. International Journal of Mass Spectrometry, 2009. 287(1): p. 58-69.

215. Minkler, P.E. and C.L. Hoppel, Separation and characterization of cardiolipin molecular species by reverse-phase ion pair high-performance liquid chromatography-mass spectrometry. Journal of lipid research, 2010. 51(4): p. 856-865.

216. Cheng, H., et al., Shotgun Lipidomics Reveals the Temporally Dependent, Highly Diversified Cardiolipin Profile in the Mammalian Brain: Temporally Coordinated Postnatal Diversification of Cardiolipin Molecular Species with Neuronal Remodeling†. Biochemistry, 2008. 47(21): p. 5869-5880.

217. Tyurina, Y.Y., et al., LC/MS characterization of rotenone induced cardiolipin

www.manaraa.com

oxidation in human lymphocytes: Implications for mitochondrial dysfunction associated with Parkinson's disease. Molecular Nutrition & Food Research, 2013. 57(8): p. 1410-1422.

218. Kim, J. and C.L. Hoppel, Monolysocardiolipin: improved preparation with high yield. Journal of lipid research, 2011. 52(2): p. 389-392.

219. Dawson, R., A hydrolytic procedure for the identification and estimation of individual phospholipids in biological samples. Biochemical Journal, 1960. 75(1): p. 45.

220. Hüttemann, M., B. Kadenbach, and L.I. Grossman, Mammalian subunit IV isoforms of cytochrome c oxidase. Gene, 2001. 267(1): p. 111-123.

www.manaraa.com

ABSTRACT

PRECLINICAL EVALUATION OF INFRARED LIGHT THERAPY IN A RAT MODEL OF NEONATAL HYPOXIC-ISCHEMIC ENCEPHALOPATHY

by

CHRISTIAN ANDREW REYNOLDS

August 2015

Advisor: Drs. Karin Przyklenk and Thomas Sanderson

Major: Physiology

Degree: Doctor of Philosophy

This work has provided two major technical contributions to the field of cerebral ischemia-reperfusion injury. First, experiments in Chapter 3 have refined and provided biochemical characterization of the rat model of HIE. Second, Chapter 4 focused on the development of a method of characterizing membrane lipids directly from their native and intact biological membranes without prior lipid extraction using the MAI-MS technology pioneered in the Trimpin laboratory. While the current study used this new method exclusively to investigate alterations in the CL profile of brain mitochondria following cerebral hypoxia-ischemia, the approach can be employed in various membrane lipid research applications. Finally, consistent with results from previous IRL efficacy studies using a rat model of adult global brain ischemia, experiments in Chapter 5 establish that IRL treatment attenuated cerebral injury resulting from hypoxia-ischemia in the neonatal rat. Thus, and perhaps most importantly, this work contributes to the development of a potential novel therapeutic approach in the management of brain injuries arising as a result of perinatal asphyxia.

www.manaraa.com

AUTOBIOGRAPHICAL STATEMENT

Christian Andrew Reynolds

Education

2015	Ph.D. in Physiology, Wayne State University School of Medicine
2008–2010	Medical School, Universidad Autónoma de Guadalajara (non-degree)
2007	B.S., Microbiology, Oregon State University

Honors

2015	Lipids@Wayne Syposium Best Poster Award – 2nd Place
2010	National Neurotrauma Society Student Travel Award
2007	Tricore Reference Laboratories Extraordinary Achievement Award

Selected Peer-reviewed publications:

1. Sanderson TH, **Reynolds CA**, Kumar R, Przyklenk K, Hüttemann M. Molecular Mechanisms of Ischemia-Reperfusion Injury in Brain: Pivotal Role of the Mitochondrial Membrane Potential in Reactive Oxygen Species Generation. *Molecular Neurobiology.* 2013. Feb;47(1):9-23.
2. **Reynolds CA**, Hüttemann M, Przyklenk K, Sanderson TH. Hypoxia-induced damage to the adult and immature brain: molecular mechanism of oxidative damage and the need for targeted therapeutic intervention. *Hypoxia: Causes, Types and Management.* Jan. 2013. 346:7-10

Manuscripts in preparation:

1. Sanderson TH, Wider J, **Reynolds CA**, Lepore B, Przyklenk K, Hüttemann M. Modulation of Cytochrome c Oxidase Activity with Specific Infrared Light Wavelengths: Non-invasive Therapy for Reperfusion Injury.
2. **Reynolds, CA**, Deleeuw, JL, Lutomski, CA, Sanderson, TH, Trimpin, S, Przyklenk, K, Solid-State Direct Injection Mass Spectrometry enables Cardiolipin Characterization from Intact Mitochondrial Membranes. Angewandte Chemie, in preparation
3. **Reynolds CA**, Przyklenk K, Hüttemann M, Sanderson, TH. Modulation of Cytochrome c Oxidase Activity with Specific Infrared Light Wavelengths: Non-invasive Therapy for Neonatal Hypoxic-Ischemic Encephalopathy
4. **Reynolds, CA**, Deleeuw, JL, Przyklenk, K, Trimpin, S, Sanderson, TH, Matrix Assisted Ionization Vacuum Ion Mobility Spectrometry Mass Spectrometry provides Evidence for Cardiolipin Remodeling Following Cerebral Hypoxia-Ischemia in the Neonatal Rat
5. Deleeuw, JL, Lutomski, CA, **Reynolds, CA**, Wager-Miller, J, Mackie, K, Trimpin, S. Rapid Characterization of Lipids by Matrix-Assisted Ionization Ion Mobility Spectrometry Mass Spectrometry.

Selected Research Support

Cardiovascular Research Institute - ISIS Grant Reynolds (Co-PI) Dec 2014-Dec 2015
Cardiolipin modification as a central linchpin in mediating neonatal brain injury

Kellogg Foundation/WSU- Perinatology Virtual Reynolds (Co-PI) Sept 2013-June 2015
A novel non-invasive infrared light-based therapy to attenuate neonatal hypoxic-ischemic brain injury

Amer Heart Assoc Predoctoral Fellowship Reynolds (PI) July 2012-June 2014
Photobioinhibition of mitochondrial complex IV: a novel approach to reduce neonatal cerebral ischemia/reperfusion injury"

www.manaraa.com